Low angle dune response to variable flow, dune translation and crestline dynamics in Fraser Estuary, British Columbia, Canada

by

Megan Lillian Hendershot

B.Sc., Simon Fraser University, 2010

Thesis Submitted in Partial Fulfillment of the
Requirements for the Degree of
Master of Science

in the
Department of Geography
Faculty of the Environment

SIMON FRASER UNIVERSITY

Spring 2014

Approval

Name:	**Megan Lillian Hendershot**
Degree:	**Master of Science**
Title:	***Low angle dune response to variable flow, dune translation and crestline dynamics in Fraser Estuary, British Columbia, Canada***
Examining Committee:	**Chair:** Dr. Geoff Mann Associate Professor

Dr. Jeremy Venditti
Senior Supervisor
Associate Professor

Dr. Michael Church
Supervisor
Professor Emeritus
Department of Geography
University of British Columbia

Dr. Ray Kostaschuk
Supervisor
Adjunct Professor

Dr. Shahin Dashtgard
External Examiner
Associate Professor
Department of Earth Sciences

Date Defended: April 28, 2014

Partial Copyright Licence

Abstract

Dune geometry and crestline dynamics in river environments are functions of the interaction between fluid flow and the channel bed, however, little is known about how they respond to variable flow conditions in tidal environments. This study examines the evolution of a dune field in Fraser Estuary, Canada using data collected during the largest tidal flux of the neap-spring cycle on the rising limb of the annual hydrograph. Chapter One examines changes in mean geometric properties. Height and lee slope angle respond directly to changes in flow, and are linked to suspended sediment concentration flux. Height and length also show a net increase, likely responding to larger scale changes in the annual hydrograph. Chapter Two addresses crestline dynamics in response to variable flow, examining planimetric morphology, translation rates, and changes in bifurcations. Mean translation increases toward low tide with increasing mean velocity, and decreases toward high tide. Highly bifurcated areas translate farther before low tide, while areas of lower bifurcation move farther after low tide. Bifurcation 'deaths' outweigh 'births' toward low tide, indicating a shift toward a more two-dimensional planimetric morphology, while births dominate post low tide, suggesting the bed is reorganizing toward a more three-dimensional morphology.

Keywords: Low angle dunes; dune geometry; crestline dynamics; tidally-dominated fluvial environment; Fraser River

For Mom and Dad, for so many reasons. You have been the best cheerleaders a person could ever ask for.

Acknowledgements

I would like to thank my senior supervisor, Dr. Jeremy Venditti, for his guidance and direction of this project, Dr. Michael Church for the many e-mails and meetings to fine tune my ideas, and Dr. Ray Kostaschuk for all the lee slope chats. Thanks to the members of the River Dynamics Research Group at SFU, in particular, Ryan Bradley for the flow and sediment data, and all the help with the little things, Maureen Attard for processing the sediment samples, and Michael Wong for the help with the data processing. Thank you to Dr. Mead Allison and Dan Duncan for the support in the field and with data processing. Thanks to Dr. Dan Parsons for answering countless e-mails about multibeam processing, and Nick Roberts for the GIS parties.

And finally, thank you to all my family and friends for being so supportive over the course of this project; I couldn't have gotten through this without you.

Funding for this project was provided through a Graduate Fellowship from Simon Fraser University and Natural Science and Engineering Research Council (NSERC) Discovery grants to Drs. Venditti, Church, and Kostaschuk.

Table of Contents

List of Tables

List of Figures

List of Symbols

D	deformation
H	mean dune height
H_{Tide}	tidal stage
H/h	relative dune height
H/L	mean dune aspect ratio
h	flow depth
L	mean dune length
L_c	bedform crestline length
L_s	length of dune stoss
L_y	straight line distance across the channel width
L_s/L	slope symmetry ratio
L/h	relative dune length
Q_w	flow discharge
q_s	bedform related mean sediment flux
R^2	coefficient of determination
r_s	Spearman rank coefficient
$<SSC>$	depth-integrated suspended sediment concentration
T	translation distance
$<u>$	depth-integrated mean flow velocity
V_b	bedform migration speed
β	bedform shape factor
$1-\rho$	proportion of the bedform cross section occupied by sediment
ρ_{bif}	bifurcation density
θ_{Lee}	lee slope angle
θ_{Stoss}	stoss slope angle

List of Acronyms

aDcp	Acoustic Doppler current profiler
DGPS	Differential global positioning system
HT	High tide
HFT	High falling tide
HRT	High rising tide
LAD	Low angle dune
LT	Low tide
LFT	Low falling tide
LRT	Low rising tide
MBES	Multibeam echo sounder
MFT	Mid falling tide
MRT	Mid rising tide
NDS	Non-dimensional span
RTK-GPS	Real time kinetic global positioning system
2D	Two-dimensional
3D	Three-dimensional

Executive Summary

The channel topography in an estuarine environment reflects the bidirectional nature of fluid flow resulting from the interaction of fluvial discharge and tidal flux. Dune height (*H*), length (*L*), aspect ratio (*H/L*), and lee slope angle (θ_{Lee}) are functions of this flow interaction and their growth, diminution, and migration under variable flows serves to characterize sediment transport within a channel. This two-part study examines the evolution of a dune field over the course of a tidal cycle in Fraser Estuary, Canada using data collected through one of the largest single tidal flux of the neap-spring cycle on the rising limb of the annual hydrograph. The first chapter focusses on the deformation of dunes over the tidal cycle by examining changes in mean geometric properties (*H*, *L*, *H/L*, and θ_{Lee}). *H* and θ_{Lee} show a direct response to flow variability, and these changes can be linked to suspended sediment concentrations, which increased with mean velocity. *H* and *L* also show a net increase over the tidal cycle, which may be a response to larger scale changes in the annual hydrograph. The second chapter focusses on crestline dynamics in response to variable flow, examining the planimetric morphology of the bed, dune translation rates, and changes in bifurcation densities. Mean dune translation increases toward low tide with increasing mean velocity, and decreases as the tidal maximum is approached. The areas on the bed with higher bifurcation density are composed of dunes that move greater distances before low tide, while the larger dunes with lower bifurcation densities move farther after low tide, showing a hysteretic response to peak flow. The number of bifurcations present in the study area changes throughout the survey period, with the number of 'deaths' outweighing the number of 'births' at the highest flows, indicating a shift toward a more two-dimensional planimetric morphology. Births dominate during low flows suggesting the bed is reorganizing toward a more three-dimensional morphology under these conditions.

Chapter 1.

Low angle dune response to variable flow in Fraser Estuary, British Columbia, Canada

1.1. Introduction

In sedimentary systems, interdependence exists between fluid flow, bed morphology, and sediment transport (Leeder, 1983). The topography of the channel bed influences the overlying flow field, while the interaction of the flow field with the labile bed gives rise to bedforms by means of sediment transport, resulting in a large-scale coupling that has been considered in the literature as far back as Sorby (1852, 1908), who related bedforms to states of flow, and textures and sedimentary structures to bedforms (Allen, 1963).

The channel topography in an estuarine environment reflects the bidirectional nature of fluid flow resulting from the interaction of fluvial discharge and tidal flux. In sand-bedded channels, as are typically found in estuaries, the most common bedforms are dunes (Venditti, 2013). Geometric properties of a dune, such as height (*H*), length (*L*), aspect ratio (*H/L*) and stoss and lee slope angles (θ_{Stoss}, θ_{Lee}, respectively), are functions of this flow interaction and the nature of dune growth, diminution, and migration through erosion and deposition of sediment under variable flows is associated with sediment transport.

Dune size has been linked to boundary layer thickness (Allen, 1963; 1968; Ashley, 1990; Southard and Boguchwal, 1990), which, in rivers, is limited by depth of flow (*h*), (Allen, 1982). Empirical correlations have been produced to show that an increase in depth generates an increase in dune dimensions (e.g. Van Rijn, 1984). Empirically, relative dune height (*H/h*) has been found to range between 1/40 and 1/2.5, and the relative wavelength of a dune (*L/h*) has also been found to be between 1 and 16 (Allen, 1982; Venditti, 2013). These ratios translate to typical ranges of order 10^0 to 10^1 m in height and order 10^0 to 10^2 m in length.

Dunes may be categorized based on cross-sectional morphology as either angle-of-repose asymmetric or low-angle symmetric (LADs) (Kostaschuk and Villard, 1996; 1999; Best and Kostaschuk, 2002). Angle-of-repose dunes display gently sloping stoss-sides with angles averaging between 2° and 6° and steep slope lee angles greater than 30°. Low-angle dunes are roughly sinusoidal in profile and may have slopes of up to 30°, but have frequently been found to measure less than 10° (*cf*. Smith and McLean, 1977; Kostaschuk and Villard, 1996; Roden, 1998; Parsons et al., 2005; Bradley et al., 2013).

Much research has been devoted to the study of flow over two-dimensional asymmetric dunes both in the field (Venditti and Bauer, 2005) and laboratory (e.g. Wiberg and Nelson, 1992; Lyn, 1993; Nelson et al., 1993; McLean et al., 1994; Bennett and Best, 1995; Venditti and Bennett, 2000; Fernandez et al., 2006; Coleman et al., 2006; Paarlberg et al., 2007). Flow over an asymmetric dune converges and accelerates as it moves up the stoss side of the dune and separates at the dune crest into a turbulent wake region which propagates downstream. An internal boundary layer that expands vertically with distance downstream extends from the flow reattachment point to

the next dune crest. The anti-phase oscillation of the water surface shows that the entire flow is affected by the dune, although the outer layer is only weakly connected to the near-bed structure, punctuated by large-scale macro-turbulent eddies generated at the bed and rising to the water surface (Venditti, 2013).

Investigations into flow over low-angle symmetric dunes have demonstrated that, in contrast to flow over asymmetric dunes, flow separation downstream of the crest is intermittent, or even non-existent (Kostaschuk and Ilersich, 1995; Kostaschuk and Villard, 1996; 1999; ten Brinke et al., 1999; Bradley et al., 2013), and is characterized by a zone of convergent accelerating flow up the stoss slope and a zone of divergent deceleration down the lee slope owing to topographic forcing (Best and Kostaschuk, 2002). Since the forces associated with fluid flow are responsible for sediment entrainment, movement, and deposition, it follows that the presence or lack of permanent flow separation downstream of a dune crest would have an influence on patterns of sediment erosion and deposition. It has been suggested through flume experiments (McLean et al., 1994; Bennett and Best, 1995; Best and Kostaschuk, 2002) and in the field (Kostaschuk, 2000) that increased turbulence produced by flow separation in the trough can encourage sediment scour. All other things equal, this would lead to a higher and steeper dune as the vertical distance between a dune's trough and crest is increased (Kostaschuk and Best, 2005). Dunes with and without flow separation would experience similar topographic forcing over the stoss, however, where flow separation is absent, flow over the downstream slope would decelerate, favouring sediment deposition and ultimately decreasing dune height and lee slope angle (Smith and McLean, 1977; Kostaschuk and Villard, 1996).

Transport stage exerts an important control on dune shape: field studies (Smith and McLean, 1977; Soulsby et al., 1991), lab experiments (Johns et al., 1990) and theoretical analysis (Kostaschuk and Best, 2005) have suggested that where suspended sediment transport dominates, dunes are low-angle symmetric and where bedload transport is dominant, dunes have been found to display the classic high-angle, asymmetric shape (Kostaschuk, 2006). Yalin's flume experiments (Yalin, 1972; Yalin and Karahan, 1976) showed that *H/L* increases with transport stage from bedload-dominated through the mixed load regime, and then declines as the transport stage increases to suspended sediment domination.

Observations from tidally influenced rivers suggest that dune geometry responds to changes in flow on the diurnal (tidal flux), synoptic (storm events), and seasonal (annual hydrograph) scales and these responses display hysteretic behavior (e.g. Pretious and Blench, 1951; Allen, 1973; 1974; 1982; Terwindt and Bower, 1986; Gabel, 1993; Julien et al.,2002; Villard and Church, 2003; 2005; Kostaschuk and Best, 2005) whereby the change in heights and lengths lag the changes in flow. Height responds more directly to flow variability while length does not change as quickly (Allen, 1982).

While the geometry of bedforms in sand-bedded channels has been well-documented, much of the work has been limited in scope to single track surveys, small-scale flume investigations, or simplified modelling, leading to a lack of ability to apply findings over a larger physical scale through three-dimensional dune topography under variable flow. As a consequence, our ability to predict sand flux in estuarine environments remains poor.

The motivation for this project is to contribute to our understanding of the

sediment flux in large, sand-bedded, fluvially-dominated, tidal environments. This requires an understanding of bed topography and, in estuarine environments where dunes dominate the channel bed, cognizance of dune response to flow variability. Here, I examine the dynamics of bed geometry at the diurnal scale in the fluvially-dominated tidal Fraser Estuary. Measurements of dune heights, lengths, aspect ratios, and lee angles over the course of the falling and rising limbs of largest diurnal tidal flux within the spring-neap tidal cycle are presented, and morphological changes through time are quantified to identify any patterns in sediment deposition and erosion at the bed in order to address the following questions: (1) *How do bedform dimensions respond to variable flow associated with the diurnal scale tidal flux?* and (2) *What processes control the evolution of low angle dunes in an estuarine environment?*

1.2. Methods

1.2.1. Field Study Site

The Fraser Estuary is located on the southwest coast of British Columbia, where the Fraser River enters the Strait of Georgia. The Fraser River has a drainage area of 234,000 km^2, with a mean annual discharge of 3410 m^3s^{-1} measured at the Mission Gauging Station, located 74 km upstream of Sand Heads (from Water Survey of Canada data collected between 1969 and 1987, and reported in McLean et al., 1999). Peak flow and sediment discharge occur in mid- to late-spring, following seasonal snowmelt, with the mean annual flood measuring 9790 m^3s^{-1} (McLean et al., 1999). Sediment discharge at the mouth of the Main Arm of the Fraser River is 17 million tonnes per year, 4.25 million of which is sandy bed material load (McLean et al., 1999).

The predominantly single-channelled Fraser River begins to bifurcate in the estuary, where the single channel splits into the North and Main Arms. Farther downstream the North Arm splits, giving rise to the Middle Arm, and the Main Arm splits to give rise to Canoe Pass. The Main Arm accommodates the majority of river discharge, approximately 70% at peak annual flow (Western Canada Hydraulic Laboratories Ltd., 1977).

The tidal pattern in the Fraser Estuary is classified as mixed but mainly semi-diurnal, with the maximum tidal range of 5 m occurring during the spring tide (Kostaschuk et al, 1989). During periods of low river discharge, a salt-wedge enters the Main Arm (Kostaschuk and Luternauer, 1989), with an upstream limit reaching as far as New Westminster (~25 km upstream of the river mouth) at low flows (Dashtgard et al., 2012) and Deas Island (~10 km upstream the river mouth) during mean annual discharge (Ages and Woollard, 1976).

In the Main Arm of the Fraser Estuary, dune heights are typically 1-2 m, and lengths are 20-50 m, although observations of dunes over 5 m high and 100 m long have been recorded (Pretious and Blench, 1951; Kostaschuk et al., 1989). Kostaschuk et al., (1989) found that heights and lengths changed seasonally in response to fluctuations in river discharge; they were relatively small in April and early May, growing large into June, then smaller dunes re-established with the decrease in sediment deposition through to September (see also Villard and Church, 2005). An annual dredging program is run typically from August through to March, which results in planing of the channel bed (Villard and Church, 2005). On a shorter time scale, dune geometry in the Fraser Estuary varies in response to tidal variation (Kostaschuk et al., 1989; Kostaschuk and Ilersich, 1995; Kostaschuk and Best, 2005).

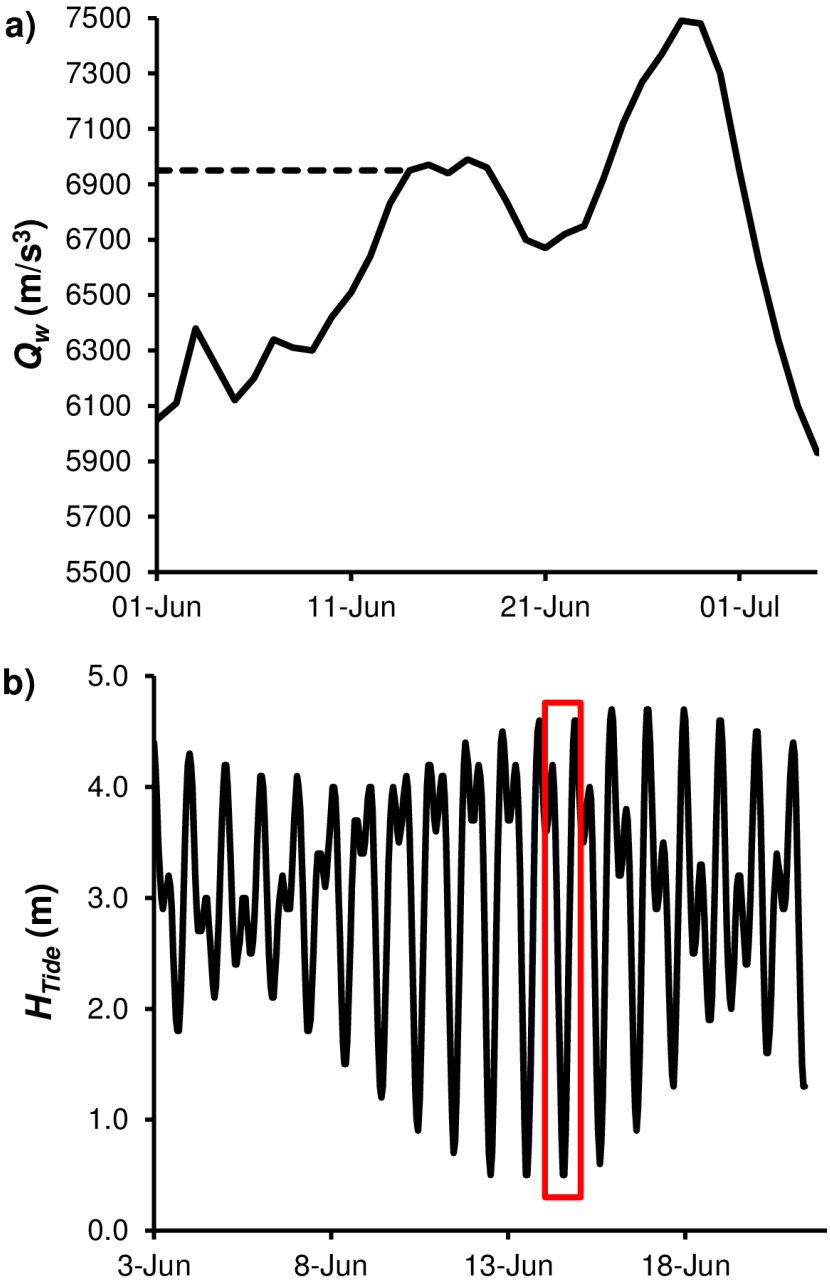

Figure 1.1. **a) Hydrograph for mean daily discharge in Fraser River at Mission for June 2010. The dashed line indicates the mean daily discharge calculated for 14 June 2010. b) Water level recorded at Steveston Gauging Station (08MH028) of the neap-spring tidal cycle during which data were collected (from Water Survey of Canada, 2011). The red box indicates the diurnal tidal cycle over which data for this project were collected.**

Observations were made on 14 June 2010, coinciding with the period of the largest tidal flux and elevated river discharge. Discharge is not recorded at Steveston, but a reasonable estimate of mean daily discharge can be obtained using the recorded mean daily discharge from the nearest station on the Fraser River (Mission Gauge Station, station number 08MH024). This yields a mean daily discharge of 6950 m^3s^{-1} for 14 June 2010 (Figure 1.1a), which preceded the peak daily mean discharge on 28 June 2010 of Q = 7490 m^3s^{-1} (Water Survey of Canada, 2011), one of the lowest annual peak flows on record. The actual value of the discharge measurement in Steveston will vary from this owing to the lag between the time of measurement in Mission and the travel time to Steveston. Tidal forcing may also affect the actual discharge at Steveston as high tidal water may hold and release river outflow. On June 14, the first high tide of the survey was 3.8 m, low tide was 0.40 m, and the second high tide was 4.3 m (Figure 1.1.b).

The study reach is located in the Main Arm of the Fraser River between Steveston and Westham Island, where the channel meets the Strait of Georgia. Data were collected along transects conducted over an area covering ~1 km in the stream-wise direction and ~0.5 km in the cross-stream direction (Figure 1.2).

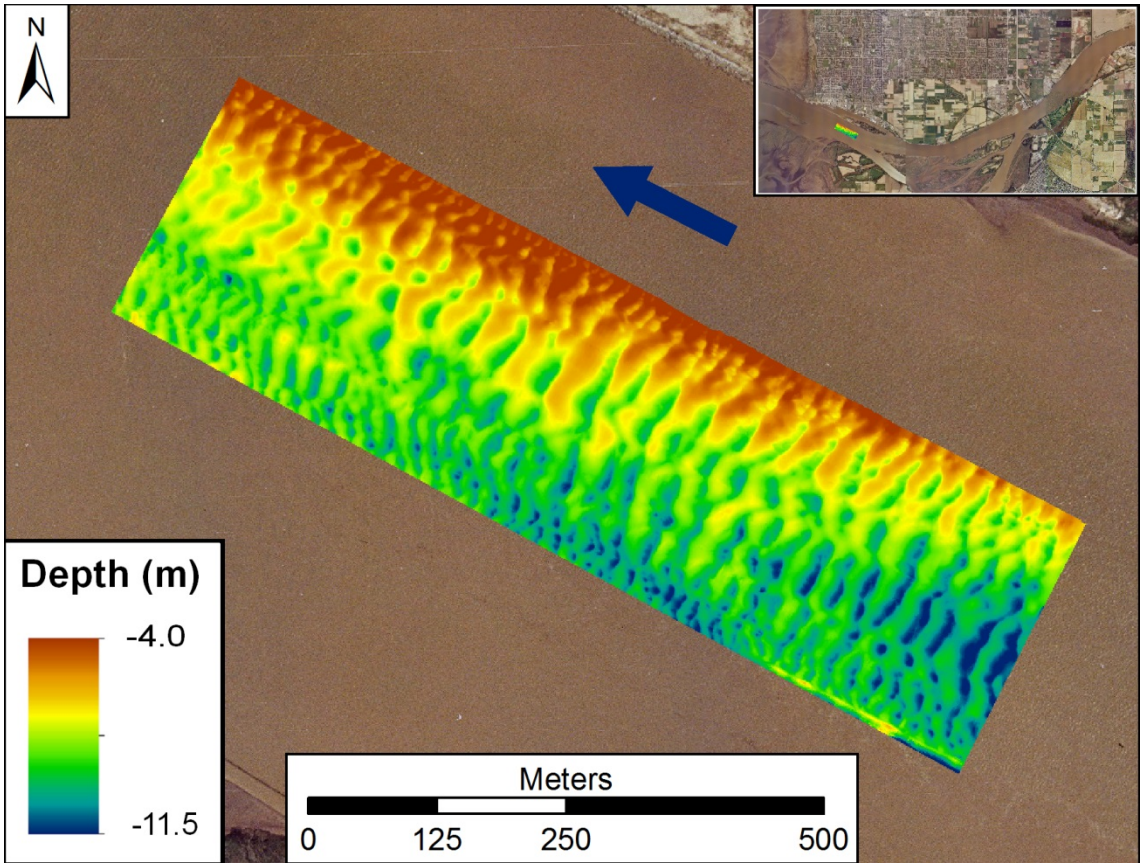

Figure 1.2. Bathymetric map of the study site. Blue arrow indicates direction of river flow. Inset shows the location of the study site within the Main Arm of the Fraser River.

1.2.2. Data Collection

Three-dimensional (3D) bathymetric data and 3D flow velocities were collected aboard the *R/V Lake Itasca* between June 12 and 17 2010 using a Reson 7101 Seabat Multibeam Echosounder (MBES) and a Teledyne RD Instruments 1200 kHz Rio Grande Workhorse acoustic Doppler current profiler (aDcp), respectively. The MBES is designed to measure relative water depth through the transmission of a wide swath of acoustic energy pulses and analysis of their reflections (Reson Inc., 2002). The sonar head emits 511 equiangular beam soundings per ping to cover a swath area of 150° (Reson Inc., 2009) with a vertical resolution of ~1.5 cm (Reson Inc., 2009).

Spatial positioning of the MBES was accomplished using a Trimble Real Time Kinematic Global Positioning System (RTK GPS) with a static base station that sent corrections to the rover head at 1 Hz. Positional accuracy of the GPS unit when running in RTK survey mode is +/- 0.01 m horizontally and +/- 0.02 m vertically. The position of the aDcp was recorded by a differential GPS (DGPS) system corrected by a Canadian Coast Guard beacon located ~1.7 km south of the study site. Positional accuracy of the DGPS is 0.25 m horizontally and 0.50 m vertically. Pitch, heave, and roll of the vessel were measured using an Applanix POS MV V3 gyroscope inertial guidance system. The system provides information to correct for the effects of horizontal and lateral vessel motion during survey operations.

Suspended sediment samples were collected on 17 June 2010. A U.S. Geological Survey P-63 point-integrated suspended sediment sampler was deployed at 0.1*h*, 0.2*h*, 0.4*h*, 0.6*h* and 0.8*h* over 40 s intervals to measure suspended sediment concentrations in the water column over the largest dune at Low Tide, Low Rising Tide, and High Rising Tide stages.

MBES measurements were collected over several tidal cycles to capture the changes in bed topography. Twenty-one surveys were conducted, each of which consisted of five parallel stream-wise traverses over the study area, and the resulting data were used to produce bed elevation maps. This study focusses on eight surveys taken over the tidal cycle occurring on 14 June 2010, chosen to correspond with the highest tidal fall of the cycle. Each survey is labelled according to its position on the tidal cycle as “High Falling Tide” (HFT), “Mid Falling Tide” (MFT), “Low Falling Tide” (LFT), “Low Tide” (LT), “Low Rising Tide” (LRT), “Mid Rising Tide” (MRT), “High Rising Tide” (HRT), and “High Tide” (HT) (refer to Figure A1).

1.2.3. Data Processing

Raw MBES data were imported into CARIS HIPS® software for post processing to correct for changes in tidal stage, pitch, heave, and sound velocity, and to remove false data points. The data were then imported into ArcGIS® and gridded at 1 m for further analysis of channel bed characteristics for each of the eight surveys. A correlation analysis was carried out on the cross-stream depth data to determine the topographic variability across the channel, and it was found that variability increased significantly at ~30 m intervals (Figure A2). In order to extract measurements from the topographic maps to calculate dune height, length, aspect ratio, and lee slope angle to represent the entire study area, 26 stream-wise transects were laid over the base maps, spaced at 10 m intervals, and points were placed at 1 m intervals along each of these lines and tagged with the position (easting and northing) and depth of bed below the water surface. These data were then used to identify local maxima (crests) and minima (troughs) as well as the lee slope angle. Height was measured as the vertical distance between each crest and associated trough, length was measured as the horizontal distance between successive troughs, and the lee slope angle (θ_{Lee}) was measured as the steepest portion of the downstream slope. The dune aspect ratio (H/L) was taken as the ratio of each individual dune's height to its length. The dune symmetry ratio (L_S/L) was calculated using the stoss side length divided by the total dune length such that a perfectly symmetrical dune has a ratio of 0.5. Successive topographic base maps were differenced to give the change in bed elevation between each survey, and qualitatively display patterns of deposition and erosion on the channel bed.

Depth-integrated suspended sediment concentrations ($\langle SSC \rangle$) were calculated along streamwise transects extending down the centre of the study site for each survey

by converting the echo intensity values recorded with the aDcp using the method of Topping et al. (2007). Mean and depth-averaged velocities were also calculated for each survey (for further details, see Bradley et al., 2013).

Frequency polygons were made to compare the distributions of dune heights, lengths, aspect ratios, and lee slope angles for each of the surveys. This was achieved by dividing each data set into equal-sized bins ranging from the lowest to highest values. Bins for dune height, length, aspect ratio, and lee slope angle were set at 0.1 m, 5 m, 0.005, and 5˚, respectively.

1.3. Results

1.3.1. Bed Topography

Bathymetric maps generated from the MBES data show a trend of decreasing elevation across the channel, with a lateral bar on the north side creating an area of higher elevation, and scour on the south side where a side channel re-enters Main Arm downstream of a series of small islands (Figure 1.2). The bed surface is covered in dunes, with the largest dunes occurring along the centre of the channel. These dunes display near-symmetric cross-sectional morphology, with a mean slope symmetry ratio (L_S/L) of 0.59, and range of 0.10 to 0.93 over the study period.

1.3.2. Dune Heights, Lengths, and Aspect Ratios

The overall distribution of dune heights and lengths appears to be pattern stable over the observed tidal cycle (Figure 1.3). Maps of height distributions for five surveys over the tidal cycle (Figure 1.3a) show that the highest dunes are consistently located in

the center of the study area, and in the upstream three-quarters of the length of the site. Maps of length distribution for the same five surveys (Figure 1.3b) show the longest dunes occur in the centre of the study area, with the dunes of maximum length corresponding to the area of the dunes with the greatest heights. Mean dune height for the entire bed, calculated for each survey over the tidal cycle, is 1.16 m, mean dune length is 25 m, and mean aspect ratio is 0.046.

Figure 1.4, panels a, b, and c, show the variation in mean dune height, length, and aspect ratio respectively, with standard error, over the tidal cycle. Overlap of error bars suggests some caution should be taken when interpreting the changes between certain survey times as this precludes confidence that any pattern of change with tidal fluctuation is explained outside the bounds of error.

No significant change in mean dune height values is observed between HFT and MFT (Figure 1.4a; Table 1) when river discharge is slowly increasing in strength as the tide ebbs. This corresponds to low <*SSC*> and <*u*>, but both are beginning to increase. At LFT, the highest <*SSC*> in the water column is recorded and <*u*> continues to increase until it reaches its peak recorded maximum of the tidal cycle at LT. *H* increases at LT, while <*SSC*> drops slightly from the previous survey time. A significant increase in *H* is observed at each survey time from LT to MRT and remains constant through to HRT. <*SSC*> drops over this time period, and <*u*> slows as the tidal influx imposes increasing opposition to river flow. At HT, *H* decreases as the tide reaches its maximum height, <*u*> falls to its lowest recorded value and <*SSC*> is also at its lowest concentration of the study period.

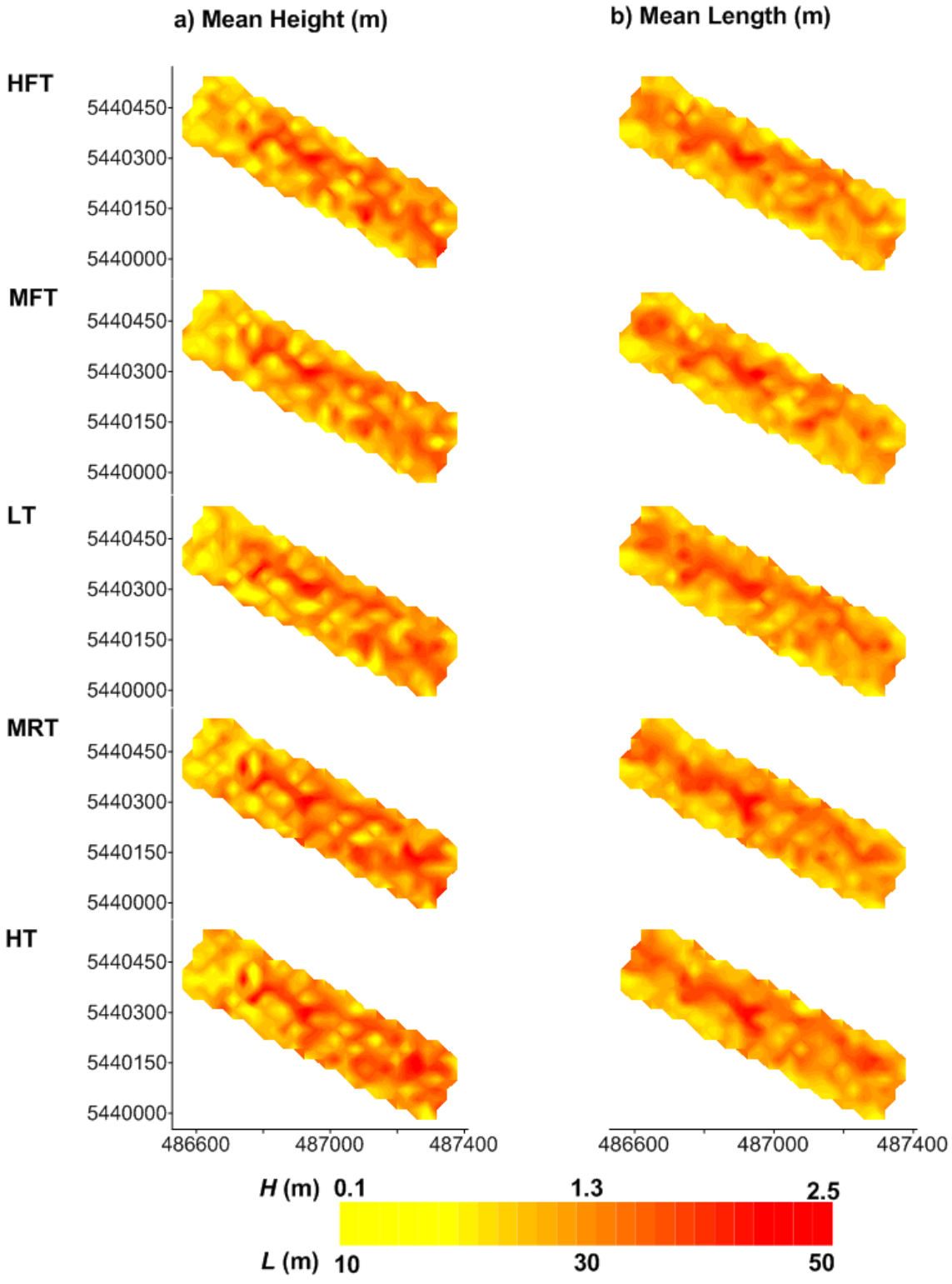

Figure 1.3. **Select spatial variability maps for distributions of dune height (left) and dune length (right). Flow is from bottom right to top left. Refer to Figures A3 to A8 for excluded maps.**

Table 1. **Mean, maximum, and minimum calculated values, as well as standard error for geometric properties for each survey time in the study period. For plots of maximum and minimum dune geometric properties, refer to Figure A9.**

	Position in Tidal Cycle	*H* (m)	*L* (m)	*H/L* (m/m)	Survey	*H* (m)	*L* (m)	*H/L* (m/m)
Mean	HFT	1.12	25	0.046	LRT	1.18	25	0.049
Maximum		2.67	62	0.096		2.65	57	0.136
Minimum		0.054	3	0.0040		0.025	5	0.0010
Standard error		0.50	9	0.016		0.54	10	0.021
Mean	MFT	1.12	25	0.044	MRT	1.21	26	0.047
Maximum		2.62	64	0.105		2.67	58	0.112
Minimum		0.040	5	0.0007		0.033	6	0.0023
Standard error		0.52	9	0.018		0.57	10	0.017
Mean	LFT	1.09	24	0.046	HRT	1.23	26	0.048
Maximum		2.82	64	0.129		2.69	60	0.104
Minimum		0.072	5	0.0034		0.073	6	0.0028
Standard error		0.51	10	0.017		0.57	10	0.017
Mean	LT	1.12	26	0.044	HT	1.18	26	0.046
Maximum		2.83	56	0.096		2.73	56	0.095
Minimum		0.059	4	0.0044		0.059	6	0.0027
Standard error		0.53	9	0.016		0.56	10	0.017

Over the course of the tidal cycle, *H* and maximum dune height display an overall increase, (Table 1, Figure A9). Maximum dune height fluctuates in a similar pattern to the mean over the survey period, although the largest dune size increases from HFT to MFT. Minimum dune height data (Table 1, Figure A9) does not show a pattern of increase over the course of the data collection, but does display a slight decrease toward low tide, and a large spike at HRT, followed by a return to a minimum height value more similar to those at previous survey times.

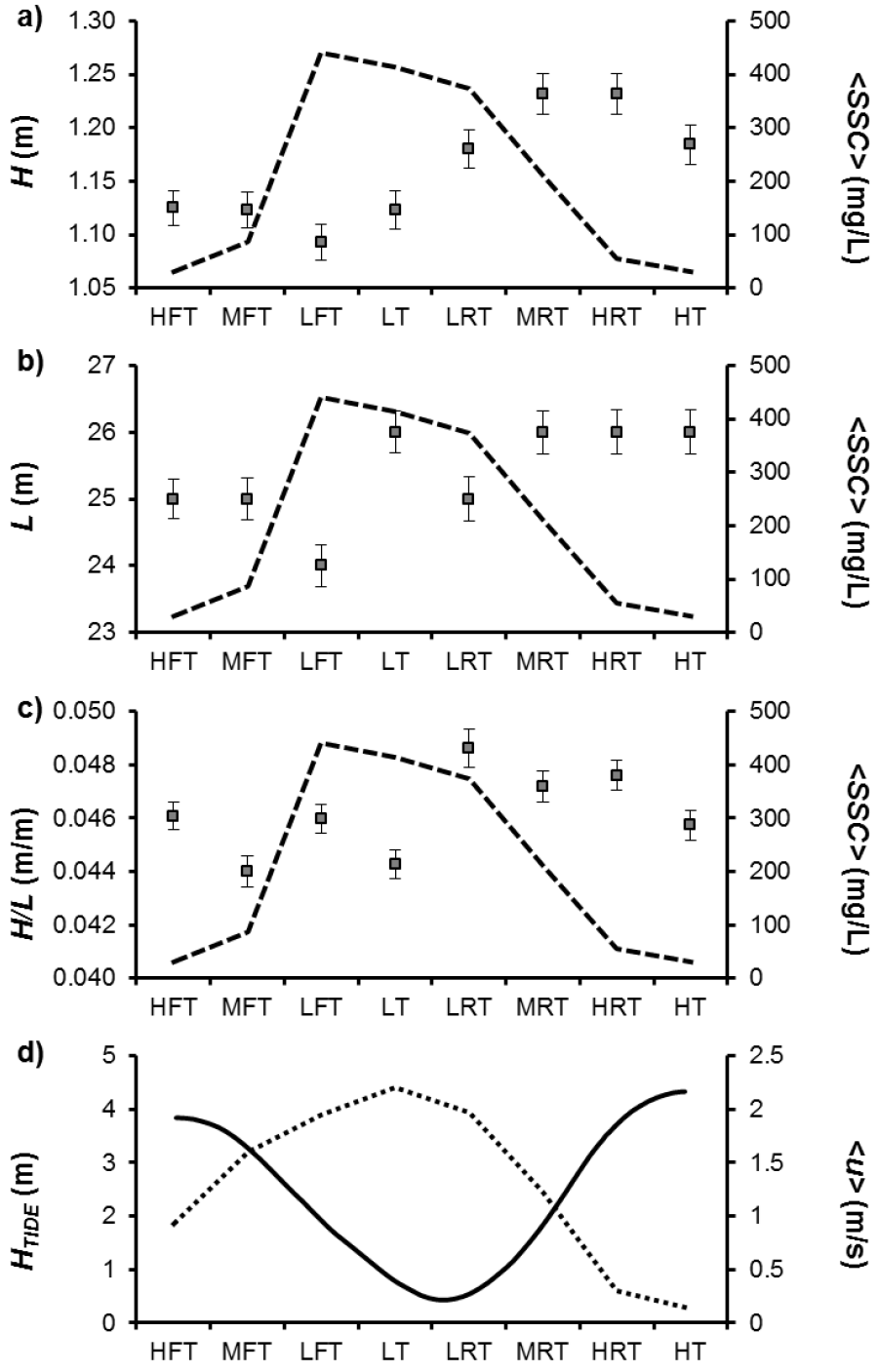

Figure 1.4. **Mean geometric properties over the study period. a) Mean dune height; b) mean dune length; c) mean dune aspect ratio. The dashed line in a, b, and c, denotes suspended sediment concentration. Error bars denote standard error of the mean. d) Tidal stage (solid line) and mean depth-integrated velocity (dashed line).**

Similar to *H*, *L* (Figure 1.4a and b; Table 1) shows a net increase over the course of the tidal cycle, however it does not appear to respond to the diurnal scale flow variability. A general pattern of decrease occurs from HFT to LFT, then increase toward HT. Error bar overlap between HFT and MFT and between MRT, HRT, and HT suggests that no significant change is occurring during those times. The difference in *L* from the beginning of the tidal cycle to the end is a modest 1 m increase. Maximum *L* (Table 1, Figure A9) increases from HFT to LFT, then drops at LT, followed by a steady increase toward HRT, and falling to the lowest measured length at HT. Minimum *L* values (Table 1, Figure A9) increase from HFT to MFT, then fall at LT, followed by an increase at MRT then retain a steady length through HT. Both maximum and minimum lengths measured over the tidal cycle show a net increase from HFT to HT.

The combination of overall increase of *H* and *L*, and the lagged cyclic response of *H* to flow variability results in a pattern of *H/L* over the tidal cycle that is distinct from those of *H* and *L*. (Figure 1.4c; Table 1). *H/L* values fluctuate between 0.044 and 0.046 between HFT and LT, but then increase to maximum observed mean value of 0.049 at LRT, as the tidal height begins to rise followed by a decreases toward HT.

The frequency polygons for *H*, *L*, and *H/L* (Figure 1.5, panels a, b, and c, respectively) show that the distributions of each geometric property retains the same general pattern over the tidal cycle. The frequency polygon distribution for height and length (Figure 1.5, panels a and b) shows a unimodal distribution, with positive skew (refer to Table A1 for skewness values). The frequency polygon for length (Figure 1.5b) also shows a unimodal distribution with positive skew.The frequency polygon for aspect ratio (Figure 1.5c) shows a curve closer to a normal distribution than those for height or length, with fluctuating skewness, where values are negative at MFT, MRT, and HT.

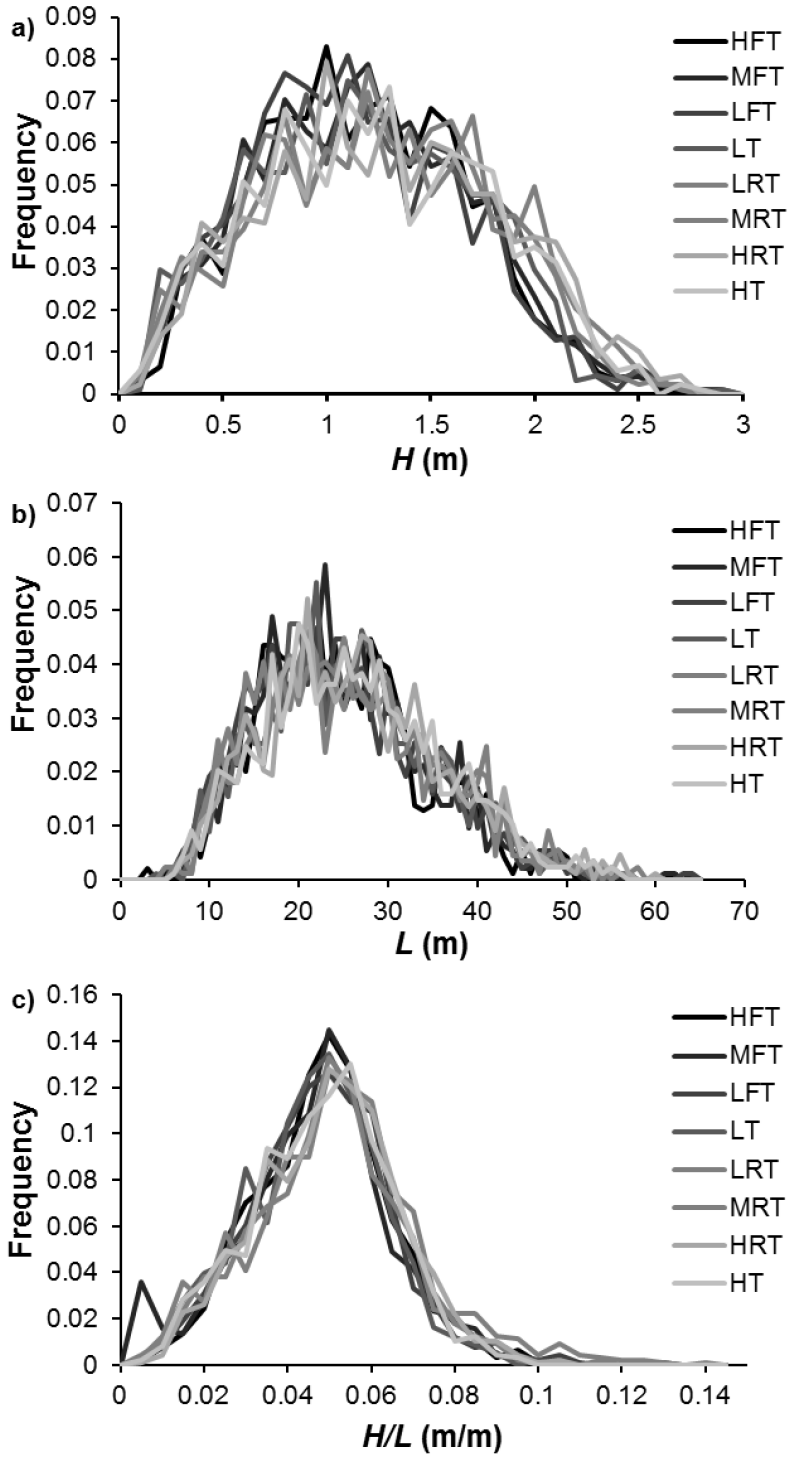

Figure 1.5. **Frequency polygons showing the distributions of geometric properties. a) Mean dune height, using 0.1 m bins; b) mean dune length, using 5 m bins; and c) mean dune aspect ratio, using bins with an interval of 0.005.**

1.3.3. Lee Slope Angles

Maps of the distribution of θ_{Lee} for 5 select surveys over the tidal cycle (Figure 1.6) show a pattern of overall decrease in angle from HFT to LT, followed by an increase from LT to HT. The steepest angles are found in the upper three-quarters of the study site, and the changes in θ_{Lee} are most pronounced in this region. Measured θ_{Lee} for the entire bed over the tidal cycle is 16.3°, indicating that the dunes in the study area are predominantly low angle symmetric. The highest measured angle is 44.1°, and the lowest is 0.5°.

The change in θ_{Lee} from HFT to MFT is insignificant based on error bar overlap, but there is a decrease toward LT (Figure 1.7; Table 1), coincident with the fastest <*u*> and second highest <*SSC*> measured during the tidal cycle. As the tide rises, the mean angle increases toward the highest recorded value at MRT, then drops slightly through to HT. Maximum angles follow a similar pattern to that of θ_{Lee}, but show a larger fluctuation (Table 1, Figure A9), with a decrease from HFT to LT, then an increase to the highest maximum value at MRT, followed by a decrease toward HT. The minimum angles for each survey period also follow a similar pattern (Table 1, Figure A9), though the magnitude of the fluctuations are on the order of 0.1°.

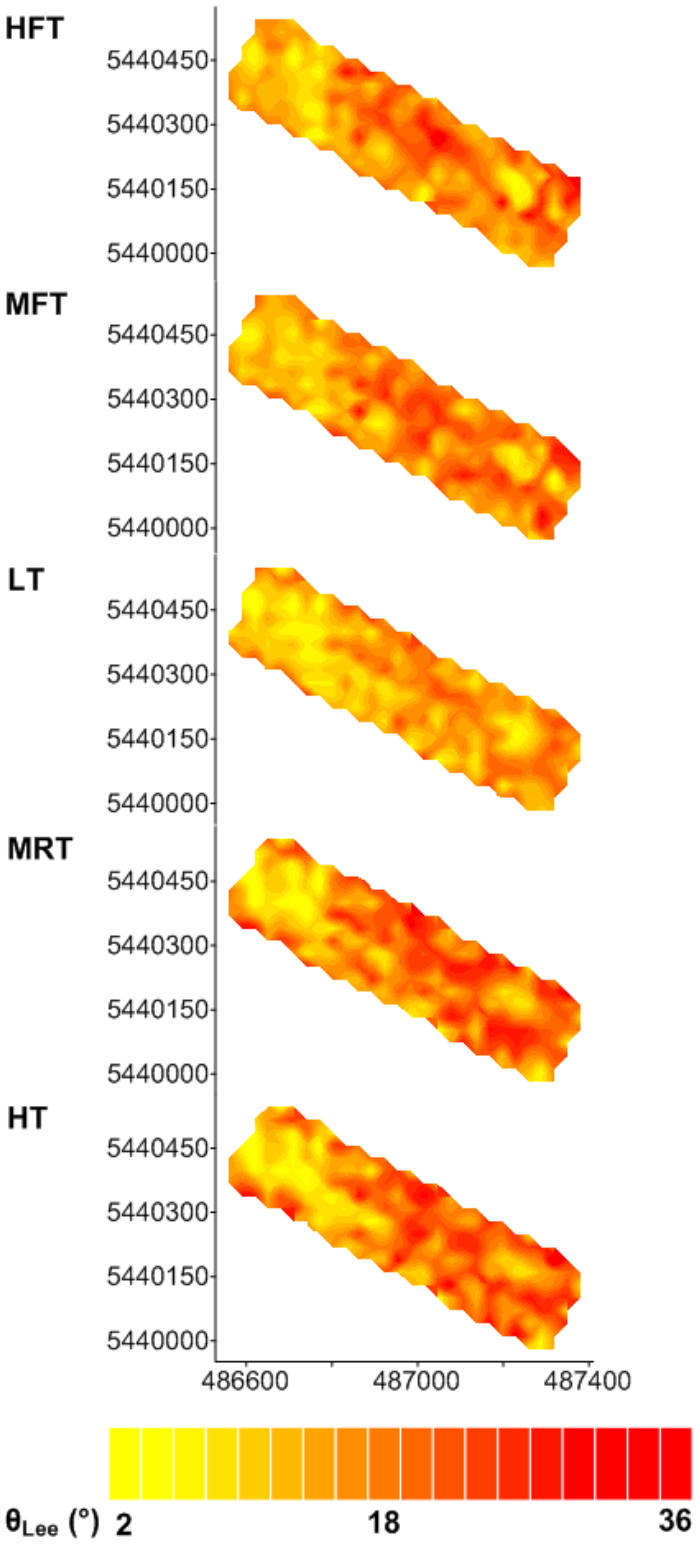

Figure 1.6. **Select spatial variability maps for distribution of lee slope angles (θ_{Lee}). River flow is from bottom right to top left. Figure A10 through A12 show the excluded spatial variability maps.**

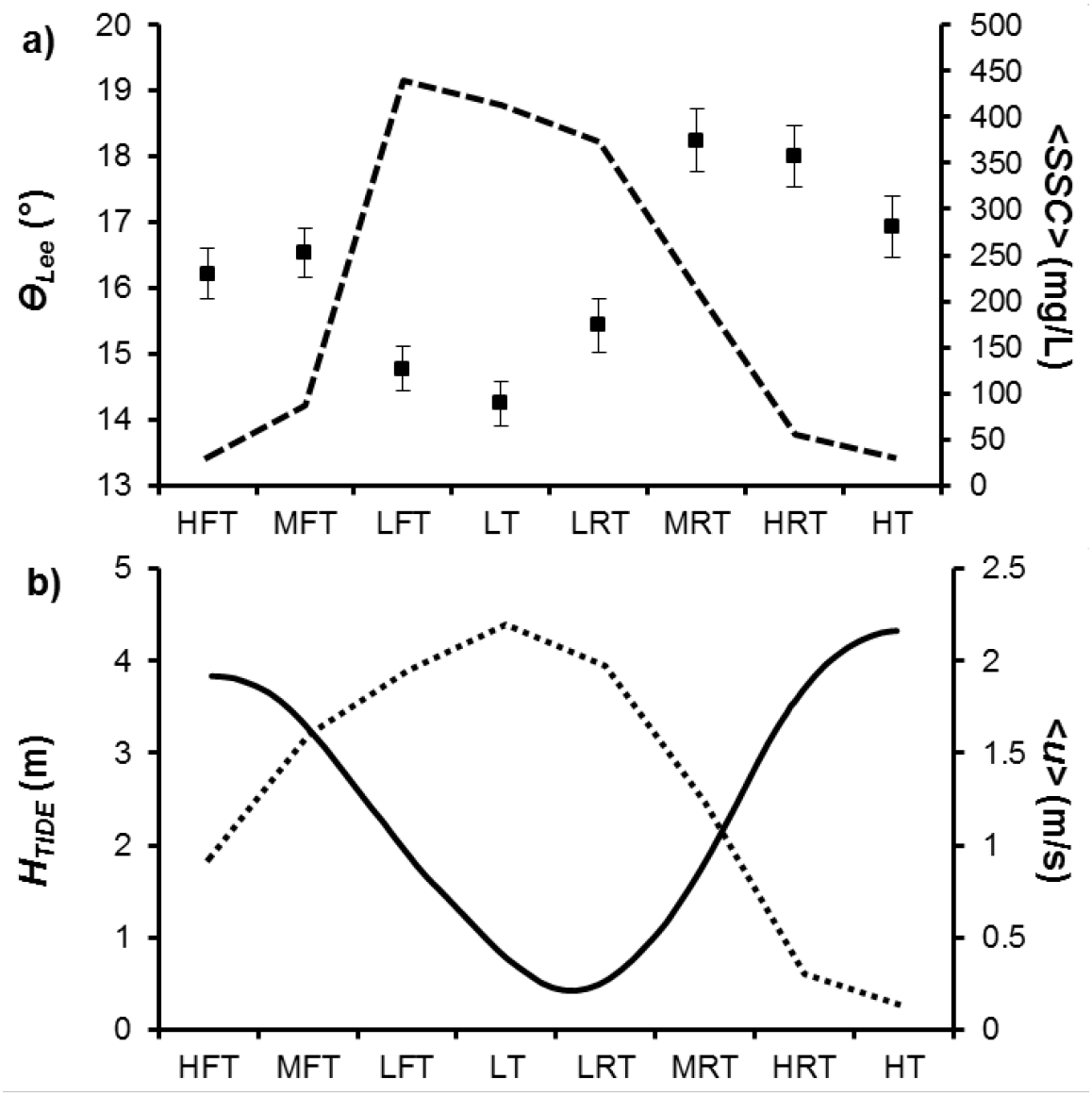

Figure 1.7. **a) Mean dune lee slope angle values over the tidal cycle. Dashed line denotes depth-integrated suspended sediment concentration. Error bars denote standard error of the mean. b) Tidal stage (solid line) and mean depth-integrated velocity (dashed line).**

The frequency polygon for θ_{Lee} (Figure 1.8) shows a unimodal distribution pattern with positive skewness that remains relatively stable over the survey period. Skewness values decrease from HFT to MRT, and then increase toward HT (see Table A1 for values). The frequency of $\theta_{Lee} > 30^{o}$, the putative threshold between high and low angle dunes, increases from about 5% at LT to nearly 25% at HT.

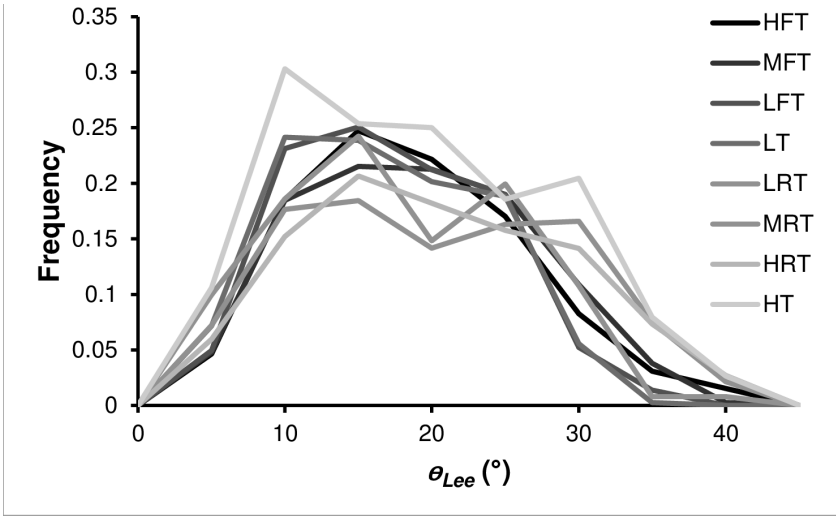

Figure 1.8. Frequency polygon showing the distribution of mean lee slope angle measurements over the tidal cycle. Bins were set at 5˚.

1.3.4. Relation between *H*, *L*, *H/L*, and θ_{Lee}

Mean values of dune geometry for each of the eight tidal stages were plotted and subjected to the Spearman Rank test as well as a test of significance to determine correlation (Figure 1.9 a, c, e, g). Mean dune height plotted against mean lee angle and length, respectively, yielded significant positive correlations, with high Spearman rank coefficients (r_s) and *P* values below the α=0.05 significance level. The correlations between mean lee slope angle and mean length as well as aspect ratio were low, and *P* values above the α=0.05 level, indicating that there is no significant relation between these geometric properties. The strong positive correlation between θ_{Lee} and *H* (Figure 1.9a) and *H* and *L* (Figure 1.9d), but not between θ_{Lee} *and L* (Figure 1.9b) indicates that the features are not self-similar. Plots of the individual data points of the geometric properties (Figure 1.9 b, d, f, h) show more scatter about the mean for θ_{Lee} against *L* and *H/L,* than against *H* or compared to *H* against *L.*

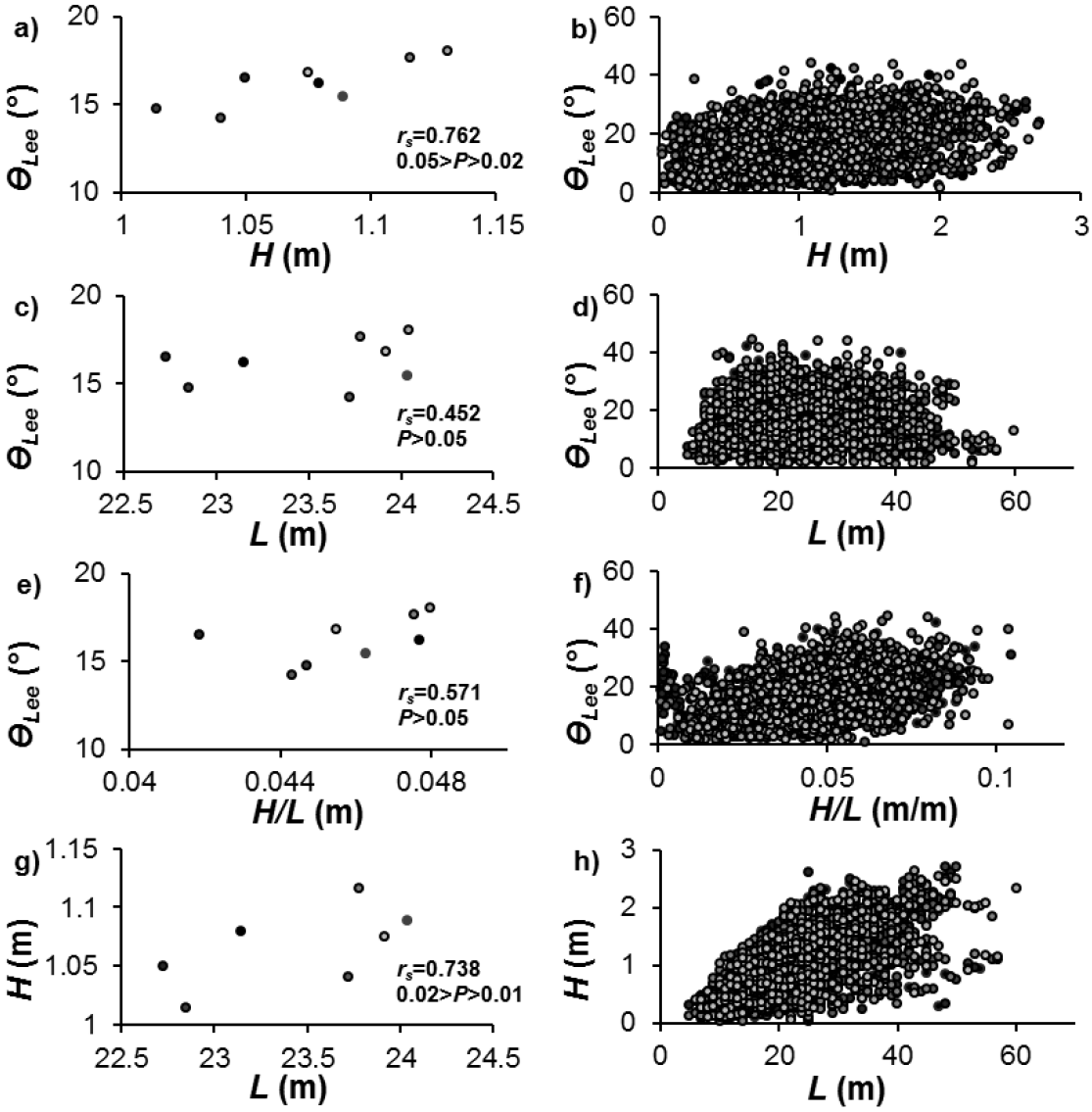

Figure 1.9. Mean dune lee slope angle at each of the eight tidal stages plotted against a) mean dune height, b) mean dune length, and c) mean dune aspect ratio; d) mean dune height against mean dune length.

1.4. Discussion

The majority of the dunes observed in this study are classified as symmetric, consistent with previous findings in the Fraser Estuary (Kostaschuk and Villard, 1996, 1999; Kostaschuk and Best, 2005; Kostaschuk et al., 2009; Bradley et al., 2013) and in other estuarine environments where suspended sediment transport dominates and flow

separation over such dunes is largely absent (e.g. Smith and McLean, 1977; Soulsby et al., 1991). Kostaschuk and Villard (1996) found that near-bed velocities of unstratified, non-separated flow over symmetric dunes (such as those observed here around low tide when river discharge is at its strongest) converged and accelerated over the stoss slope and diverged and decelerated down the lee slope (results further supported by Gabel, 1993), while suspended sediment concentration and transport rates increased up the stoss and decreased down the lee, likely a consequence of preferential erosion on the stoss and deposition in the lee (Kostaschuk and Villard, 1999).

Gabel (1993) found that histograms of dune heights and lengths were unimodal or bimodal with positive skew to symmetrical distributions at low flows, and retained this shape under high flows, but with a shift to higher values and more variance, similar to Allen's (1976) models. Histograms of data from the present study conform to the shape of the distribution seen in the above studies, but show no discernible pattern of change with changing flow.

1.4.1. How do dune dimensions respond to tidal scale variable flow?

The results of the present study show that significant change in mean dune height, length, and aspect ratio occurred over the study period. Height decreased slightly with increasing velocity toward low tide, and then increased with declining velocity toward the highest tidal stage, concurrent with observations of Kostaschuk and Best (2005). A relatively large increase in mean length occurs between LFT and LT, and is associated with a period of dune 'death', when smaller dunes in the more heavily bifurcated channel sides are combining (see Chapter 2), resulting in an overall increase

in longer dunes. The pattern of change in height suggests that the response to variability in flow is more direct than that of length. This result is in agreement with previous findings that suggest this occurs owing to the large volume of sediment that must be deposited or eroded in order to increase or decrease length compared to height (Allen and Friend, 1976; Terwindt and Brouwer, 1986; Rhodes, 1992; Gabel, 1993). Height and length both show a general pattern of increase throughout the cycle, suggesting they are adjusting in response to a longer term velocity change. In addition, given that the growth or reduction in length is facilitated by sediment transport, an increase in the length of a dune would therefore be paired with a decrease in the length of another (Dalrymple and Rhodes, 1995) without significant sediment input from upstream or dune amalgamation. The data for the present study were collected on the rising limb of the hydrograph, two weeks prior to peak discharge, and it is highly feasible that lengths are responding to changes in flow of this scale although the temporal limitation of this study precludes the ability to prove this.

Since the change in height is responding more directly to flow variability than the change in length, the change in the dune aspect ratio would be expected to most closely follow the pattern of change of dune height. However, the observations presented here indicate that dune aspect ratio fluctuates throughout the tidal cycle with a general decrease toward LRT and increase thereafter toward HT.

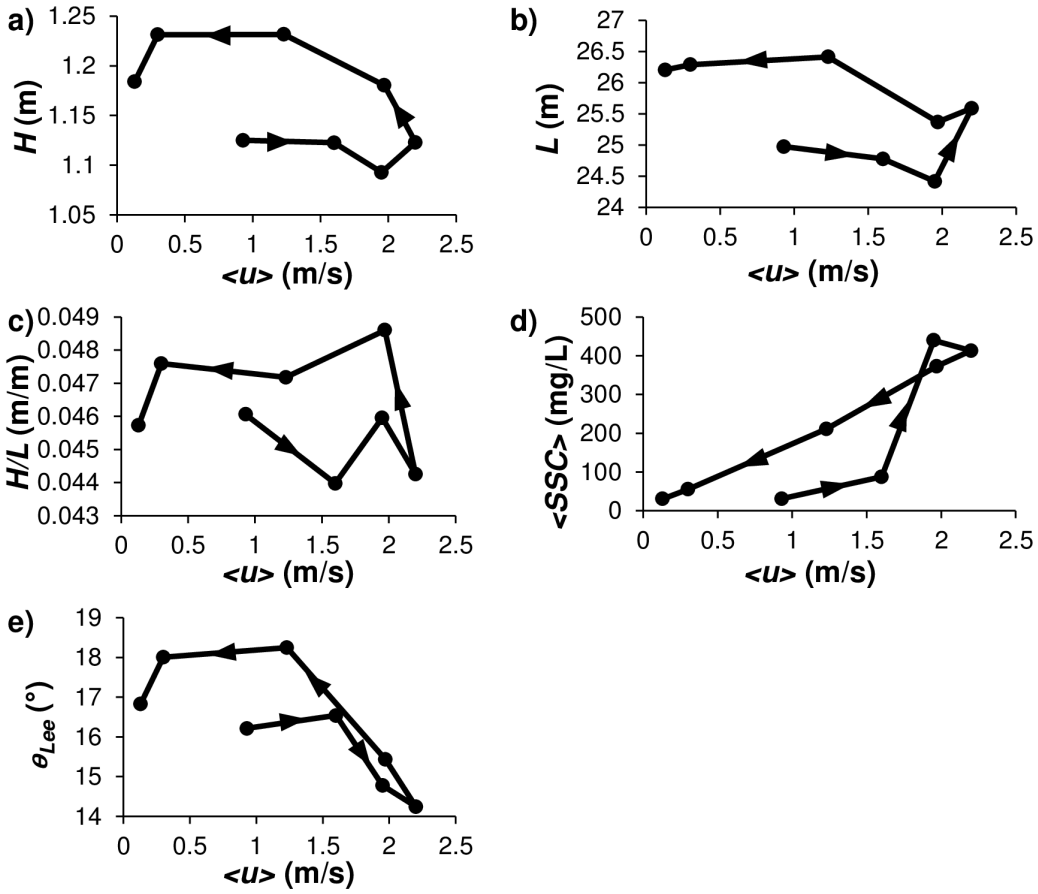

Figure 1.10. Plots of geometric properties (a,b,c,e) and suspended sediment concentration (d) against mean depth-integrated velocity. Arrows indicate direction of loop.

When plotted as functions of flow velocity, mean *H*, *L*, *H/L*, θ_{Lee}, and <*SSC*> show counterclockwise hysteretic trajectories for all variables (Figure 1.10), indicating that the response of the mean geometry lags diurnal scale flow fluctuations. Numerous studies have examined the lag between flow and dune size on a variety of time scales: the diurnal tidal scale (e.g. Kostaschuk and Best, 2005); the bi-monthly neap-spring lunar scale (e.g. Allen et al., 1969; Allen and Friend, 1976; Terwindt and Brouwer, 1986; Davis and Flemming, 1991; Rhodes, 1992) and the seasonal freshet scale (e.g. Villard and Church, 2005), and have shown that flow-driven changes in dune properties generally lag changes in flow. This lag occurs because the relation between fluid flow,

dune morphology, and sediment transport tends toward equilibrium, and as flow changes, the dune adjusts its shape to the new equilibrium through the movement of sediment (Allen, 1982). This adjustment requires that a certain volume of sediment be moved, the magnitude of which is dependent on the size of the dune, and the movement of this sediment requires time to adjust (Dalrymple and Rhodes, 1995). Wider, more rounded hysteretic loops suggest a greater lag time than tighter, more rectilinear ones. Theoretical analysis (Dalrymple and Rhodes, 1995), empirical studies (Gabel, 1993; Julien et al., 2002; Kostaschuk et al., 1989, Kostaschuk and Ilersich, 1995; Wilbers, 2004; Wilbers and ten Brinke, 2003) and this current study have shown that change in mean height and length lags change in velocity. Similar relations are reported for changes in lee angle values, although diagrams presented in Kostaschuk and Best (2005) show clockwise hysteretic loops for height and aspect ratio. That height adjusts more directly to changes in velocity could allow for greater variability of response (Dalrymple and Rhodes, 1995), and this could explain the height result of Kostaschuk and Best (2005). Although, it is equally possible that their data reflects sampling bias: their data were collected by taking multiple surveys of a single transect line in the middle of the channel. Data collected along a single transect line would require a very high degree of locational precision, and since dune height has been shown to be highly variable along the crestline of a dune (Allen, 1982; Parsons et al., 2005) any deviation from the original transect could introduce false variability.

Though analysis and comparison of hysteresis diagrams between studies has indicated relatively consistent patterns in the response of dune geometry to changes in flow, it is important to note that caution should be taken in comparing the results of different studies. Firstly, in comparing studies of differing time scales (diurnal against

lunar against synoptic against seasonal), the magnitude of change in regimes involved, most notably flow and depth, are not necessarily consistent between the different time scales. When considering the diurnal scale, changes in flow are relatively large, whereas depth variability is small; on the synoptic scale, both regimes can be considered medium to large in magnitude, and seasonal changes would typically see large fluctuations in both flow and depth. To compare diurnal to seasonal scale bedform response to flow variability then becomes suspect with respect to compatibility given the differing regimes. Furthermore, Dalrymple and Rhodes (1995) identify the issue of the time intervals over which data were collected being wider than the scale they are meant to represent, leading to inconsistencies between results. The strength of this study lies in the quality of the bathymetric data and results gleaned from one tidal cycle to infer diurnal flux and response.

1.4.2. What controls the evolution of low angle dunes over a semi-diurnal tidal cycle?

There are at least three hypotheses for the low leeface angles of LADs in equilibrium, two of which relate to bedload-dominated dunes and the third to environments where bed-material transport is primarily in suspension. Carling et al. (2000) proposed a model of dune form evolution based on observations in the Rhine River. They hypothesize that the occurrence of low-angle lee sides on coarse-grained large dunes is controlled by secondary dunes on the stoss sides which limit the sediment supply to the crestal region, resulting in degradation of the lee side. Sukhodolov et al. (2006) examined dunes in the shallow (depth = 0.35 m), sand-bedded Embarrass River and found leeface angles of 12° or less. They suggest that these LADs are due to low stoss-side bedload transport conditions that reduce the rate of delivery of material to the

bedform crest, resulting in more rounded crests and gentle lee slopes. However, these explanations are not applicable to the majority of LADs that are found in large, deep, sand-bedded, lowland rivers and estuaries such as the Columbia River (Smith and McLean, 1977), Fraser River (Kostaschuk et al., 2004), Mississippi River (Nittrouer et al, 2008), Rio Paraná (Shugar et al., 2010) and Jamuna River (Roden, 1998) where most bed-material is transported in suspension.

Several numerical, laboratory and field studies have demonstrated the importance of the transport and deposition of suspended bed-material in dune dynamics and morphology in sand-bed flumes, rivers and estuaries. Numerical simulations and field measurements over estuarine dunes conducted by Johns et al. (1990) demonstrated that a combination of high flow velocity and fine sand bed-material resulted in a lowering of the dune crest and filling of the trough by deposition from suspension. Flume experiments by Hand and Bartberger (1988), Saunderson and Lockett (1983) and Bridge and Best (1988) demonstrated that high flow velocities result in a relatively uniform sediment concentration profile with height above the bed, giving rise to a more rounded dune crest and a more symmetrical dune long profile. Field measurements performed by Smith and McLean (1977), Kostaschuk and Villard (1996), Kostaschuk (2000) and Kostaschuk et al. (2009) suggest that increased sand transport in suspension, relative to bedload, was associated with flatter dunes and lower leeface angles. Amsler and Schreider (1999) used simulated values of the ratio of suspended bed-material load (q_s): bedload (q_b) to show that higher q_s/q_b ratios were associated with a diminishment of dune height during floods in the Rio Paraná, Argentina. Kostaschuk (2006) conducted an empirical examination of several large rivers and concluded that deposition of suspended sediment in the trough and on the dune lee side acts to reduce dune height and lower the lee slope angle. Kostaschuk et al. (2009) used

field measurements over a dune in the Rio Paraná to show that about 17% of the suspended bed-material transported over the crest is deposited on the 22^{o} leeface before it reaches the trough. Kostaschuk et al. (2009) also used the results of Kostaschuk and Villard (1996) from the Fraser River and found that the percentage of sand deposited between the crest and trough over dunes in Fraser River ranged from 25-56% and the corresponding leefaces were 8-19°, with the higher deposition rates associated with lower lee slope angles.

Sediment transport, along the bed or in suspension, is what controls the geometry of dunes, and the patterns of ebb and flow of the tidal heights should result in predictable patterns of sediment movement via erosion and deposition which can explain the trend in height change over the tidal cycle. The patterns of deposition and erosion of the bed as a result of differencing the bed topography between survey times (Figure 1.11) provides qualitative support to the geometric changes observed, and serves to link this study to previous work.

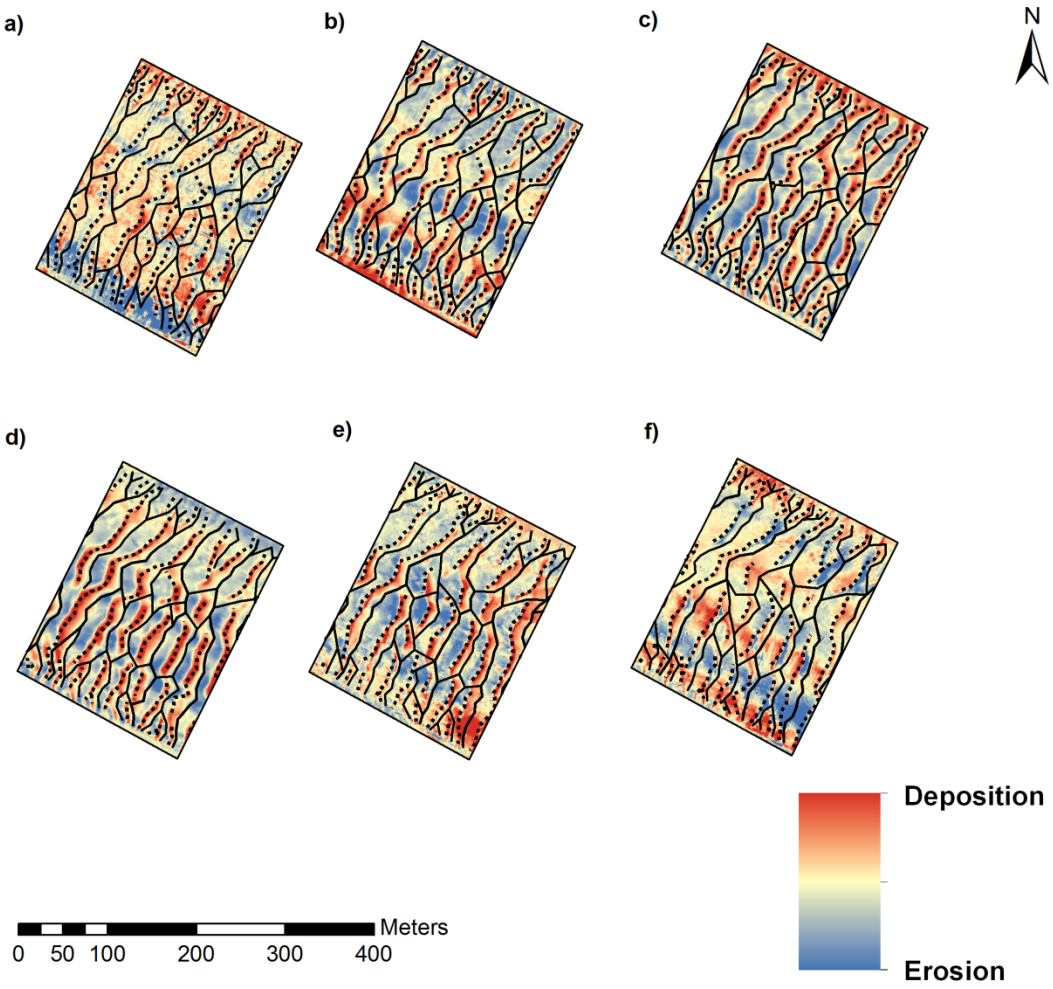

Figure 1.11. Difference maps between surveys over the tidal cycle. a) HFT to MFT, b) MFT to LFT, c) LFT to LT, d) LT to LRT, e) LRT to MRT, f) MRT to HT. Solid lines indicate crestlines while dotted lines are the troughlines. For full map that span the entire study site, refer to Figures A23 to A29.

The change in bed topography between HFT and MFT (Figure 1.11a) is minimal relative to the other time sequences; the map shows isolated patches of deposition and erosion mostly occurring in the lower lee slope, and patches of erosion, most notably on the south side of the channel. This is reflected in the mean dune height, length, and lee angle values calculated for HFT and MFT, none of which show significant change from the first survey time to the next. The difference in topography between MFT and LFT

(Figure 1.11b) displays a more discernible pattern of deposition and erosion: erosion is occurring predominantly on the stoss slope, along the crest, and along the uppermost lee portion of the majority of the dunes in the study site, while deposition is occurring in the lowermost lee and downstream trough. This pattern favours a decrease in dune height and lee angle since dunes would be lowering through crestal erosion and infilling of troughs, promoting further reduction in height and slope angle. Indeed, the mean heights and lee angles decrease from MFT to LFT.

From LFT to LT (Figure 1.11c) the area around the trough over which deposition is occurring is increasing, extending farther up the lee slope. Erosion is still occurring over the stoss slope, along the crestline and upper lee slope. This pattern would again favour a decrease in height and more so lee angle, since deposition is occurring farther up the lee, and less erosion is occurring at the crest. Interestingly, neither mean height nor lee angle change significantly between LFT and LT, and yet, length shows an increase, likely owing to dune amalgamation at the channel sides. Between LT and LRT, erosion ceases in the uppermost lee area, is limited at the crest, but is still occurring on the stoss slope, while deposition is still occurring in the trough and increasingly up the lee slope, almost to the crest in some locations. An increase in height and lee angle is observed over this time, perhaps due to a build-up of sediment higher up on the lee slope, while length has decreased, which could be a result of stoss slope erosion over a larger area being deposited higher up in the lee.

The change in topography between LRT and MRT (Figure 1.11d) is much less than the three previous surveys (Figure 1.11 a through c), coinciding with the decrease in mean velocity and suspended sediment concentration. Deposition is occurring up to the crests and in the upper stoss in some areas, and height and lee angle have

increased. Length has increased, which may be due to the erosion of sediment over a wider area on the stoss slope and deposition over a smaller area in the lee. From MRT to HT (Figure 1.11e) the general pattern seen in the previous surveys is no longer evident, and areas of erosion can be seen in some parts of the lower lee and trough, which could be scour, while deposition is still occurring in other troughs and lees. Mean height, length, and lee slope angle values do not change significantly over this time interval, reflecting that velocity and sediment movement has slowed on the approach to high tide.

1.5. Conclusions

The following conclusions can be drawn from the study of variability of dune geometry over a tidal cycle in the Fraser Estuary:

1) Mean dune height, length, aspect ratio, and lee slope angles display counter-clockwise hysteretic patterns when plotted against mean velocity.

2) The patterns of deposition and erosion over the tidal cycle support the observed changes in height and lee slope angle, which are linked to suspended sediment concentration, and the change in height and lee angle in response to diurnal flow variability suggest that suspension of bed material controls their decrease with higher mean velocity.

3) Mean height and length show net increases over the study period, which cannot be connected to diurnal scale velocity flux, and most likely reflects adjustment in response to increasing discharge on the seasonal scale.

4) As the tide rises, height and lee slope angle increase significantly due to persistent deposition on the crest and erosion in the trough. Trough erosion may be caused by enhanced turbulence as currents decelerate. An

increasing importance of bedload over suspended load as current velocities decrease may also increase lee slope angles.

Chapter 2.

Dune Translation and Crestline Dynamics in Fraser Estuary, Canada

2.1. Introduction

Bedforms are expressions of the interaction between moving fluid and the erodible bed over which it flows. The patterns of bedforms which arise, in turn, exert constraints on the overlying flow. In sand-bedded alluvial environments, these sedimentary expressions most often take on the form of dunes (Venditti, 2013). In estuaries, the bidirectionality of fluid flow caused by tidal fluctuations creates an environment where the channel bed is forced to continually adjust to the variability of flow. This perpetual adjustment to cyclical fluctuations in flow strength results in adjustments to the characteristics of the bedform field including: bedform metrics such as height and length; crestline sinuosity, migration and sediment flux; and creation and destruction of individual dunes.

Dunes may be classified based on their planimetric morphology as two-dimensional (2D) or three-dimensional (3D) (Allen, 1982). Two-dimensional dunes display regularity in their geometry, and have approximately straight crestlines oriented transverse to flow, while 3D dunes display non-uniformity in their height, length and spacing, and have highly sinuous transverse-flow crestlines (Ashley, 1990). Venditti et al. (2005b) proposed a threshold separating 2D and 3D dunes, predicated on the dune's

ability to resist deformation caused by perturbations passing downstream through a dune field. They calculated the non-dimensional span (NDS), or crestline sinuosity, defined as the ratio (L_c/L_y) of the length of the bedform crestline, L_c, to the distance across the channel, L_y. They found that when the NDS is less than 1.2, the dunes are 2D and defects, defined as transient excesses or deficiencies of sand, propagate downstream from one dune to the next without permanent deformation of the crestlines. When the NDS is greater than 1.2, crestline defects pass downstream and increase in number, leaving permanently distorted, 3D dunes.

The response of flow to 2D bathymetry has been studied extensively through lab experiments over high-angle asymmetric (Raudkivi, 1963, 1966; Lyn, 1993; Nelson et al., 1993; McLean et al., 1994; Venditti and Bennett, 2000) and low-angle symmetric dunes (Wiberg and Nelson, 1992; Best and Kostaschuk, 2002). However, natural bedforms in alluvial and estuarine environments are predominantly three dimensional (Allen, 1982; Parsons et al. 2005), which alters the flow field in a manner significantly different to that found over 2D bedforms (Maddux et al., 2003a, Maddux et al., 2003b; Venditti, 2007). Increasingly, studies have focused on the more complex interactions between flow and bed morphology in natural systems (e.g. Gabel, 1993; Mohrig and Smith, 1996, Wilbers, 2004; Parsons et al., 2005) and recreating them in the laboratory (e.g. Maddux et al., 2003a, 2003b; Venditti et al., 2005a, 2005b, 2005c; Venditti, 2007; Martin and Jerolmack, 2013).

In 3D dune fields, the crestlines of dunes can be generalized as lobe-shaped or saddle shaped. The former display crests with topographic highs that bow in the downstream direction, while the crests of the latter have topographic lows that bow upstream. Through laboratory experiments, Maddux et al. (2003a, 2003b) observed flow

over dunes arranged with straight crestlines, but with heights that varied in the cross-stream direction. They found that this arrangement resulted in a shift of maximum streamwise velocity to its highest value at the halfway point between the highest and lowest portion of the crest (referred to by the authors as the 'crestal node"), rather than the dune's maximum elevation point, where maximum streamwise velocity occurs over 2D dune morphology.

Laboratory experiments by Venditti (2007) examined the flow and drag associated with fully 3D dunes and found that lobe-shaped dune crestlines generate more strongly defined wake structures and increased turbulent mixing than 2D systems. The 3D bed configuration also effects a vertical divergence of mean and secondary flows generated in the upward direction that further enhances turbulence. Field work by Parsons et al. (2005) on the flow structure over a 3D dune field in the Rio Parana, Argentina found that the 3D dune morphology had a significant effect on flow structure in that vertical velocities were greater and flow separation zones were smaller over both lobe and saddle shaped dunes. Their results concurred with Venditti's (2007) lab results with respect to the lobe pattern, but contradicted the findings over the saddle pattern.

Our understanding of the response of a dune population to fluid flow remains largely incomplete. The field-scale occurrence of dune birth, death, and piracy has received little attention, though several studies have documented the rise of dune fields from flat beds under steady flow conditions (see Venditti, 2013, for a review). Laboratory experiments suggest that bedform 'birth', or initiation, occurs by two main mechanisms (Gyr and Schmidt, 1989): 1) defect bedform initiation, observed in the laboratory (Raudkivi, 1963; 1966; Southard and Dingler, 1971; Leeder, 1980; Best, 1992, Venditti et al., 2005c), and 2) instantaneous bedform initiation (Venditti et al., 2005c). Dune

'death' describes the disappearance of a pre-existing dune, and may occur via two different processes. One method occurs when more sediment is eroded from a bedform than is deposited, and if enough sediment goes into suspension and is carried downstream, dunes may wash out into upper stage plane beds (Venditti, 2013). The second method involves two dunes amalgamating into one. Gabel's (1993) field study found no correlation between rates of birth or death and discharge, and suggests that these are functions of localized variability in sediment transport. Dune 'piracy' involves the detachment of a bifurcated crestline from one primary crestline and subsequent reattachment to another. No studies to date have attempted to quantify the importance of piracy in an active dune field.

Dune migration is a function of the shear stress exerted at the channel boundary by the overlying flow. The flow entrains sediment on the upstream side of the dune and deposits it in the lee, resulting in a coherent downstream shift of the dune. As such, the symbiotic relation between flow and bed morphology ultimately controls migration through sediment transport. Bedform related sediment transport (q_s) is composed of two components: deformation and translation (McElroy and Mohrig, 2009) where translation (T) refers to the downstream shift of bedforms, and deformation (D) refers to the change in size and shape of a bedform as bed sediments are entrained into suspension and redeposited downflow. Combined, these two components of the sediment load are responsible for the evolution of bedform fields in rivers and estuaries.

Measured values of dune geometry can be used to calculate a bedload transport rate, which is equal to the translation component of the total transport when sediment suspension is negligible, using the modified Exner equation of Simons and Richardson (1965):

$$q_s = (1-\rho)\beta H V_b \quad (1)$$

where q_s is the sediment flux rate per unit width, ρ is the fraction of the bed occupied by sediment (assumed to be 0.6), β is the bedform shape factor, found to be reasonably estimated by 0.56 (from Venditti et al., 2005a; similar values found in van den Berg, 1987; ten Brinke et al., 1997). H is the bedform height, and the bedform migration speed, V_b, can be calculated by the distance translated (T) over a given time interval.

A characteristic feature of 3D dunes is the presence of secondary crestlines within the bedform field. These may be discontinuous (non-channel spanning) crestlines as identified by Parsons et al. (2005), or smaller crestline branches extending off a larger, channel-spanning crestline, referred to as bifurcations (Colombini and Stocchino, 2008) or defects (Werner and Kocurek, 1999; Ewing et al., 2006; Huntley et al., 2008). Very little attention has been given to the dynamics of crestline bifurcations, and the majority of existing information is from numerical modelling of aeolian dune dynamics (e.g. Werner, 1995; Werner and Kocurek, 1997) or near-shore seabed dynamics (e.g. Huntley et al, 2008).

Allen (1973a) proposed two mechanisms to explain the initiation of crestline defects. The first results from the process of a secondary, climbing bedform growing in height on the stoss-side of an existing bedform, and splitting from the initial bedform on which it climbs to form a bifurcation. The second more infrequent mechanism is a result of crestline splitting at spurs, which are flow parallel ridges that extend along the stoss slope of a bedform (Allen, 1969). Because secondary bedforms are generally smaller, than primary bedforms in a population, they tend to have faster migration rates (Coleman and Melville, 1994; Landry and Werner, 1994). Their relatively greater

mobility, via sediment deposition and erosion, may lead to bifurcation piracy, which involves the severing of the defects from one primary dune and reattachment to another.

Numerical modelling of ripples under nearshore conditions by Huntley et al. (2008) explored the effect of defect density on the evolution of bed topography. They found that the presence of defects strongly affected the rate of topographic response to variable flow conditions in that beds with low defect densities resisted changes in bedform characteristics (height and length), and beds with higher defects experienced more changes to bedform morphologies. Werner and Kocurek (1997) argue that crestline defects control the overall evolution of the bedform field through their influence on crestline orientation and through crestline splitting.

The majority of our understanding of crestline dynamics in rivers is from work in steady, unidirectional flows, yet natural river systems rarely experience such conditions for extended periods of time owing to fluctuations on the diurnal (tides in estuarine reaches), synoptic (storm events), and seasonal (annual hydrograph) scales. The result is constant readjustment of the bed in response to flow variability, and measuring the response is often made more challenging by the presence of a time lag (Pretious and Blench, 1951; Allen, 1973; 1974; 1982; Terwindt and Brouwer, 1986; Gabel, 1993; Julien et al., 2002; Villard and Church, 2003; 2005; Kostaschuk and Best, 2005).

Previous work on dune migration in variable flows has considered translation rates with the intent of calculating bed material transport over longer time scales, such as that of the rising flood hydrograph (e.g. Pretious and Blench, 1951; Kostaschuk et al., 1989). However, data collection in previous studies was limited (by instrumentation) to single track surveys, and no observations to date have considered migration over the

diurnal scale. Translation rates, observed in laboratory experiments (Lin and Venditti, 2013), show a strong correlation to transport stage under unidirectional flow conditions, but further work is required in natural settings with variable flow conditions in order to understand how crestlines, bifurcations, bedform dimensions, and bedform translation vary with flow.

In Chapter 1, I quantified reach-scale changes in dune geometry over the course of a tidal cycle, examining how mean dune height, length, aspect ratio, and lee slope angle responded to flow variability. I found that dune heights and lee slope angles both decreased with increasing mean velocity and suspended sediment concentrations toward low tide, and then increased as the tidal flux approached its maximum height. Changes in mean length were small, and showed a trend of overall increase, suggesting that they were responding to longer term flow variability associated with the rising hydrograph. Mean dune aspect ratios fluctuated owing to the discordance of change of height with respect to length. These results are consistent with previous studies which found that rising velocities were coincident with increased suspended sediment transport rates (Smith and McLean, 1977; Johns et al., 1990; Kostaschuk and Ilersich, 1995; Kostaschuk and Best, 2005), where sediment is being entrained on the stoss and crest and deposited in the lower lee and trough, resulting in decreases in height and lee angle. Conversely, falling velocities and suspended sediment concentrations observed on the approach to high tide were coincident to increasing mean dune height and lee angles.

The motivation for this project is to contribute to our understanding of the sediment flux in large sand-bedded, fluvially-dominated, tidal environments. This requires an understanding of bed topography, and in estuarine environments where dunes dominate the channel bed, an understanding of dune response to flow variability. The purpose of

this paper is to examine the dynamics of dunes at the diurnal tidal scale in the fluvially-dominated Fraser Estuary. Measurements of dune crestline sinuosity, translation and changes in bifurcation over the course of the largest falling and rising limbs in the lunar cycle of a mixed semi-diurnal tide regime are used to address the following research questions: 1) *What is the structure of the crestlines in a natural estuarine bedform field?* 2) *How do crestlines change in response to variable flow? 3) How are the dynamics of dunes linked to dune dimensions and translation?*

2.2. Methods

2.2.1. Field Study Site

The Fraser Estuary is located on the southwest coast of British Columbia, where the Fraser River enters the Strait of Georgia. The Fraser River has a drainage area of 234,000 km^2, with a mean annual discharge of 3410 m^3s^{-1} measured at the Mission Gauging Station, located 74 km upstream of Sand Heads (from Water Survey of Canada data collected between 1969 and 1987, and reported in McLean et al., 1999). Peak flow and sediment discharge occur in mid- to late-spring, following seasonal snowmelt, with the mean annual flood measuring 9790 m^3s^{-1} (McLean et al., 1999). Sediment discharge at the mouth of the Main Arm of the Fraser River is 17 million tonnes per year, 4.25 million of which is sandy bed material load (McLean et al., 1999).

The predominantly single-channelled Fraser River begins to bifurcate in the estuary, where the single channel splits into the North and Main Arms. Farther downstream the North Arm splits, giving rise to the Middle Arm, and the Main Arm splits to give rise to Canoe Pass. The Main Arm accommodates the majority of river

discharge, approximately 70% at peak annual flow (Western Canada Hydraulic Laboratories Ltd., 1977).

The tidal pattern in the Fraser Estuary is classified as mixed but mainly semi-diurnal, with the maximum tidal range of 5 m occurring during the spring tide (Kostaschuk et al, 1989). During periods of low river discharge, a salt-wedge enters the Main Arm (Kostaschuk and Luternauer, 1989), with an upstream limit reaching as far as New Westminster (~25 km upstream of the river mouth) at low flows (Dashtgard et al., 2012) and Deas Island (~10 km upstream the river mouth) during mean annual discharge (Ages and Woollard, 1976).

In the Main Arm of the Fraser Estuary, dune heights are typically 1-2 m, and lengths are 20-50 m, although observations of dunes over 5 m high and 100 m long have been recorded (Pretious and Blench, 1951; Kostaschuk et al., 1989). Kostaschuk et al., (1989) found that heights and lengths changed seasonally in response to fluctuations in river discharge; they were relatively small in April and early May, growing large into June, then smaller dunes re-established with the decrease in sediment deposition through to September (see also Villard and Church, 2005). An annual dredging program is run typically from August through to March, which results in planing of the channel bed (Villard and Church, 2005). On a shorter time scale, dune geometry in the Fraser Estuary varies in response to tidal variation (Kostaschuk et al., 1989; Kostaschuk and Ilersich, 1995; Kostaschuk and Best, 2005).

Observations were made on 14 June 2010, coinciding with the period of the largest tidal flux and elevated river discharge. Discharge is not recorded at Steveston, but a reasonable estimate of mean daily discharge can be obtained using the recorded

mean daily discharge from the nearest station on the Fraser River (Mission Gauge Station, station number 08MH024). This yields a mean daily discharge of 6950 m^3s^{-1} for 14 June 2010 (Figure 2.1a), which preceded the peak daily mean discharge on 28 June 2010 of Q = 7490 m^3s^{-1} (Water Survey of Canada, 2011), one of the lowest annual peak flows on record. The actual value of the discharge measurement in Steveston will vary from this owing to the lag between the time of measurement in Mission and the travel time to Steveston. Tidal forcing may also affect the actual discharge at Steveston as high tidal water may hold and release river outflow. On June 14, the first high tide of the survey was 3.8 m, low tide was 0.40 m, and the second high tide was 4.3 m (Figure 2.1.b).

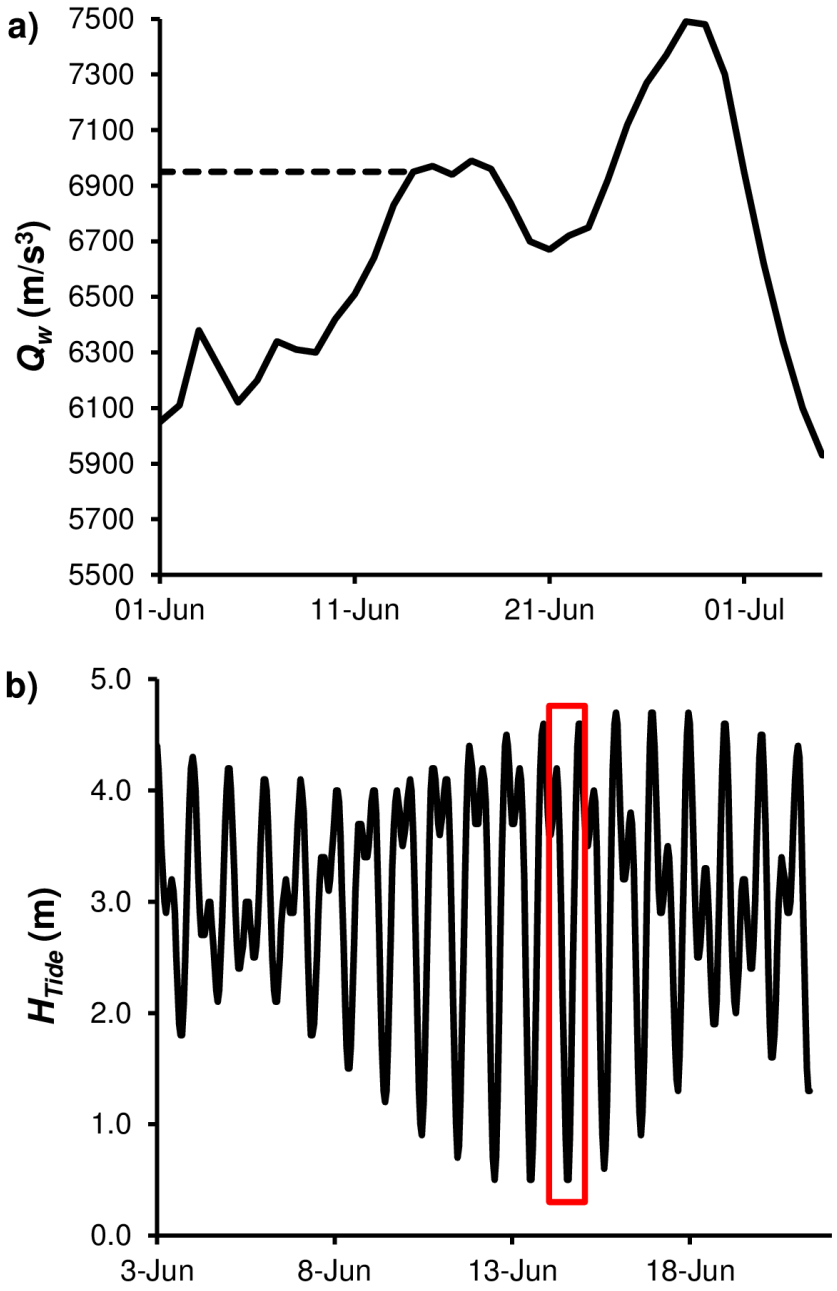

Figure 2.1. **Hydrograph for mean daily discharge in Fraser River at Mission for June, 2010. The dashed line indicates the mean daily discharge calculated for 14 June 2010. b) Water level recorded at Steveston Gauging Station (08MH028) of the neap-spring tidal cycle during which data were collected (from Water Survey of Canada, 2011). The red box indicates the diurnal tidal cycle over which data for this project were collected.**

The study reach is located in the Main Arm of the Fraser River between Steveston and Westham Island, where the channel meets the Strait of Georgia. Data were collected along transects conducted over an area covering ~1 km in the stream-wise direction and ~0.5 km in the cross-stream direction (Figure 2.2).

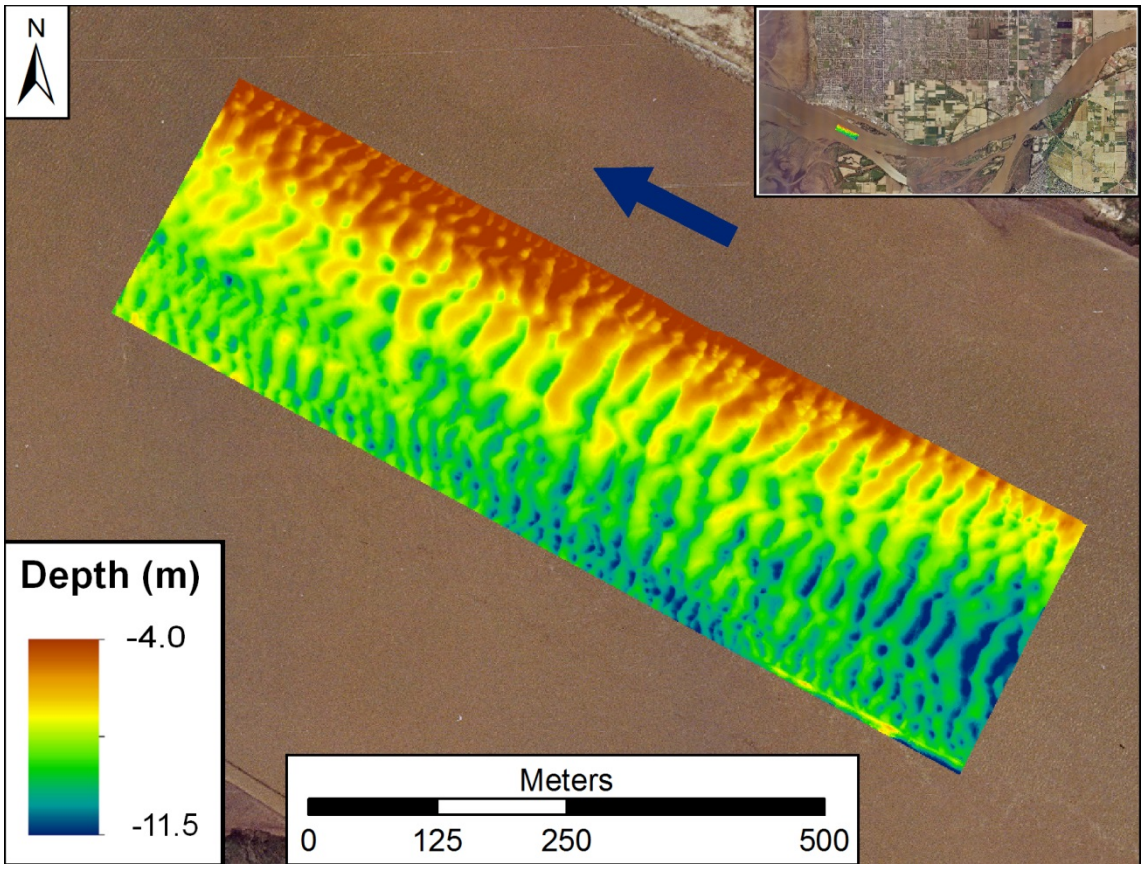

Figure 2.2. Bathymetric map of the study site. Blue arrow indicates direction of river flow. Inset shows the location of the study site within the Main Arm of the Fraser River.

2.2.2. Data Collection

Three-dimensional (3D) bathymetric data and 3D flow velocities were collected aboard the *R/V Lake Itasca* between June 12 and 17 2010 using a Reson 7101 Seabat Multibeam Echosounder (MBES) and a Teledyne RD Instruments 1200 kHz Rio Grande Workhorse acoustic Doppler current profiler (aDcp), respectively. The MBES is designed

to measure relative water depth through the transmission of a wide swath of acoustic energy pulses and analysis of their reflections (Reson Inc., 2002). The sonar head emits 511 equiangular beam soundings per ping to cover a swath area of 150° (Reson Inc., 2009) with a vertical resolution of ~1.5 cm (Reson Inc., 2009).

Spatial positioning of the MBES was accomplished using a Trimble Real Time Kinematic Global Positioning System (RTK GPS) with a static base station that sent corrections to the rover head at 1 Hz. Positional accuracy of the GPS unit when running in RTK survey mode is +/- 0.01 m horizontally and +/- 0.02 m vertically. The position of the aDcp was recorded by a differential GPS (DGPS) system corrected by a Canadian Coast Guard beacon located ~1.7 km south of the study site. Positional accuracy of the DGPS is 0.25 m horizontally and 0.50 m vertically. Pitch, heave, and roll of the vessel were measured using an Applanix POS MV V3 gyroscope inertial guidance system. The system provides information to correct for the effects of horizontal and lateral vessel motion during survey operations.

Suspended sediment samples were collected on 17 June 2010. A U.S. Geological Survey P-63 point-integrated suspended sediment sampler was deployed at 0.1h, 0.2h, 0.4h, 0.6h and 0.8h over 40 s intervals to measure suspended sediment concentrations in the water column over the largest dune at Low Tide, Low Rising Tide, and High Rising Tide stages.

MBES measurements were collected over several tidal cycles to capture the changes in bed topography. Twenty-one surveys were conducted, each of which consisted of five parallel stream-wise traverses over the study area, and the resulting data were used to produce bed elevation maps. This study focusses on eight surveys

taken over the tidal cycle occurring on 14 June 2010, chosen to correspond with the highest tidal fall of the cycle. Each survey is labelled according to its position on the tidal cycle as “High Falling Tide” (HFT), “Mid Falling Tide” (MFT), “Low Falling Tide” (LFT), “Low Tide” (LT), “Low Rising Tide” (LRT), “Mid Rising Tide” (MRT), “High Rising Tide” (HRT), and “High Tide” (HT) (refer to Figure A1).

2.2.3. Data Processing

Raw MBES data were imported into CARIS HIPS® software for post processing to correct for changes in tidal stage, pitch, heave, and sound velocity, and to remove false data points. The data were then imported into ArcGIS® and gridded at 1 m for further analysis of channel bed characteristics for each of the eight surveys. A correlation analysis was carried out on the cross-stream depth data to determine the topographic variability across the channel, and it was found that variability increased significantly at ~30 m intervals (Figure A2). In order to extract measurements from the topographic maps to calculate crestline sinuosity, dune translation rates and sediment flux, 26 stream-wise transects were laid over the base maps, spaced at 10 m intervals, and points were placed at 1 m intervals along each of these lines and tagged with the position (easting and northing) and depth of bed below the water surface. These data were then used to identify local maxima (crests) and minima (troughs). Successive topographic base maps were differenced to give the change in bed elevation between each survey, and qualitatively display patterns of deposition and erosion on the channel bed.

Crestlines were identified by connecting the points of highest local maxima along each of the 26 stream-wise transects and plotted in ArcGIS® to amalgamate other

parameters (dune height, length, lee slope angle). In order to determine movement of the dunes, 21 primary crestlines were identified. This was achieved by identifying all the crestlines of the shortest cross-stream length that continuously span the width of the study area; all other crestlines are labelled secondary crestlines, which includes crestlines that do not span the entire width of the channel, and bifurcations, which occur when a crestline splits into two separate branches. The primary dunes are labelled from the upstream-most crestline (Dune 1) to the most seaward crestline (Dune 21). The crestline non-dimensional span (*NDS*) was calculated as the length of each primary crestline (L_c) divided by the straight line distance between its endpoints (L_y).

To measure translation, the displacement of each primary and secondary crestline was measured between crest points of each of the 26 stream-wise transects between each survey period. The sediment flux rate associated with the migrating bedforms was then calculated using Equation 1. The number of secondary crestlines attached to each primary crestline was counted for each survey period to determine the occurrence of birth, death and piracy over the tidal cycle, and secondary crestline density was determined by drawing grids over areas of similar bifurcation pattern (determined visually) and dividing by the area of the grid. It should be noted that the accuracy of the detectable displacement is controlled by the resolution of the DEM.

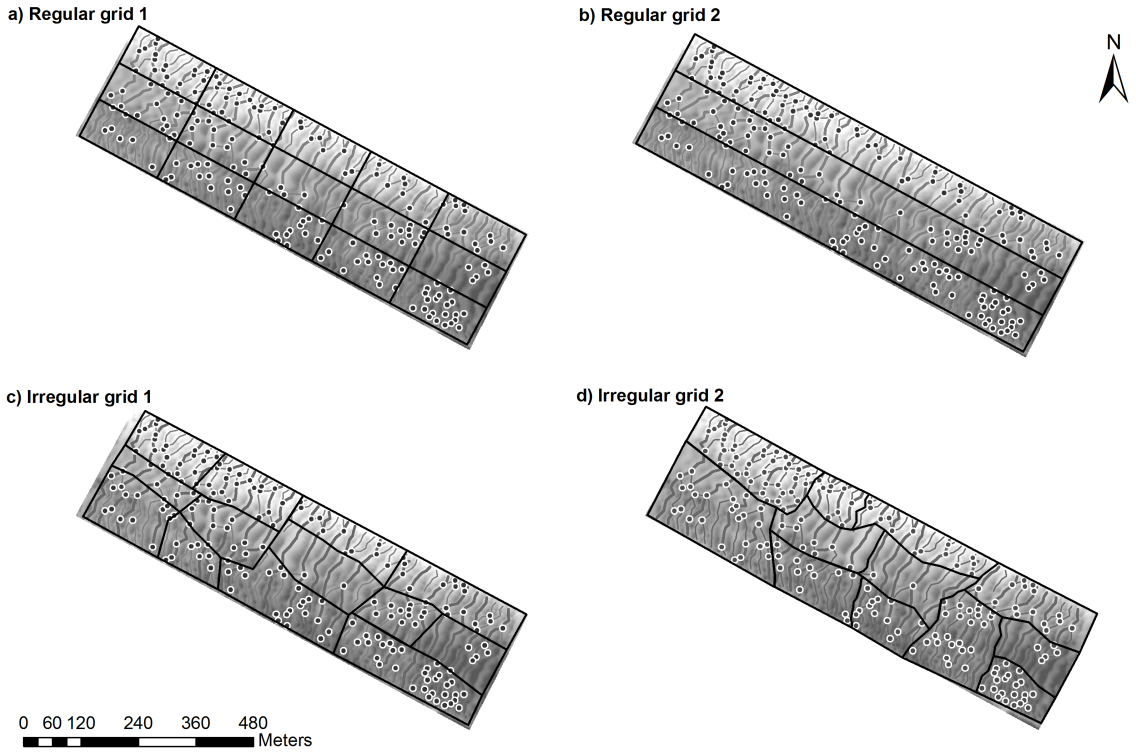

Figure 2.3. Grid patterns for dividing the channel. Black lines indicate polygon borders and circles are the bifurcation intersection points.

In order to explore the patterns of translation, sediment transport, and bifurcation, and test whether relations between these processes exist, four different grids were constructed and applied to the data set (Figure 2.3). One is composed of 15 equal-size rectangular polygons (referred to herein as 'Regular Grid 1', or RG1), a second consists of three downstream-spanning rectangles of equal area ('Regular Grid 2', or RG2) and two consist of polygons constructed to capture areas of similar bifurcation distribution ('Irregular Grid 1', or IG1 and 'Irregular Grid 2', or IG2). Regular Grid 2 was applied to capture larger dunes in the centre of the channel, and the smaller, more strongly bifurcated dunes at the sides of the study area. Irregular Grid 1 was constructed by grouping areas of like bifurcation based on the location and extent of the secondary crestlines, while Irregular Grid 2 was constructed using the bifurcation points where a

crestline splits to give rise to another attached crestline. The number of bifurcation points in each polygon was then divided by the polygon area to obtain a density value. In ArcGIS®, points were placed where bifurcations arose from primary crestlines, and these points were compared at sequential survey times in order to identify bifurcation births (generation of a new secondary crestline), deaths (disappearance of a secondary crestline), or piracy (detachment of a secondary crestline from one primary or other secondary crestline and reattachment to another).

In order to ensure that individual, migrating points were recognized from one survey to the next, successive grids were overlaid in ArcGIS®. Both primary and secondary crestlines were compared for similarities, such as distinguishing local sinuosities (for larger dunes) and relative positions of attachment to primary dunes (for secondary dunes). To identify the occurrence of piracy, because the attachment point would change, the locations and shapes of the individual crestlines were compared between surveys to ensure that the correct crestline was being identified.

2.3. Results

2.3.1. Bed Topography and Dune Geometry

Bathymetric maps generated from the MBES data show a trend of decreasing elevation across the channel, with a lateral bar to the north creating an area of higher elevation, and scour on the south side where Sea Reach Channel re-enters Main Arm downstream of a series of small islands. The bed surface is covered in dunes, with the largest dunes occurring along the centre of the channel. I showed in Chapter 1 that these dunes display near-symmetric cross-sectional morphology, with a mean slope

symmetry ratio, which is the ratio of the length of the stoss slope to the total length of the dune (L_{stoss}/L), of 0.59, and range of 0.10 to 0.93 over the study period.

2.3.2. Crestlines and Bifurcations

Figure 2.4a shows the primary crestlines extracted from the MBES data and reveals a pattern of linear, 2D dunes that span the width of the study site. These crestlines have low sinuosity, with varying patterns of subtle lobe and saddle morphology along each individual dune. Calculations of the non-dimensional span (L_c/L_y) of each primary crestline for each survey over the fall and rise of the tidal cycle (Figure 2.5) yield values that are equal to or below the threshold value for 2-3D transition of 1.2 (Venditti et al., 2005b) for all but two dune crestlines (Dune 17 at HRT and Dune 13 at HT). Fluctuation in L_c/L_y is observable in the dunes over the course of the tidal cycle (sinuosity range = 1.03 – 1.22; std. dev. = 0.04), however, a Wilcoxon Rank Sum test indicates these changes are not significant at the 95% level, with P-values ranging from 0.43 to 0.87.

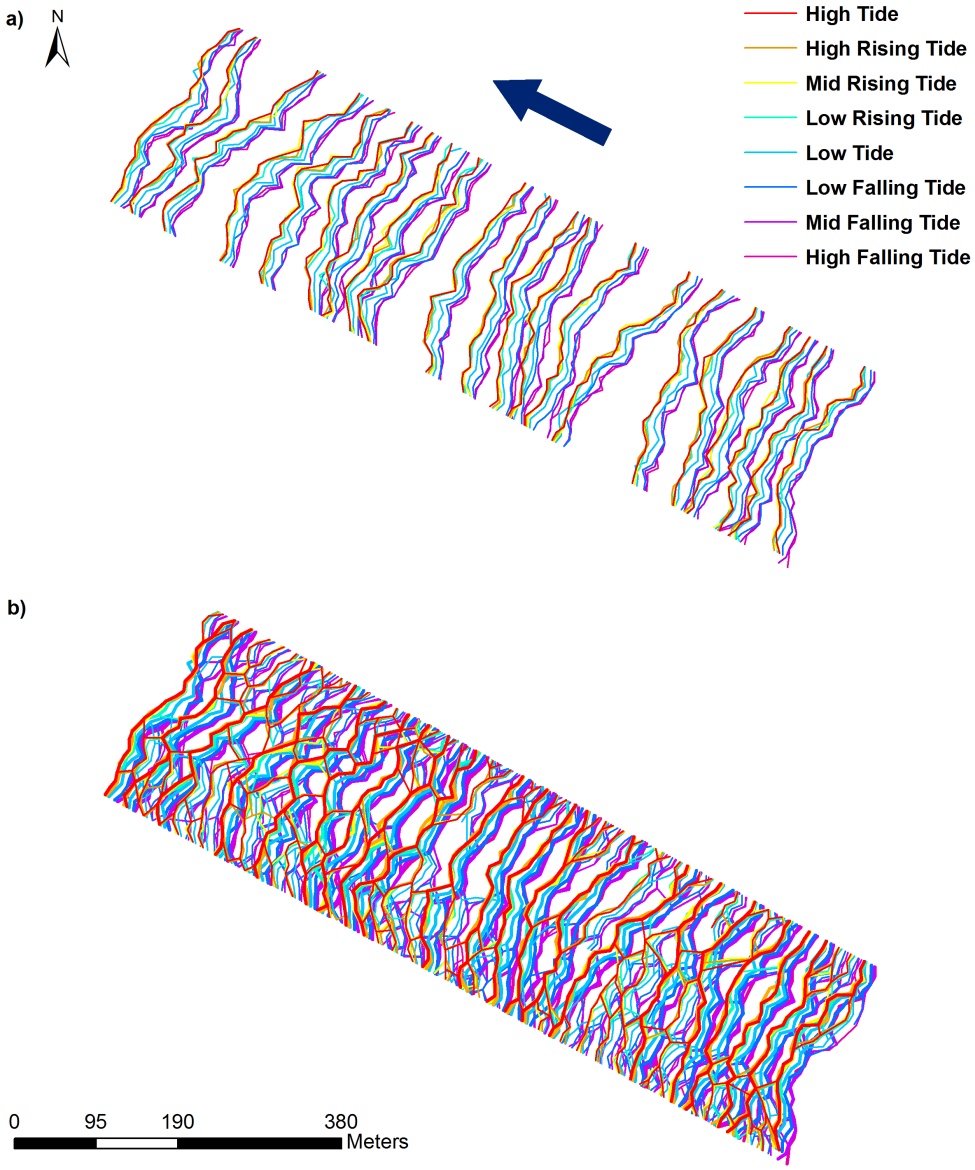

Figure 2.4. Lines created by connecting points of local maximum elevation to denote a) primary crestlines, and b) secondary or bifurcated crestlines (shown with primary crestlines) over the study site for each survey. Blue arrow indicates flow direction for both panels.

Inclusion of secondary dunes in the analysis (Figure 2.4b) results in a more complex 3D pattern, with the majority of the bifurcations having occurred along the sides of the study site, where areas of higher elevation (north side) and lower elevation (south side) occur. In the downstream one-third of the study reach, there is a higher number of

secondary dunes within the centre, displaying a more linguoid pattern of interconnecting crestlines, compared to the bifurcations along the sides, which display a more dendritic pattern.

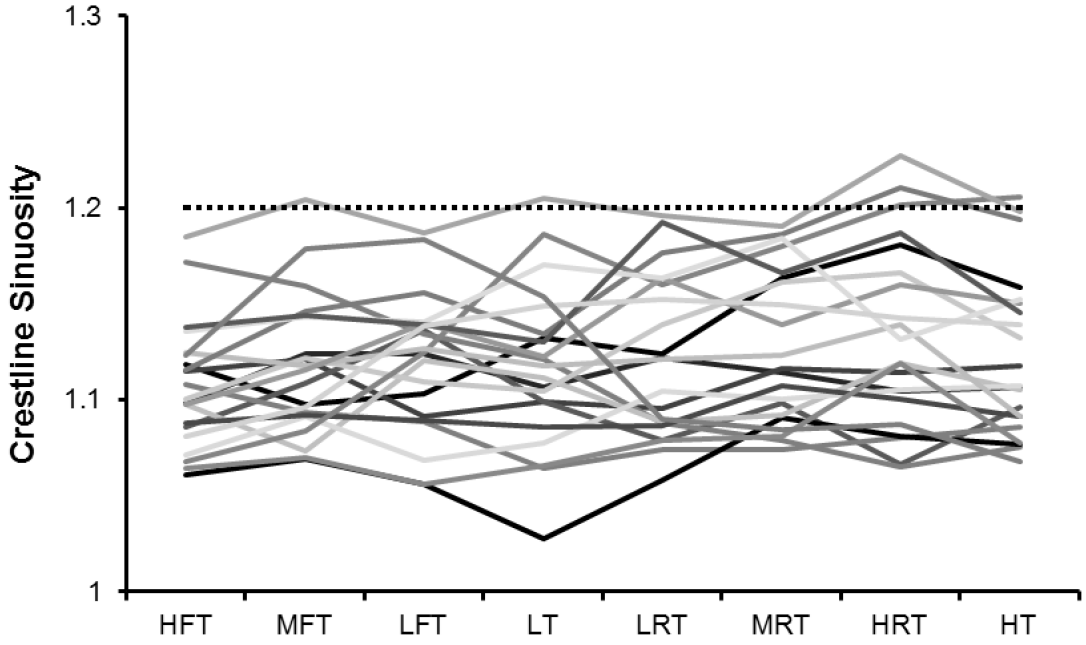

Figure 2.5. Crestline sinuosity calculated for each of the 21 primary crestlines in the study site at each survey time. Dashed line represents the 2D-3D threshold as defined by Venditti et al. (2005b).

The total number of secondary dunes on the bed of the study site initially increased from HFT to LFT, rising from a count of 235 to 239 (Figure 2.6). As the tidal minimum was reached, the total count dropped to the lowest number of secondary dunes of the study period, 222, and then increased toward HT, with the last count at that time being 242. This change in total number of secondary dunes is reflected in the occurrence of birth, death, and piracy over the study period (Figure 2.6). For the majority of the survey times, the number of births outnumbered deaths, with the exception of HFT-MFT, where an equal number of each is occurring, and at LFT-LT, where just over twice as many deaths occurred as births (33 vs 16). Piracy appears to have been a

relatively rare occurrence over the course of this study, only happening at and after low tide, and not exceeding 3 events per survey.

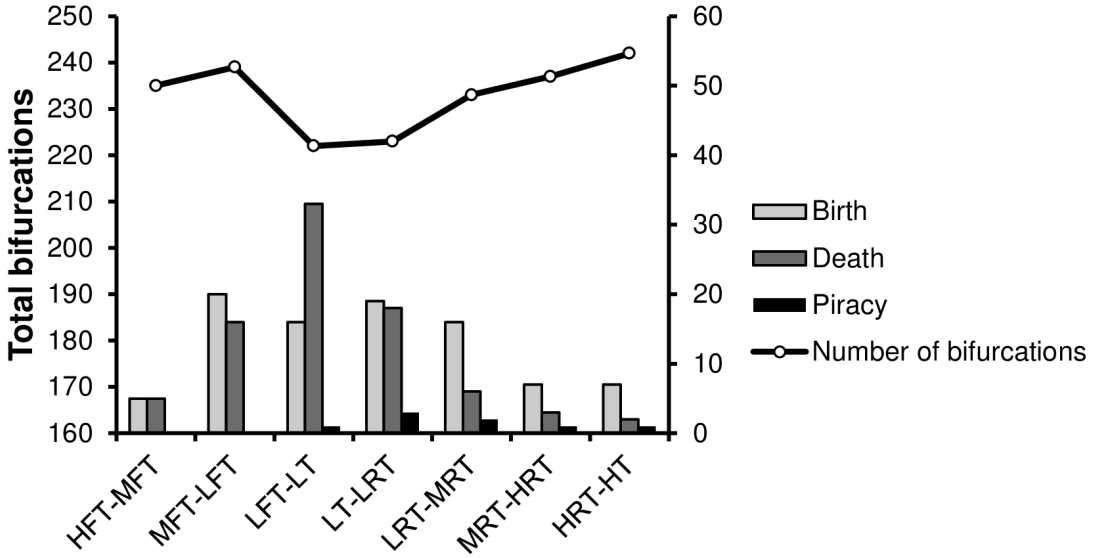

Figure 2.6. Changes in secondary crestlines over the tidal cycle. The line connects the points of total secondary crestline numbers at each survey time, while the bars represent the number of changes of secondary crestlines associated with primary dunes (birth, death, and piracy).

Spatial distribution of secondary crestline fluctuations varied over the tidal cycle, and although no obvious pattern is discernible for the occurrence of birth, death, or piracy (Figure 2.7), the largest number of changes occurred between LFT and LRT. Between HFT and MFT, all but one event occurred on the south side of the study site, with a cluster of secondary crestline births occurring in the mid portion of the southern polygon, and deaths clustered at the downstream end. Between MFT and LFT, most of the changes occurred along the sides of the study area although no clear pattern is visible, while between LFT and LT, death dominated, particularly along the south side.

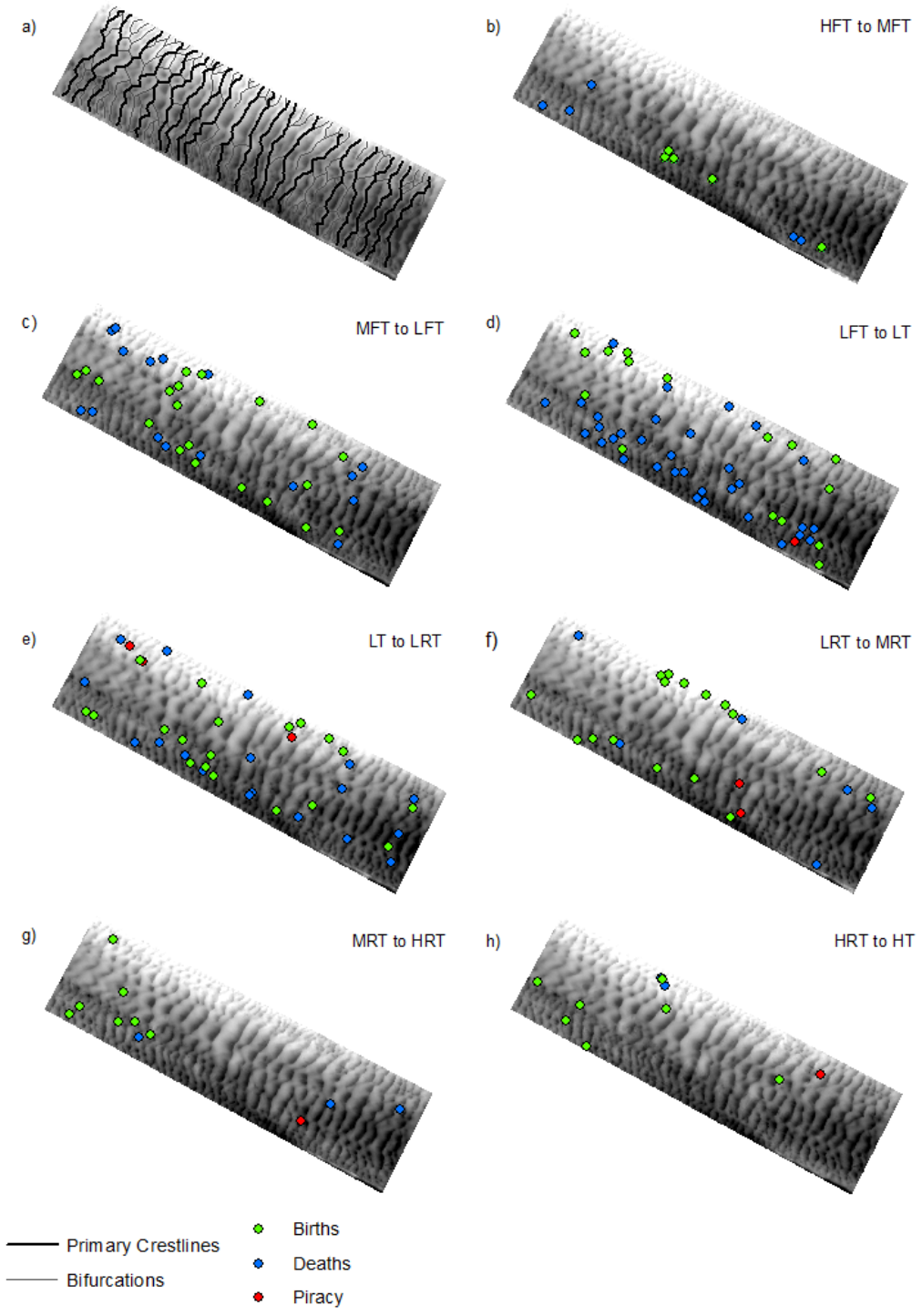

Figure 2.7. **Points of secondary crestline birth, death, and piracy over the tidal cycle. a) Bed topography with primary and bifurcated crestlines overlaid for reference. Panels b) to h) show the change in bifurcations compared to the previous survey for MFT through HT.**

Figure 2.8 shows the spatial variability of both distance translated and sediment flux calculated using Equation 1. Data presented here are limited to the two surveys taken between LFT and LRT, when the majority of the movement occurred. Between LFT and LT, the distribution of translation distances appears patchy. In the survey after low tide, a pattern emerges such that the lowest rates of dune translation are along the north side, with a general increase in translated distance from the sides of the study site toward the centre. Similar to the spatial patterns of translation, the spatial distribution of sediment flux is patchy between LFT and LRT, and conforms to a more consistent pattern between LT and LRT, where the largest volume of sediment was moved down the centre, and decreases toward the streamwise margins of the study site.

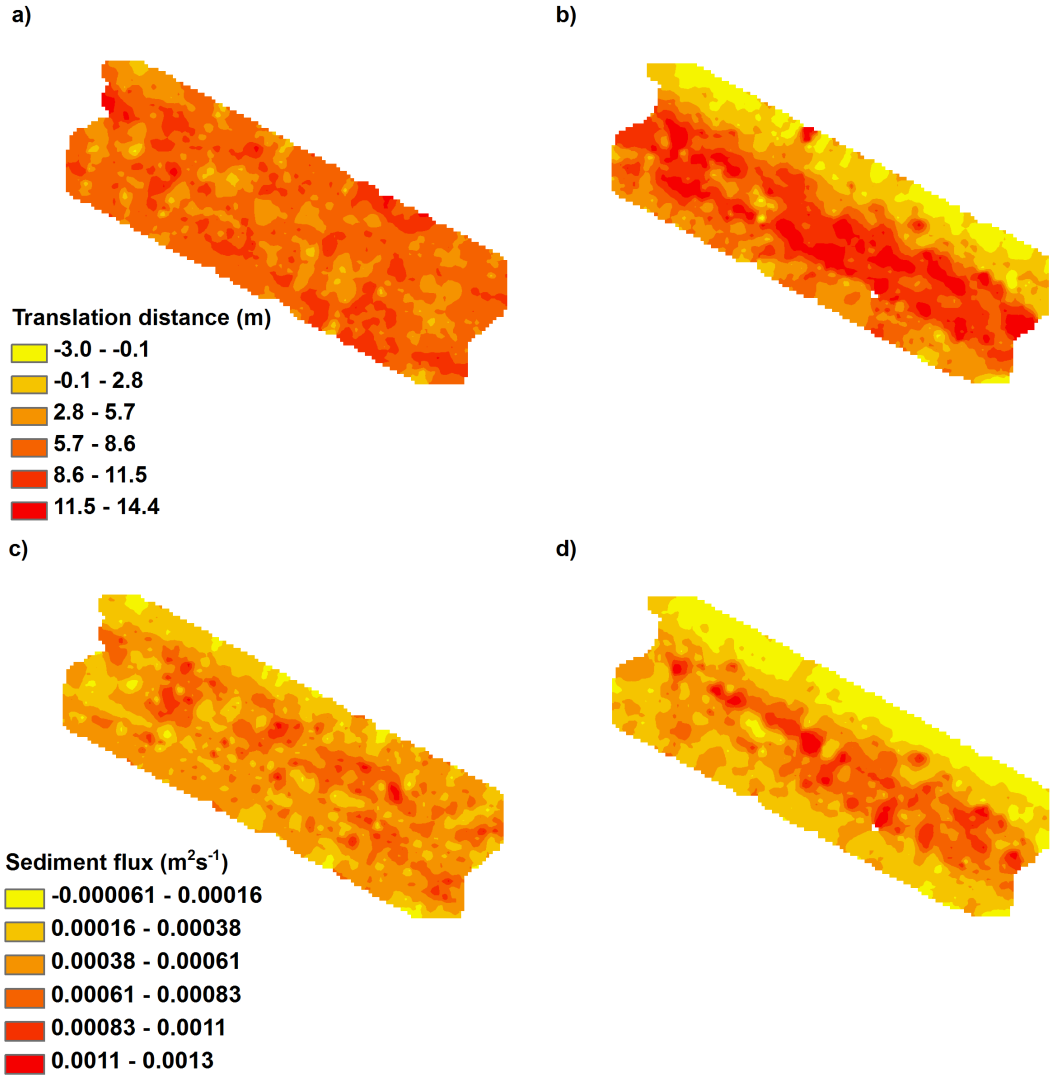

Figure 2.8. Maps of spatial variability of translation between a) LFT and LT, and b) LT and LRT and of sediment flux per unit width between c) LFT and LT, and d) LT and LRT.

During the study period, dune translation displayed a general pattern of increase toward low tide, and decrease toward high tide (Figure 2.9 a, c, e). Negative values of *T* were measured at individual points within the study field because *T* was calculated using the points of maximum elevation and in some cases this point was located upstream of the point in the previous measurement. This may be due to dune avalanching or secondary crestline birth, death, or piracy, and is reflected in the lower bounds of the

given ranges. Overall, the bulk mass of the dunes within the field moved downstream or remained stationary. Mean dune movement between HFT and MFT was low. Along the sides of the study site, mean translation distance was 1 m, while mean movement along the centre was close to 0 m. The peak mean translation distance of 7 m occurred between LFT and LT along the both side sections of the survey area, while the mean translation distance in the centre peaked between LT and LRT, also at 7 m. These peaks were followed by a sharp decrease in mean translation toward HT, to 1 m for the side sections and -1 m along the centre.

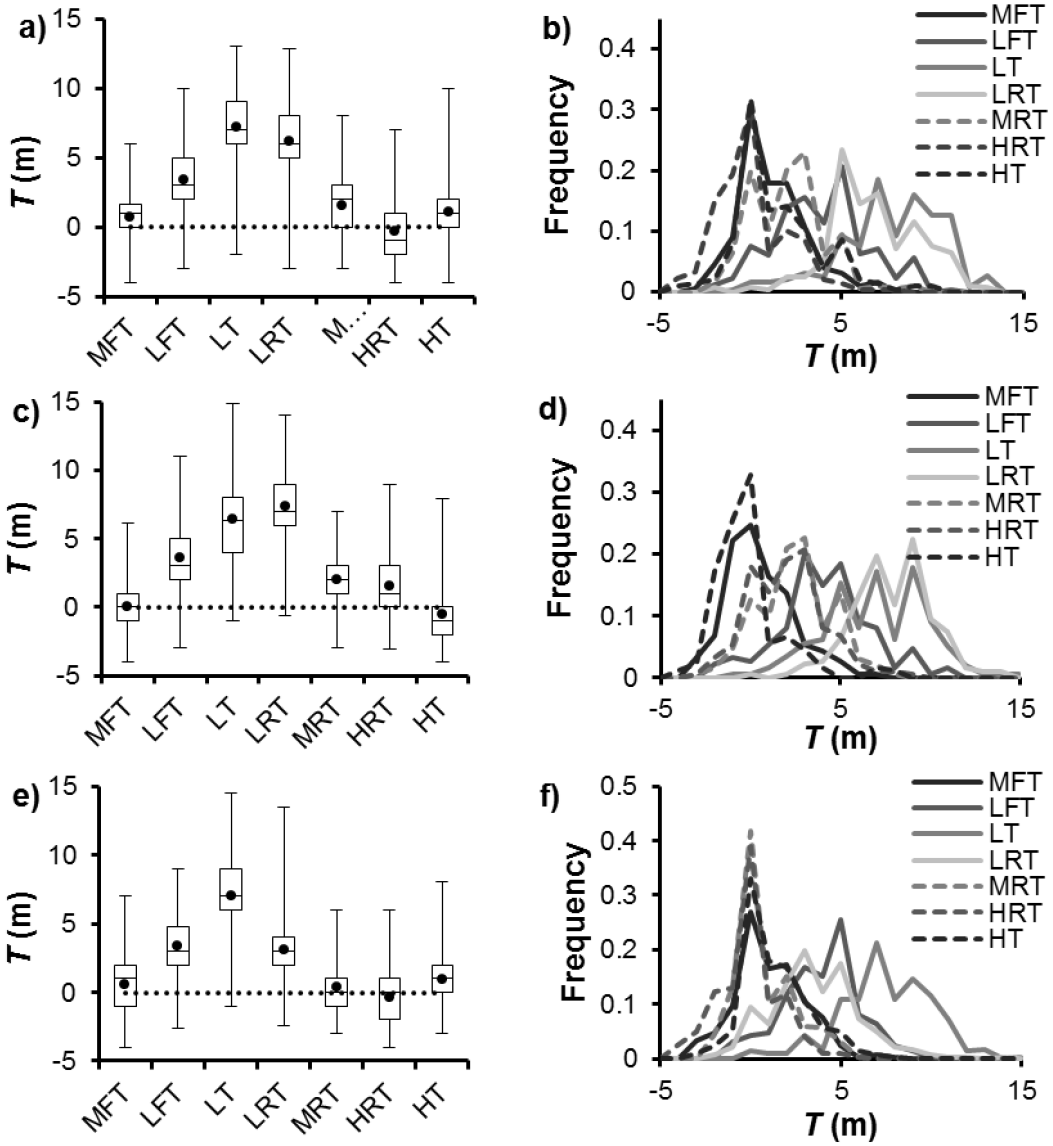

Figure 2.9. Box and whisker plots showing minimum, 25th percentile, median, 75th percentile, and range of translation distances of dunes in the study site at a) south side, c) centre, and e) north side. Black dots indicate mean distance translated, and dotted lines indicate the boundary between positive and negative translation distances. Frequency polygons showing the distribution of translation distances for each survey period for b) south side, d) centre channel, and f) north side. Frequency bins were set at 1 m.

The frequency distribution of distance translated by all of the dunes for each of the survey times varies over the tidal cycle (Fig. 2.9 b, d, f). The distributions are positively-skewed for HFT to MFT, showing an asymmetric spread about the mean with

the bulk of the distribution occurring around the low end of the range and the distibution tail extending toward larger translation distances. This then shifts to a near-normal, almost symmetric distribution from MFT to LFT, then to a negatively-skewed shaped from LFT to LT, when the bulk of the dunes are moving longer distances. The distributions shift back to a positive skew after low tide, and persist to High Tide. The polygons show a consistent pattern of translation where the peak translation increases on the falling limb of the tidal cycle, and decreases on the rising limb. The centre of the study area experiences the greatest movement between LT and LRT when there are the fewest bifurcations, while the sides experience greatest movement between LFT and LT when there are the most bifurcations.

2.3.3. Translation, Bifurcation Density, and Dune Geometry

Figure 2.10 shows the relations between translation distance and dune geometry using the data from all the grid polygon configurations (see Figure 2.2). The way the bedform data are separated spatially does not change the underlying patterns. The plotted relation is for Irregular Grid 2 polygon arrangement (shown as black squares), chosen because it most appropriately segregates areas of like bifurcation densities.

The plots of *T* against both *H* and *L* (Figure 2.10 a through d) show that the signs of the correlations reverse between LFT to LT (negative correlation) and LT to LRT (positive correlation). Smaller dunes, both in height and length, move longer distance than larger ones between LFT and LT, while the larger dunes move farther between LT and LRT. Spearman's rank coefficient (r_s) values for *L* and *H* vs *T* between LFT and LT and between LT and LRT indicate reasonable correlation for a natural system. The

relation between θ_{Lee} and *T* has a negative correlation over both survey periods, and is weak.

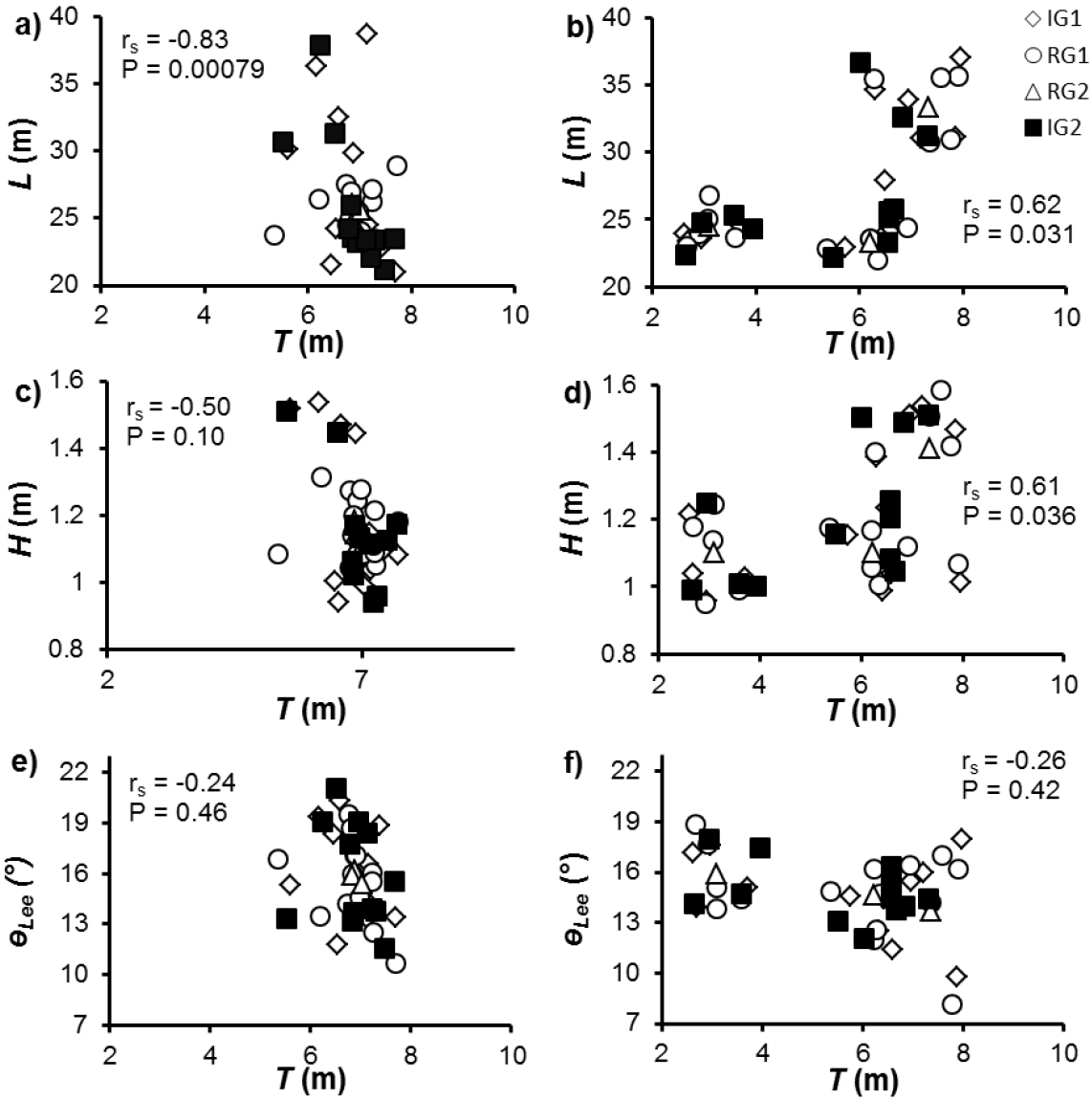

Figure 2.10. Plots of mean values of length (*L*) vs translation distance (*T*) at a) LFT to LT and b) LT to LRT, height (*H*) vs *T* at c) LFT to LT and d) LT to LRT, and lee slope angle (θ_{Lee}) vs *T* from e) LFT to LT, and f) LT to LRT. The reported statistical parameters pertain to those obtained from Irregular Grid 2 (black squares).

Comparisons of relations between bifurcation density (ρ_{bif}) and dune geometry (Figure 2.11) show that, in general, a negative correlation exists between ρ_{bif} and both *H*

and *L*, where the higher and longer dunes are found in areas of lower bifurcation density. The plots of ρ_{bif} against θ_{Lee} show that the data points are highly scattered for the two separate surveys around low tide, and no discernible correlation exists.

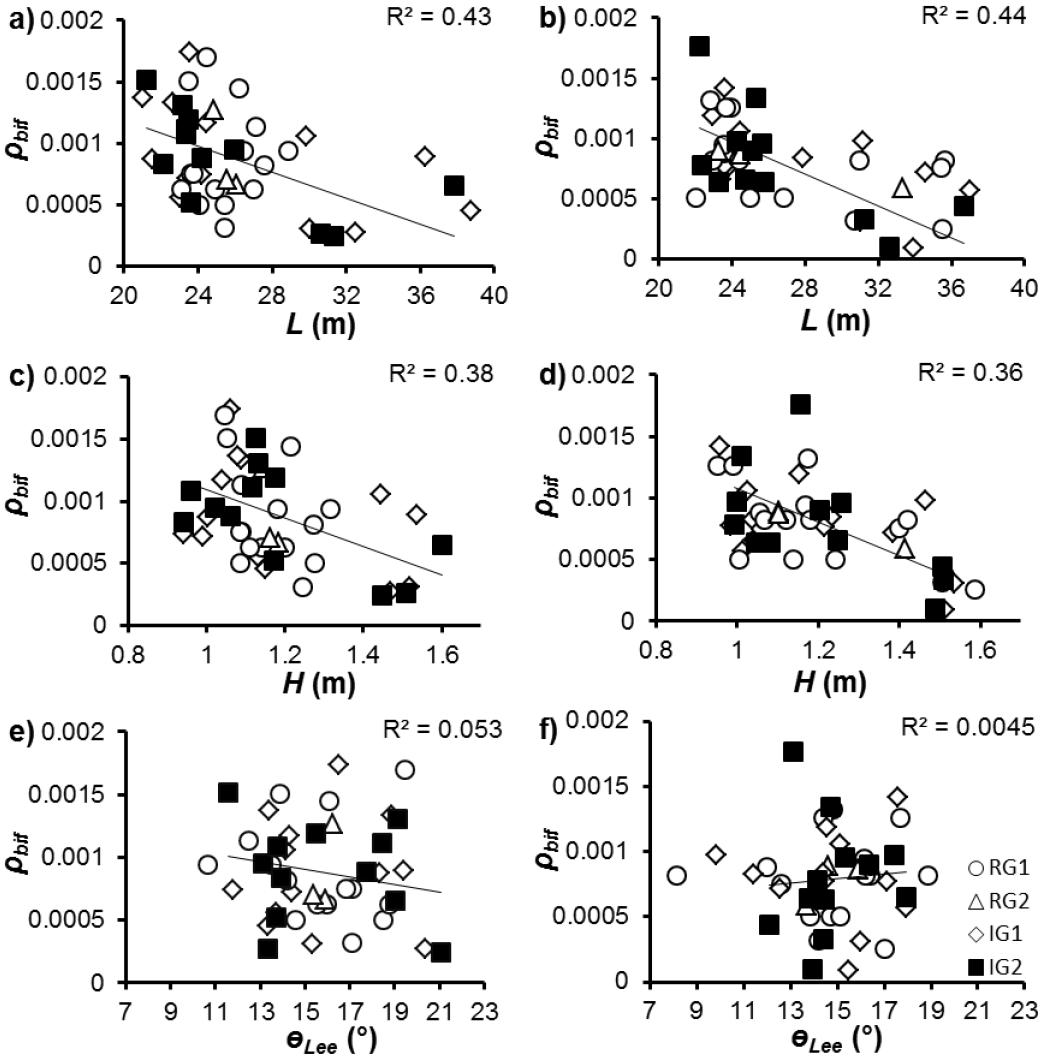

Figure 2.11. Plots of mean values of bifurcation density (ρ_{bif}) vs length (*L*) at a) LFT to LT, and b) LT to LRT, ρ_{bif} vs height (*H*) at c) LFT to LT, and d) LT to LRT and ρ_{bif} vs lee slope angle (θ_{Lee}) at e) LFT to LT, and f) LT to LRT. The trendlines (and values reported in text) pertain to those obtained from Irregular Grid 2 (black squares).

Plots comparing ρ_{bif} and *T* show opposing correlations between the LFT-LT period and the LT-LRT period, the former having a positive correlation, the latter having

a negative correlation. Comparing ρ_{bif} to q_s (Figure 2.12), the correlations are negative for both LFT to LT and LT to LRT. In order to investigate the differences between correlations of ρ_{bif} vs T and q_s, plots of q_s vs T were made for both time periods, and it was found that a negative correlation exists between LFT and LT, and a positive correlation between LT and LRT.

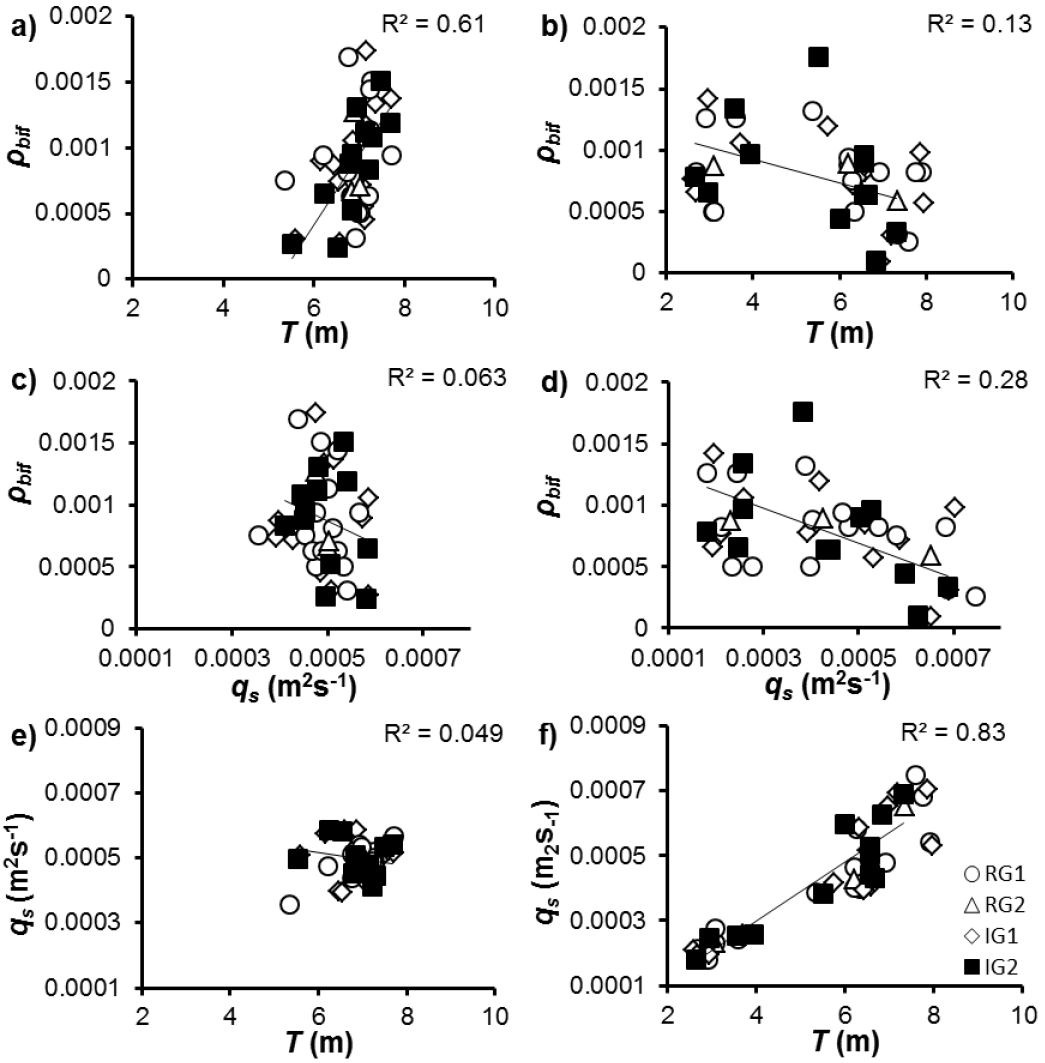

Figure 2.12. Plots of mean values of bifurcation density (ρ_{bif}) vs translation distance (T) at a) LFT to LT and b) LT to LRT, ρ_{bif} vs sediment flux (q_s) at c) LFT to LT and d) LT to LRT, and q_s vs T at e) LFT to LT and f) LT to LRT. The trendlines (and values reported in text) pertain to those obtained from Irregular Grid 2 (black squares).

2.4. Discussion

2.4.1. What is the Structure of the Crestlines in a Natural Dune Field?

Observations reported in this study were made in a tidally influenced, fluvially dominated reach of the Fraser Estuary, where river outflow velocities are heavily modulated by tidal influx. The crestlines in the study site displayed a 3D pattern throughout the course of the observed tidal cycle. When the dunes are separated into primary, channel-spanning continuous ridges, and smaller, secondary crestlines (bifurcations, defects), a single description of their planimetric morphology becomes complicated. The primary crestlines displayed a more two-dimensional morphology, and retained this configuration as they migrated under the influence of flow, while the bifurcated crests were more dynamic in response to flow and were found to appear, disappear, and shift with frequencies reflecting the strength of the river discharge.

Experiments on the development of sand ripples (Baas et al., 1993) and on dunes Venditti et al., (2005b) under unidirectional flow in flumes have shown that straight, low sinuosity ripples (2D) are intermediate in planform, and, given enough time, will develop into linguoid-shaped (3D) equilibrium morphology. A 3D morphology arises from a 2D bed through the propagation of perturbations in the dune crestlines downstream through time at a rate greater than the dune translation rates. This effects dune splitting, and creates the 3D dune morphology. The experiments by Baas et al., (1993) and Venditti et al (2005b) suggest that 2D bedforms are not in equilibrium with flow and that all systems eventually attain a 3D morphology, given steady flow for a long enough period of time. Here, I have shown that the 2D pattern of the primary crestlines persists over the course of the tidal cycle, suggesting that the variability of flow does not

afford the larger, channel-spanning dunes the equilibrium conditions necessary to become fully 3D. However, three-dimensionality of the bedform field exists via the presence and dynamic nature of secondary crestlines.

2.4.2. How do Crestlines Change in Response to Variable Flows?

Observations of bifurcated ripples in aeolian environments (Sharp, 1963; Werner and Kocurek, 1997) suggest that the number of defects associated with a ripple decreases over time, as the bed adjusts to an equilibrium state. Venditti et al. (2005b) found that an increase in shear stress forced a 3D dune field to reorganize to a 2D configuration, but this was transient, and the bed reverted to 3D as it equilibrated to the flow conditions. This indicates that while there may be similarities in fundamental attributes shared by bedforms, such as shape, spacing, and orientation to flow, that caution must be taken when comparing observations where fluid viscosities and densities differ (wind vs. water) and where different bedform types are present (ripples vs dunes). The number of bifurcations present on the bed over the course of the study period fluctuates, showing a pattern of decrease toward low tide, and then increasing after the maximum velocity toward high tide. The number of bifurcation 'deaths' outweighs 'births' on the falling tide, which indicates that the system is reorganizing to a more 2D morphology as shear stress increases with increasing tidal flux. Bifurcation birth dominates the rising limb of the tidal flux suggesting a shift toward a 3D bed configuration.

Werner and Kocurek (1997) suggest that defect density and relative migration speed exert a major control on the overall morphology of ripples. They argue that, on the basis of numerical modelling of aeolian sand dynamics, higher defect densities result

in faster field-scale reorientation rates than is seen in more linear formations with a lower proportion of defects. This does not appear to be the case with the dunes in this study, where the smaller dunes move at greater rates toward low tide, but do not influence the orientation or sinuosity of the larger dunes over the course of the study period. Rather, smaller dunes appear, die off and reorganize independently of the larger dunes.

2.4.3. How are the Dynamics of Dunes Linked to Dune Dimensions and Translation?

The primary crestlines in this study are associated with dunes that are generally greater, both in height and length, than bifurcated dunes, and this may be a key reason for their more planimetrically stable nature relative to the bifurcated crestlines. Toward low tide, mean channel velocity was approaching its maximum speed. Over low tide, the mean translation distance was higher where the bifurcation densities were higher and so the dunes that were smaller (both in terms of mean height and length) translated further. Previous studies have reported that smaller defects migrate more rapidly than larger crestlines to which they are connected (Coleman and Melville, 1994; Venditti et al., 2005a); my observations concur with these findings toward the low tide mark. Interestingly, the areas of lower bifurcation density are moving more sediment than those with a higher density of bifurcations, even though dunes in the higher density areas are translating farther. A larger dune requires the movement of a greater volume of sediment in order to shift compared to smaller dunes under the same flow conditions (Allen, 1982), and as such, would experience a greater mass transfer (higher q_s) for a translation distance of equal length.

Following low tide, dunes in areas of lower bifurcation density, which still correspond to the areas with the longest and highest dunes are now migrating farther and moving more sediment compared to the dunes in the higher bifurcation density areas.

There is a distinct difference in the relation between sediment flux and translation distance on the approach to low tide and immediately after it (Figure 2.12 panels e, f). Since translation distance is a function of sediment transport of the bed-material eroded from the upstream portion of the dune and deposited at the downstream end, it follows that their values would be strongly positively correlated. And yet, the results show that on the approach to low tide, there is no correlation between q_s and T, and what we are observing are similar flux rates for the entire bed, regardless of dune size or bifurcation density. The calculated value of q_s, using Equation 1, is also proportional to H, and so one would expect that if the bifurcated crestlines are translating approximately the same distances as the primary crestlines (under the assumption that the primary dunes have longer lengths and higher heights compared to bifurcated dunes, which is the general case, see Figure 2.11, panels a through d) then per dune, the amount of sediment moved would be less for the bifurcated dunes compared to the primary dunes. However, if there are enough bifurcated dunes migrating, then the total sediment moved could potentially be more than that moved by the primary dunes. The data show that the dunes in the more heavily bifurcated areas are actually moving farther than the dunes in the less bifurcated areas between LFT and LT (Figure 2.12, panel a), and when the total mass per polygon is compared for the bed, the more heavily bifurcated areas have greater total dune volume (Figure A30) .

After low tide, there is a strong positive correlation between q_s and T. The greatest number of bifurcation deaths are occurring on the channel bed between LFT and LT (Figure 2.7), which involves the amalgamation of the dune that 'dies' with a neighbouring dune. If many bifurcated dunes have amalgamated between LFT and LT, fewer smaller dunes can exist in these areas, so we would expect that measured dune values are getting larger and taller. The relations between H and L vs T, respectively, show positive correlations, and ρ_{bif} and T shows a negative correlation, so the areas with larger dunes and lower bifurcation densities are moving more sediment.

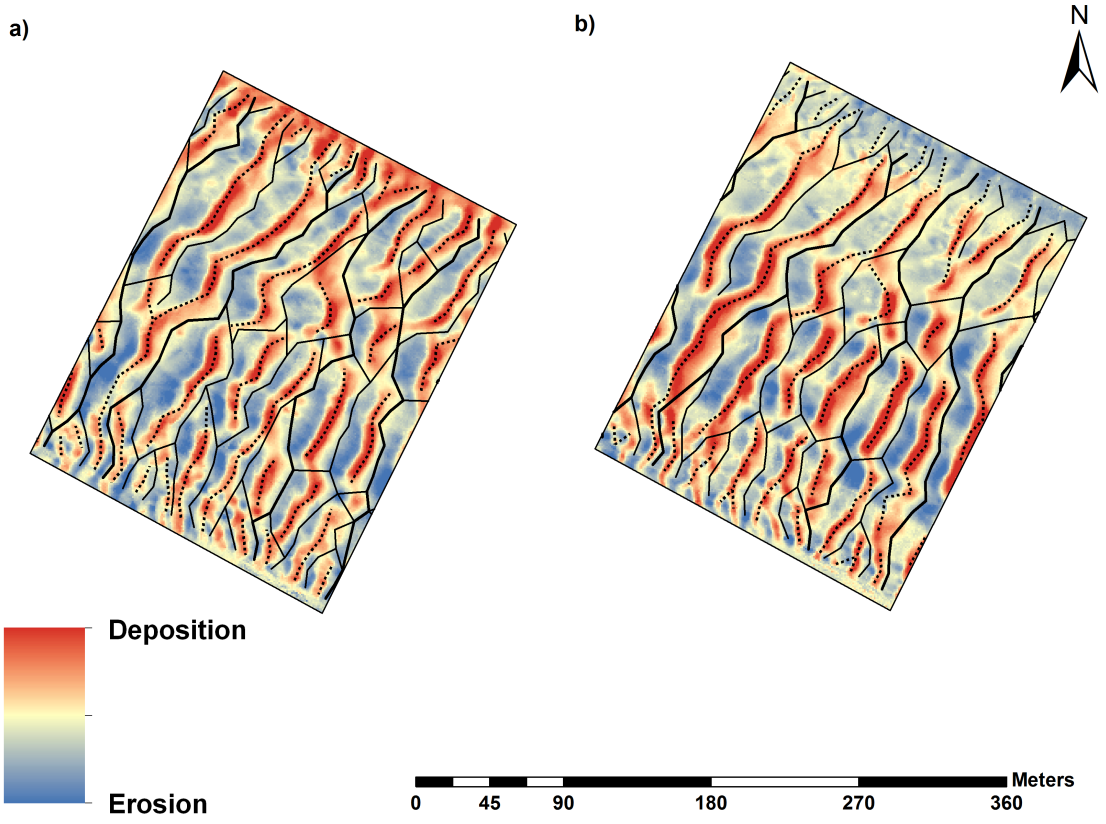

Figure 2.13. Maps showing the difference in elevation between a) LFT and LT and b) LT and LRT. Red indicates an increase in elevation (deposition) and blue indicates a decrease in elevation (erosion). Black lines denote crestlines (both primary and secondary), and dotted lines are the troughlines.

2.5. Conclusions

1. The bed of the study site displays a 3D planimetric morphology over the course of the observed tidal cycle, yet the primary crestlines show little change in sinuosity and maintain an overall 2D morphology. The reluctance of the primary crestlines to shift to a more 3D pattern is reflective of the bed's inability to reach equilibrium under constantly varying flow conditions.

2. Bifurcated crestlines appear and disappear throughout the study period. The number of bifurcation deaths outweighs births at high flows, reflecting the reorganization to a more 2D morphology. Bifurcation birth dominates at lower flow strengths, suggesting a shift toward a 3D bed configuration.

3. Larger dunes (with respect to both height and length) are found in areas of lower bifurcation density, while the higher density areas are populated with a greater number of smaller dunes.

4. Mean dune translation increases toward low tide, and decreases as the tidal maximum is approached. The areas on the bed with higher bifurcation density are composed of dunes that move farther before low tide, while the larger dunes with lower bifurcation densities move farther after low tide.

References

Ages, A., Woollard, A. (1976). The tides in the Fraser Estuary. Pacific Marine Science Report 76-5. Institute of Ocean Sciences, Victoria, B.C.

Allen, J.R.L. 1963. Henry Clifton Sorby and the sedimentary structures of sands and sandstones in relation to flow conditions. *Geol. Mijnbouw*. **42**: 223-228.

Allen, J.R.L., 1968. Current Ripples: their relation to patterns of water and sediment motion. Elsevier, New York, NY.

Allen, J.R.L., 1969. On the geometry of current ripples in relation to stability of fluid flow. *Geographiska Annaler*, **51**, 61-96.

Allen, J.R.L., 1973a. Features of cross-stratification due to random and other changes in bed forms. *Sedimentology*, **20**, 189-202.

Allen, J.R.L. (1973b). Phase differences between bed configuration and flow in natural environments, and their geological relevance. *Sedimentology*, **20**, 323-329.

Allen, J.R.L. (1974). Reaction, relaxation and lag in natural sedimentary systems: general principles, examples and lessons. *Earth Science Reviews*, **10**, 263-342.

Allen, J.R.L. 1976. Computational models for dune time-lag: general ideas, difficulties, and early results. *Sedimentary Geology*. **15**: 1-53.

Allen, J.R.L., 1982. Sedimentary structures: their character and physical basis. Vol.1. in: *Developments in Sedimentary structures*. Elsevier. Amsterdam.

Allen, J.R.L., Friend, P.F. (1976). Changes in intertidal dunes during two spring-neap cycles, Lifeboat Station Bank, Wells-Next-The-Sea, Norfolk. *Sedimentology*, **23**, 329-346.

Amsler, M. L., Schreider, M. I. (1999). Dune height prediction at floods in the Paraná River, Argentina. *River Sedimentation: theory and applications*, 615-620.

Ashley, G.M. (1990). Classification of large-scale subaqueous bedforms: a new look at an old problem. *Journal of Sedimentary Petrology*, **60**, 160-172.

Baas, J.H., 1994. A flume study on the development and equilibrium morphology of current ripples in very fine sand. Sedimentology, 41, 185-209.

Baas, J.H. (1999). An empirical model for the development and equilibrium morphology of current ripples in fine sand. *Sedimentology*, **46**, 123-138.

Baas, J.H., Oost, A.P., Sztano, O.K., de Boer, P.L., Postma, G. (1993). Time as an independent variable for current ripples developing towards linguoid equilibrium morphology. *TerraNova*, **5**, 29-35.

Bennett, S. J., Best, J.L. (1995), Mean flow and turbulence structure over fixed, two-dimensional dunes: Implications for sediment transport and bedform stability, *Sedimentology*, **42**, 491‐513.

Bennett, S.J., Best, J.L. (1996). Mean flow and turbulence structure over fixed ripples and the ripple-dune transition. In: *Coherent Flow Structures in Open Channels.* Eds: Ashworth, P.J., Bennett S.J., Best J.L., McLelland S.J. John Wiley, Hoboken, NJ, pp. 281-304.

Best, J.L. (1992). On the entrainment of sediment and initiation of bed defects: insights from recent developments within turbulent boundary layer research. *Sedimentology*, **39**, 797-811.

Best J.L. (2005). The fluid dynamics of river dunes: A review and some future research directions. *Journal of Geophysical Research*, **110**, F04S02, doi:10.1029/2004JF000218.

Best, J.L., Kostaschuk, R. (2002). An experimental study of turbulent flow over a low-angle dune. *Journal of Geophysical Research*, **107**, doi:10.1029/2000JC000294.

Bradley, R.W., Venditti, J.G., Kostaschuk, R.A., Church, M.A., Hendershot, M.L., Allison, M.A. (2013). Flow and sediment suspension events over low angle dunes: Fraser Estuary, Canada. *Journal of Geophysical Research*, **118**, doi:10.1002/jgrf.20118.

Bridge, J.S., Best, J.L., (1988). Flow, sediment transport and bedform dynamics over the transition from dunes to upper-stage plane beds: implications for the formation of planar laminae. *Sedimentology*, **35**, 753-763.

Carling, P.A., Gölz, E., Orr, H.G., Radecki-Pawlik, A. (2000). The morphodynamics of fluvial sand dunes in the River Rhine near Mainz, Germany, Part I: Sedimentology and morphology. *Sedimentology*, **47**, 227-252.

Coleman, S. E., Melville, B. W. (1994). Bed-form development. *Journal of Hydraulic Engineering*, **120**, 544-560.

Coleman, S.E., Melville, B.W. (1996). Initiation of bedforms on a flat sand bed. *Journal of Hydraulic Engineering*, **122**, 301-310.

Coleman S.E., Nikora, V.I., McLean, S.R., Clunie, T.M., Schicke, T., Melville, B.W. (2006). Equilibrium hydrodynamics concept for developing dunes. *Physics of Fluids*, **18**, 105104, doi:10.1063/1.23583332.

Colombini, M., Stocchino, A. (2007). Bifurcation patterns in dune and antidune stability. *Proceedings of the 5th IAHR Symposium on River, Coastal, and Estuarine Morphodynamics*. 949-960.

Dalrymple, R.W., Rhodes, R.N. (1995). Estuarine Dunes and Bars. In: Geomorphology and Sedimentology of Estuaries. (Ed. G.M.E. Perillo). Elsevier, Amsterdam.

Dashtgard, S.E., Venditti, J.G., Hill, P.R., Sisulak, C.F., Johnson, S.M., De La Croix, A.D. (2012). Sedimentation across the tidal-fluvial transition in the Lower Fraser River, Canada. *The Sedimentary Record*, **10**, doi:10.2110/sedred.2012.4.

Davis, R.A., Flemming, B.W. (1991). Time-series study of mesoscale tidal bedforms, Martens Plate, Wadden Sea, Germany. In: Clastic Tidal Sedimentology. (Eds. D.G. Smith, G.E. Reinson, B.A. Zaitlin, and R.A. Rahmani) Canadian Society of Petroleum Geologists Special Publication. Pp. 275-282.

Ewing, R.C., Kocurek, G., Lake, L.W. (2006). Pattern analysis of dune-field parameters. *Earth Surface Processes and Landforms,* **31**, 1176-1191.

Fernandez, R., Best, J., López, F. (2006). Mean flow, turbulence structure, and bed form superimposition across the ripple-dune transition. *Water Resources Research*, **42**, W05406, doi:10.1029/2005WR004330.

Gabel, S.L. (1993). Geometry and kinematics of dunes during steady and unsteady flows in the Calamus River, Nebraska, USA. *Sedimentology*, **40**, 237-269.

Gyr, A., Schmid, A. (1989). The different ripple formation mechanism. *Journal of Hydraulic Research,* **27**, 61-74.

Hand, B.M., Bartberger, C.E. (1988). Leeside sediment fallout patterns and the stability of angular bedforms. *Journal of Sedimentary Petrology*, **58**, 33-42.

Huntley, D.A., Coco, G., Bryan, K.R., Murray, A.B. (2008). Influence of "defects" on sorted bedform dynamics. *Geophysical Research Letters,* **35***.* L02601. doi:10.1029/2007GL030512.

Johns, B., Soulsby, R.L., Chesher, T.J. (1990). The modelling of sandwave evolution resulting from suspended and bedload transport of sediment. *Journal of Hydraulic Research,* **28**, 355-374.

Julien, P.Y., Klaassen, G.J., ten Brinke, W.B.M., Wilbers, A.W.E. (2002). Case study: bed resistance of Rhine River during the 1998 flood. *Journal of Hydraulic Engineering*, **128**, 1042-1050.

Kostaschuk, R. (2000). A field study of turbulence and sediment dynamics over subaqueous dunes with flow separation. *Sedimentology*, **47**, 519-531.

Kostaschuk, R. (2006). Sediment transport mechanics and subaqueous dune morphology. In: *River, Coastal and Estuarine Morphodynamics*. London. Taylor and Francis. 795-801.

Kostaschuk, R.A., Luternauer, J.L. (1989). The role of the salt wedge in sediment resuspension and deposition: Fraser River Estuary, Canada. *Journal of Coastal Research*, **5**, 93-101.

Kostaschuk, R.A., Church, M.A., Luternauer, J.L. (1989). Bedforms, bed material, and bedload transport in a salt-wedge estuary: Fraser River, British Columbia. *Canadian Journal of Earth Science*, **26**, 1440-1452.

Kostaschuk, R.A., Church, M.A., Luternauer, J.L. (1992). Sediment transport over salt-wedge intrusions: Fraser River estuary, Canada. *Sedimentology*, **39**, 305-317.

Kostaschuk, R.A., Ilersich, S.A. (1995). Dune geometry and sediment transport: Fraser River, British Columbia. In: *River Geomorphology*, (Ed. E. J. Hickin), pp. 19-36. John Wiley and Sons, Chichester.

Kostaschuk, R.A., Villard, P.V. (1996). Flow and sediment transport over large subaqueous dunes: Fraser River, Canada. *Sedimentology*, **43**, 849-863.

Kostaschuk, R.A., Villard, P.V. (1999). Turbulent sand suspension over dunes. *Special Publications of the International Association of Sedimentologists*, **28**, 3-13.

Kostaschuk, R., Best, J. (2005). Response of sand dunes to variations in tidal flow: Fraser Estuary, Canada. *Journal of Geophysical Research*, **110**, F04S04, doi:10.1029/2004JF000176.

Kostaschuk, R., Shugar, D.H, Best, J.L., Parsons, D.R., Lane, S.N., Hardy, R., Orfeo, O. (2009). Suspended sediment transport and deposition over a dune: Río Paraná, Argentina. Earth Surface Processes and Landforms, 34, 1605-1611.

Landry, W., Werner, B.T. (1994). Computer simulations of self-organized wind ripple patterns. *Physica D: Nonlinear Phenomena*, **77**, 238-260.

Leeder, M.R. (1980). On the stability of lower stage plane beds and the absence of ripples in coarse sand. *Journal of the Geological Society of London*, **137**, 423-429.

Leeder, M.R. (1983). On the interactions between turbulent flow, sediment transport and bedform mechanics in channelized flows. *Special Publications of the International Association of Sedimentologists*, **6**, 5-18.

Lin, C.Y., Venditti, J.G. (2013). An empirical model of subcritical bedform migration. *Sedimentology*, **60**, doi: 10.1111/sed.12056.

Lyn, D.A., 1993. Turbulence measurements in open-channel flow over bedforms. *Journal of Hydraulic Engineering*. **119**: 306-326.

Maddux, T.B., Nelson, J.M., McLean, S.R. (2003a). Turbulent flow over three-dimensional dunes: 1. Free surface and flow response. *Journal of Geophysical Research*, **108**, doi:10.1029/2003JF000017.

Maddux, T.B., McLean, S.R., Nelson, J.M. (2003b). Turbulent flow over three-dimensional dunes: 2. Fluid and bed stresses. *Journal of Geophysical Research*, **108**, doi:10.1029/2003JF000018.

Martin, R.L., Jerolmack, D.J. (2013). Origin of hysteresis in bed form response to unsteady flows. *Water Resources Research*, **49**, 1314-1333.

McLean, S.R., J.M. Nelson, and S.R. Wolfe. (1994). Turbulence structure over two-dimensional bedforms: Implications for sediment transport. *Journal of Geophysical Research.* **99**: 12,729-12,747.

McLean, D.G., Church, M.A., Tassone, B. (1999). Sediment transport along lower Fraser River. 1. Measurements and hydraulic computations. *Water Resources Research,* **35**, 2533-2548.

McElroy, B., Mohrig, D. (2009). Nature of deformation of sandy bed forms. *Journal of Geophysical Research*, **114**, F00A04, doi:10.1029/2008JF001220.

Mohrig, D., Smith, J. (1996). Predicting the Migration Rates of Subaqueous Dunes. *Water Resources Research*, **32**, 3207-3217.

Nelson, J.M., S.R. McLean, and S.R. Wolfe. (1993). Mean flow and turbulence over two-dimensional bedforms. *Water Resources Research*. **29**: 3935-3953.

Nittrouer, J.A., Allison, M.A., Campanella, R. (2008). Bedform transport rates for the lowermost Mississippi River. *Journal of Geophysical Research*, **113**, F03004, doi:1029/2007JF000795.

Paarlberg A.J., Dohmen-Janssen, C.M., Hulscher, S.J.M.H., Termes, P. (2007). A parameterization of flow separation over subaqueous dunes. *Water Resources Research*, **43**, W12417, doi:10.1029/2006WR005425.

Parsons, D.R., Best, J.L., Orfeo, O., Hardy, R.J., Kostaschuk, R., Lane, S.N. (2005). Morphology and flow fields of three-dimensional dunes, Rio Paraná, Argentina: Results from simultaneous multibeam echo sounding and acoustic Doppler current profiling. *Journal of Geophysical Research,* **110**, doi:10.1029/2004JF000231.

Pretious, E.S., Blench, T. (1951). Final report on special observations on bed movement in the lower Fraser River at Ladner Reach during the 1950 freshet. National Research Council of Canada, Fraser River Model Project.

Raudkivi, A.J. (1963). Study of sediment ripple formation. ASCE, *Journal of the Hydraulics Division*, **89**, 15-33.

Raudkivi, A.J. (1966). Bedforms in alluvial channels. *Journal of Fluid Mechanics*, **26**, 507-514.

Reson Inc. (2002). 8101 Multibeam sounder, Users Manual, 281 pp., Goleta, Calif.

Reson Inc. (2009). SeaBat 7101 High-Resolution Multibeam Echosounder System, Operator's Manual. 168 pp, Denmark.

Rhodes, R.N. (1992). Hydrodynamics and the morphology, migration and structure of subaqueous dunes, Minas Basin, Canada. M.Sc. Thesis, Queen's University, Kingston, Ontario.

Roden, J.E. (1998). The sedimentology and dynamics of mega-dunes, Jamuna River, Bangladesh. Ph.D. Thesis, Department of Earth Science, University of Leeds, Leeds, UK.

Saunderson, H. C., Lockett, F. P. J. (1983). Flume experiments on bedforms and structures at the dune-plane bed transition. *Modern and Ancient Fluvial Systems: International Association of Sedimentologists,* Special Publication, **6**, 49-58.

Sharp, R.P. (1963). Wind Ripples. *Journal of Geology*, **71**, 617-636.

Shugar, D.H., Kostaschuk, R., Best, J.L., Parsons, D.R., Lane, S.N., Orfeo, O., and Hardy, R. (2010). On the relationship between flow and suspended sediment transport over the crest of a sand dune, Rio Parana, Argentina. *Sedimentology*, **57**, 252-272.

Simons, D.B., Richardson, E.V., Nordin, C.F. (1965). Bedload equation for ripples and dunes. USGS Professional Paper, 462-H, 1-9.

Smith, J.D. and S.R. McLean. (1977). Spatially averaged flow over a wavy surface. *Journal of Geophysical Research*, **82**, 1735-1746.

Sorby. H.C. (1852). On the oscillations of the currents drifting the sandstone beds of the southeast of Northumberland, and on the general direction in the coalfield in the neighbourhood of Edinburgh. *Proceedings of the Yorkshire Geological Society*, **3**, 232-240.

Sorby. H.C. (1908). On the application of quantitative methods to the study of the structure and history of rocks. *Quarterly Journal of the Geologic Society of London,* **64**, 171-232.

Soulsby, R.L., Atkins, R., Waters, C.B., Oliver, N. (1991). Field measurements of suspended sediment over sandwaves. In: *Sand Transport in Rivers, Estuaries, and Sea*. Eds: R.L. Soulsby and R.E. Bettess. A.A. Balkema, Brookfield, Vt.

Southard, J.B., Boguchwal, L.A. (1990a). Bed configurations in steady unidirectional water flow part 1. Scale model study using fine sands. *Journal of Sedimentary Research*, **60**, 649-657.

Southard, J.B., Boguchwal, L.A. (1990b). Bed configurations in steady unidirectional water flow part 2. Synthesis of flume data. *Journal of Sedimentary Petrology*, **60**, 658-679.

Southard, J.B., Dingler, J.R. (1971). Flume study of ripple propagation behind mounds on flat sand beds. *Sedimentology*, **16**, 251-263.

Sukhodolov, A.N., Fedele, J.J., Rhoads, B.L. (2006). Structure of flow over alluvial bedforms: an experiment on linking field and laboratory methods. *Earth Surface Processes and Landforms*, **31**, 1292-1310.

ten Brinke, W.B.M. (1997). Temporal variability in aggregate size and settling velocity in the Oosterschelde (The Netherlands). *Cohesive Sediments*, pp. 63-73.

ten Brinke, W.B.M., Wilbers, A.W.E., Wesseling, C. (1999). Dune Growth, decay and migration rates during a large-magnitude flood at a sand and mixed sand–gravel bed in the Dutch Rhine River System. *Fluvial Sedimentology VI*, 15-32.

Terwindt, J.H.J., Brouwer, M.J N. (1986).The behaviour of intertidal sandwaves during neap-spring tide cycles and the relevance to paleoflow reconstructions. *Sedimentology*. **33**: 1-31.

Topping, D. J., Wright, S.A., Melis, T.S., Rubin, D.M. (2007). High-resolution measurements of suspended-sediment concentration and grain size in the Colorado River in Grand Canyon using a multi-frequency acoustic system. In *Proceedings of the 10th International Symposium on River Sedimentation*, August 1–4, Moscow, Russia.

van den Berg, J.H. (1987). Bedform migration and bed-load transport in some rivers and tidal environments. *Sedimentology*, **34**, 681-698.

Venditti, J.G., Bennett, S.J. (2000). Spectral analysis of turbulent flow and suspended sediment transport over fixed dunes. *Journal of Geophysical Research*, **105**, 22035-22047.

Venditti, J.G., Bauer, B.O. (2005). Turbulent flow over a dune: Green River, Colorado. *Earth Surface Processes and Landforms*, **30**, 289-304, doi: 10.1002/esp.1142.

Venditti, J.G., Church, M.A., and Bennett, S.J. (2005a). Morphodynamics of small-scale superimposed sandwaves over migrating dune bedforms, *Water Resources Research*, **41**, W10423, doi:10.1029/2004WR003461.

Venditti, J.G., Church, M.A., and Bennett, S.J. (2005b). On the transition between 2D and 3D dunes. *Sedimentology*, **52**, 1343–1359, doi: 10.1111/j.1365-3091.2005.00748.x.

Venditti, J.G., Church, M., Bennett, S.J. (2005c). Bed form initiation from a flat sand bed. *Journal of Geophysical Research*, **110**, F01009. doi: 10.1029/2004JF000149.

Venditti, J.G. (2007). Turbulent flow and drag over fixed two- and three-dimensional dunes. *Journal of Geophysical Research*, **112**, F04008. doi:10.1029/2006JF000650.

Venditti, J.G. (2013), Bedforms in sand-bedded rivers. In *Treatise on Geomorphology*, Fluvial Geomorphology, vol. 9, edited by J. F. Shroder (Editor-in-chief), E. Wohl, pp. 137–162, (Volume Editor), Academic Press, San Diego.

Villard, P.V., Church, M.A. (2003). Dunes and associated sand transport in a tidally influenced sand-bed channel: Fraser River, British Columbia. *Canadian Journal of Earth Science*, **40**, 115-130.

Villard, P.V., Church, M.A. (2005). Bar and dune development during a freshet: Fraser River Estuary, British Columbia, Canada. *Sedimentology*, **52**, 737-756.

Western Canada Hydraulic Laboratories Ltd. (1977). *Feasibility study, development of a forty-foot draft navigation channel, New Westminster to Sandheads*. Unpublished report to Public Works Canada.

Werner, B.T. (1999). Complexity in natural landform patterns. *Science*, **284**, doi: 10.1126/science.284.5411.102.

Werner, B.T., Kocurek, G. (1997). Bedform dynamics: Does the tail wag the dog?, *Geology*, **25**, 771– 774.

Werner, B.T., Kocurek, G. (1999). Bedform spacing from defect dynamics. *Geology*, **27**, 727-730.

Wiberg, P.L., Nelson, J.M. (1992). Unidirectional flow over asymmetric and symmetric ripples. *Journal of Geophysical Research*, **97**, 12745-12761.

Wijbenga, J.H.A., Klaassen, G.J. (1983). Changes in bedform dimensions under unsteady flow conditions in a straight flume. *Special Publication of the International Association of Sedimentologists*, 6, 35-48.

Wilbers, A. W. E. 2004. Prediction of bedform characteristics and bedform roughness in large rivers, Ph.D. thesis, Utrecht Univ., Utrecht, Netherlands.

Wilbers, A.W.E., ten Brinke, W.B.M. (2003). The response of subaqueous dunes to floods in sand and gravel bed reaches of the Dutch Rhine. *Sedimentology*, **50**, 1013-1034.

Yalin, M.S. 1972. *Mechanics of sediment transport*. Pergamon Press, Oxford.

Yalin, M.S., Karahan, E. (1979). Steepness of sedimentary dunes. *Journal of the Hydraulic Division*, **105**, 381-392.

Appendix

Supplemental figures

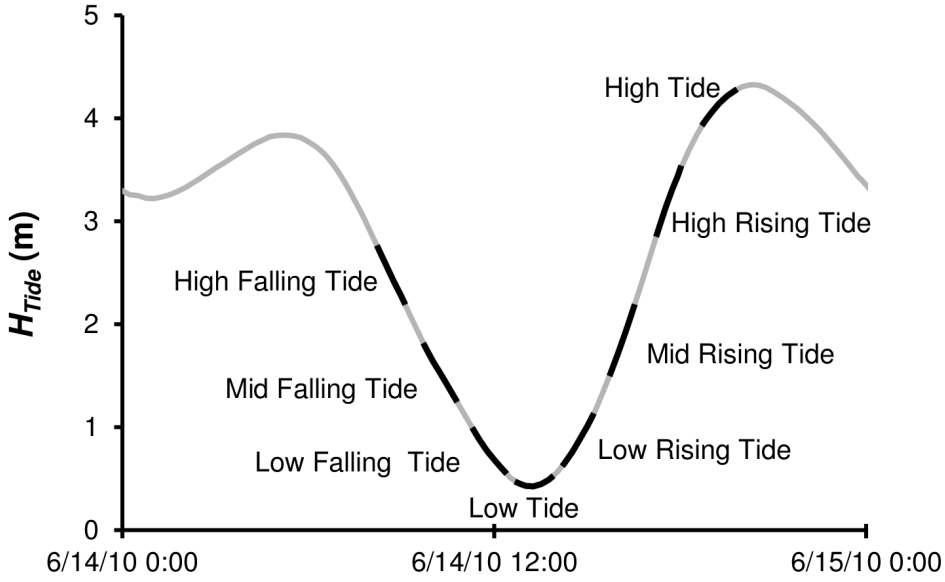

Figure A1. **Tidal cycle for 14 June 2010. Grey line shows the tidal stage (m) over which data were collected and the black lines are the individual surveys taken to characterize the fall and rise of the tide.**

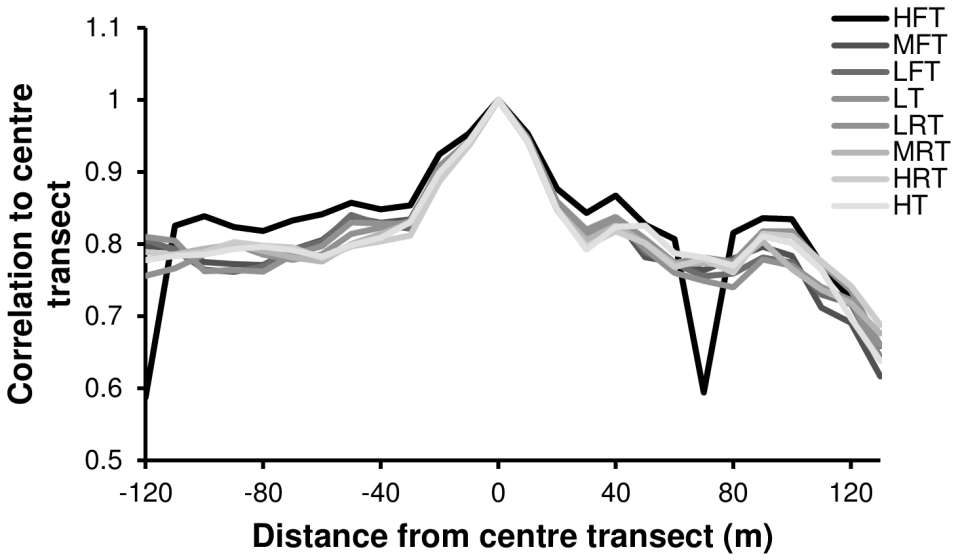

Figure A2. **Cross-stream correlation of topographic data for each survey period over the tidal cycle.**

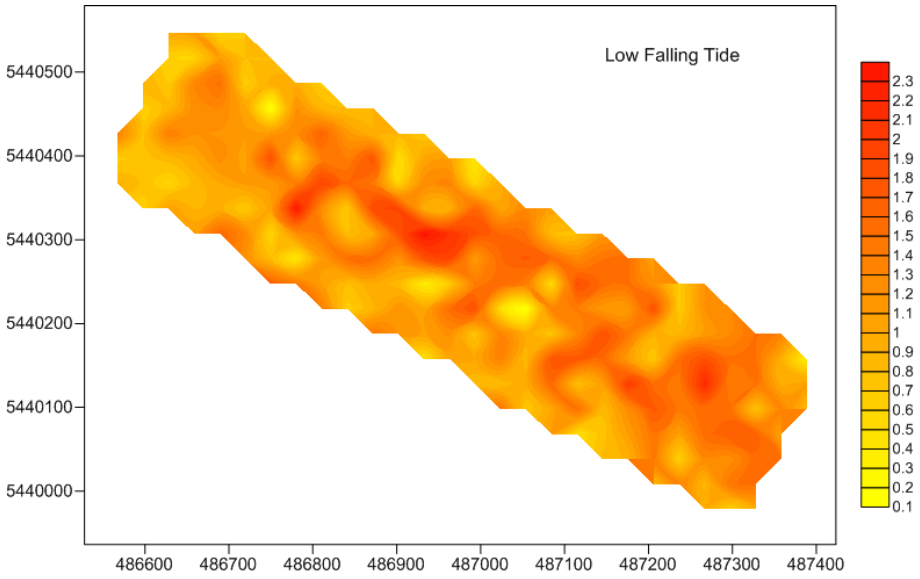

Figure A3. **Spatial variability map of dune height distribution (in metres) at Low Falling Tide.**

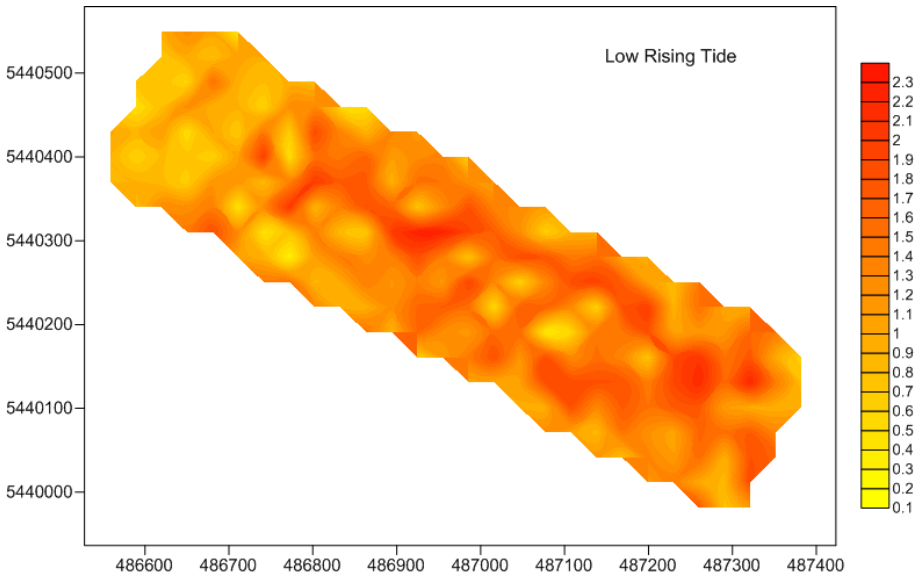

Figure A4. **Spatial variability map of dune height distribution (in metres) at Low Rising Tide.**

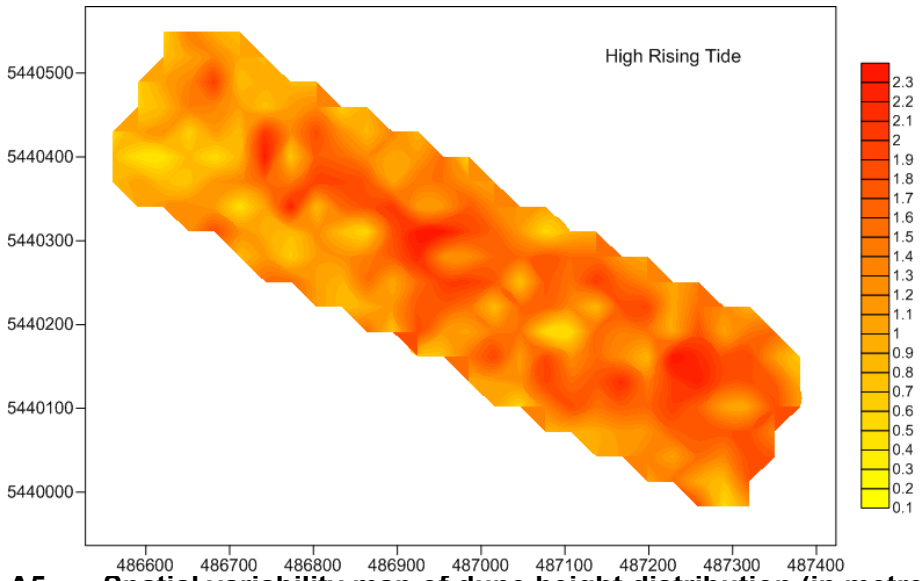

Figure A5. **Spatial variability map of dune height distribution (in metres) at High Rising Tide.**

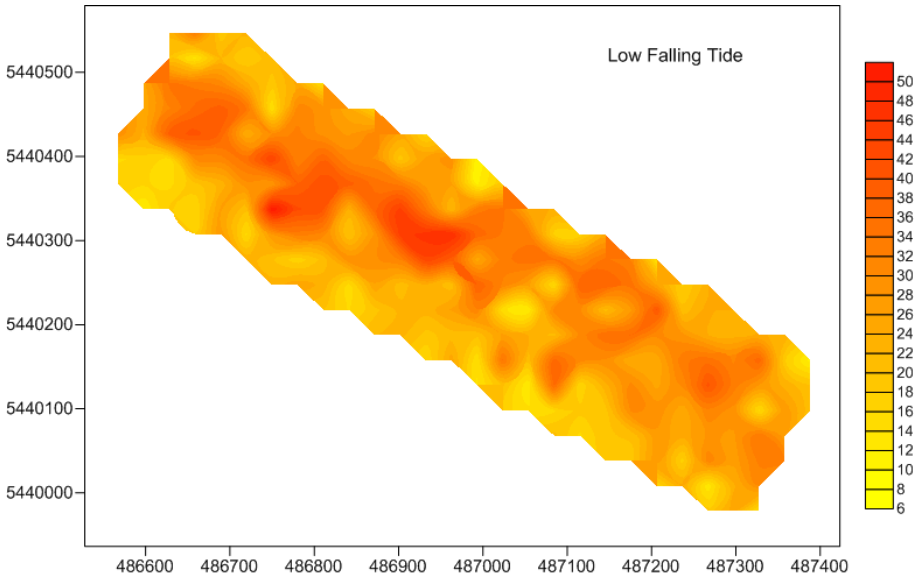

Figure A6. **Spatial variability map of dune length distribution (in metres) at Low Falling Tide.**

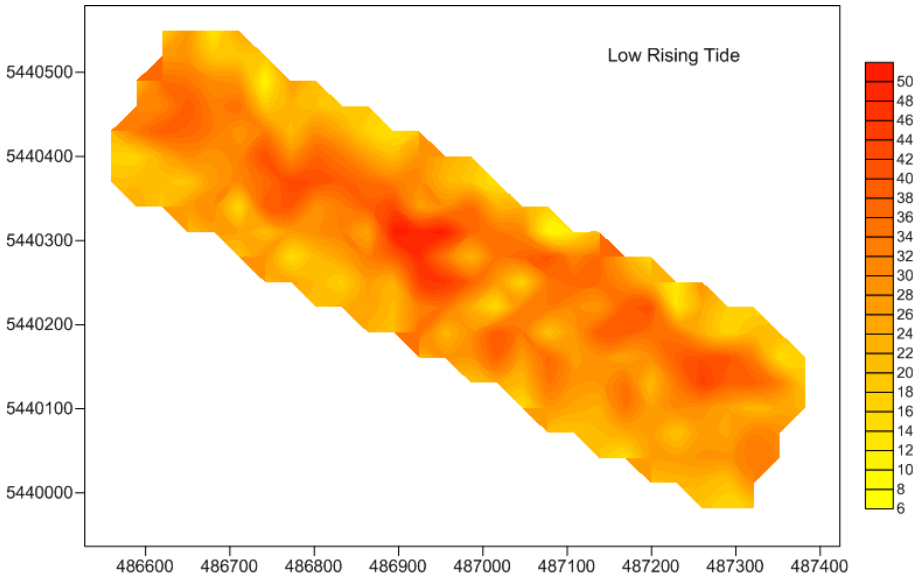

Figure A7. **Spatial variability map of dune length distribution (in metres) at Low Rising Tide.**

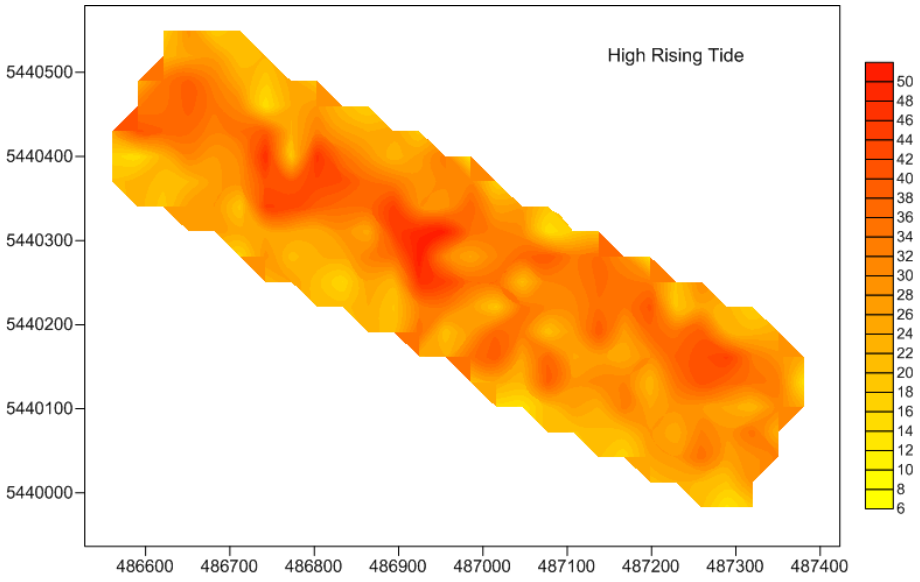

Figure A8. **Spatial variability map of dune length distribution (in metres) at High Rising Tide.**

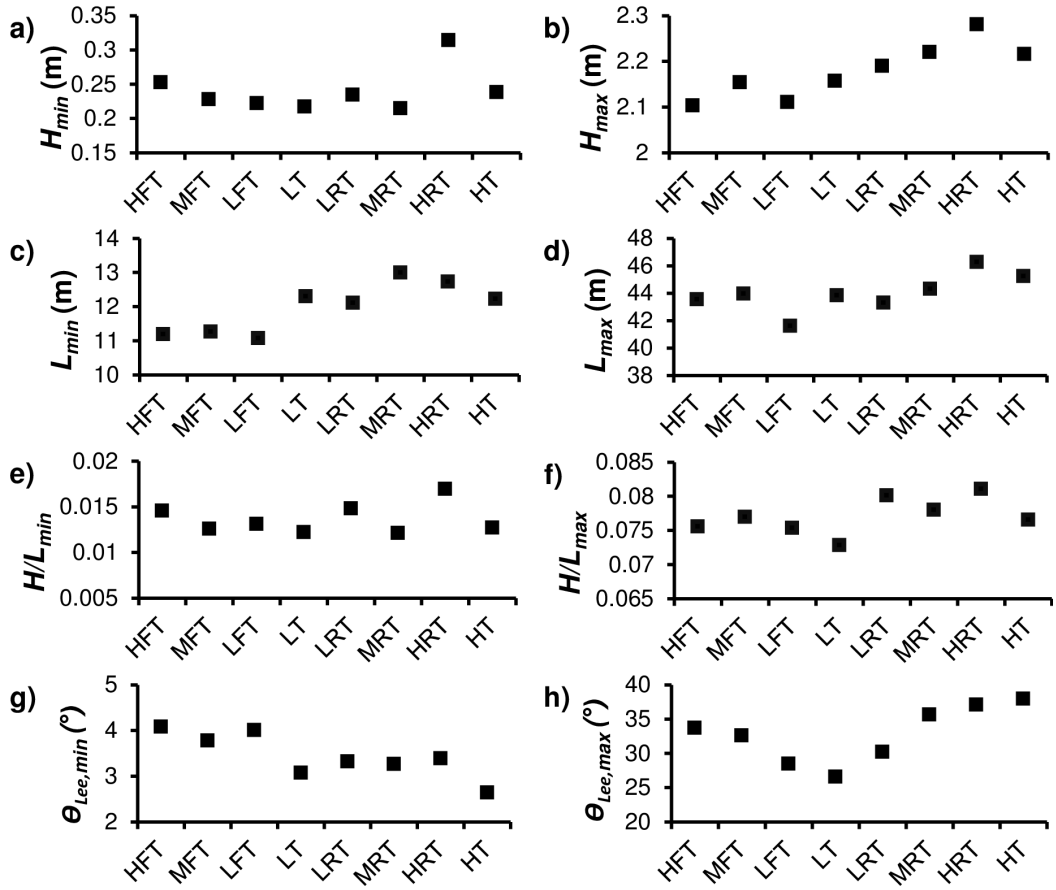

Figure A9. Maximum and minimum measured values of dune geometric properties over the survey period.

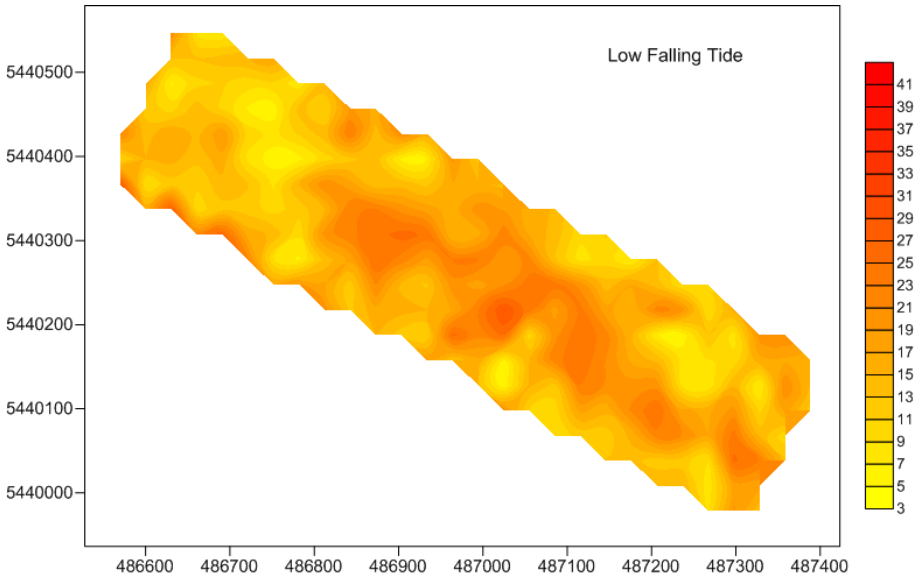

Figure A10. Spatial variability map of dune lee slope angle distribution (in ˚) at Low Falling Tide.

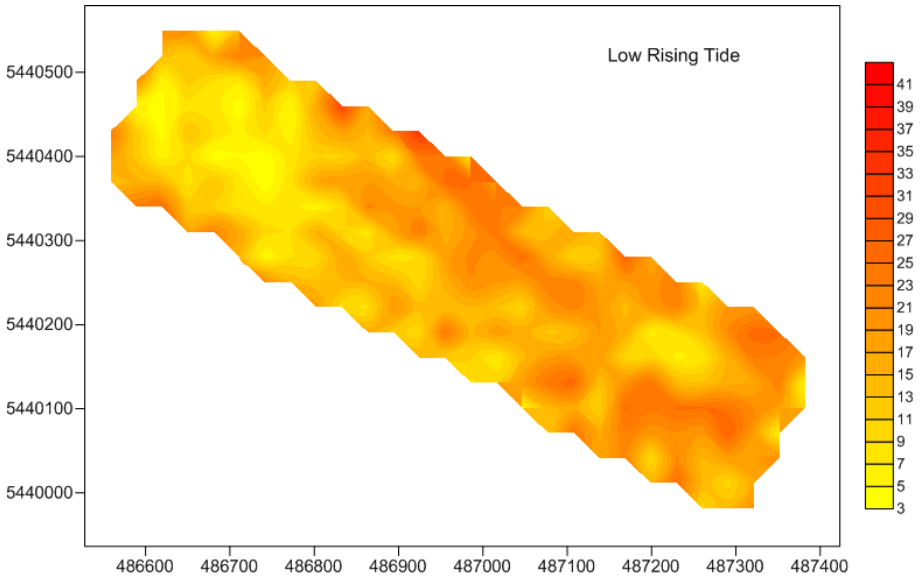

Figure A11. Spatial variability map of dune lee slope angle distribution (in ˚) at Low Rising Tide.

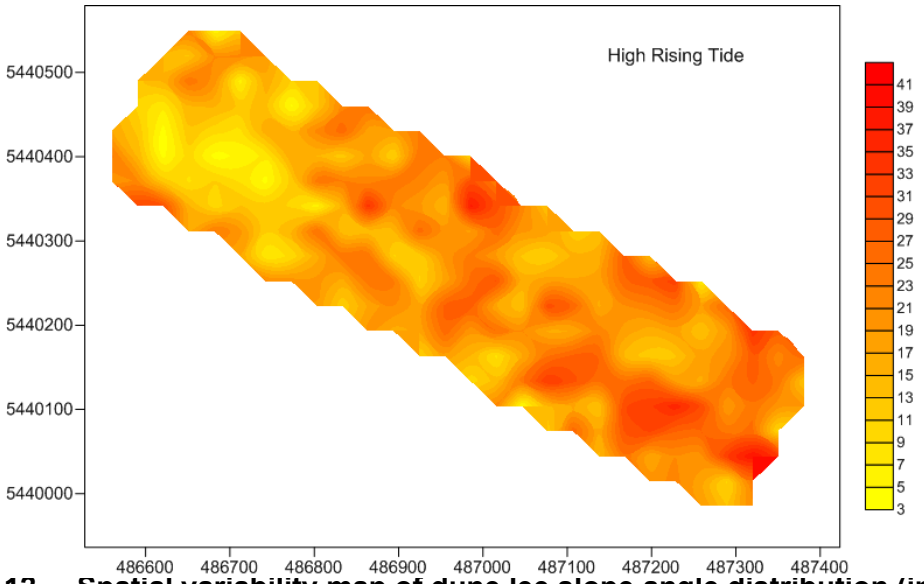

Figure A12. Spatial variability map of dune lee slope angle distribution (in ˚) at High Rising Tide.

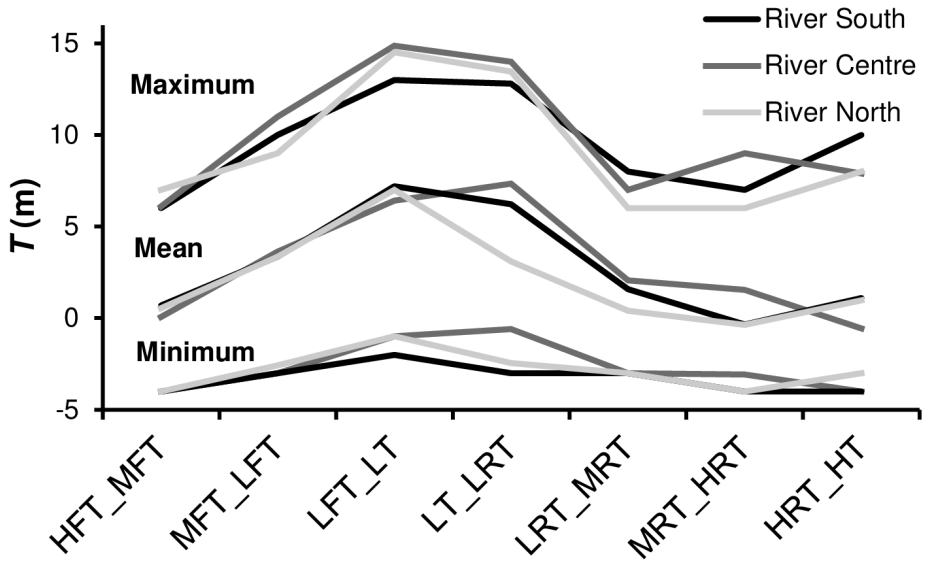

Figure A13. Maximum, mean, and minimum measured translation distances measured over the survey period for the south, centre, and north sections of the study site.

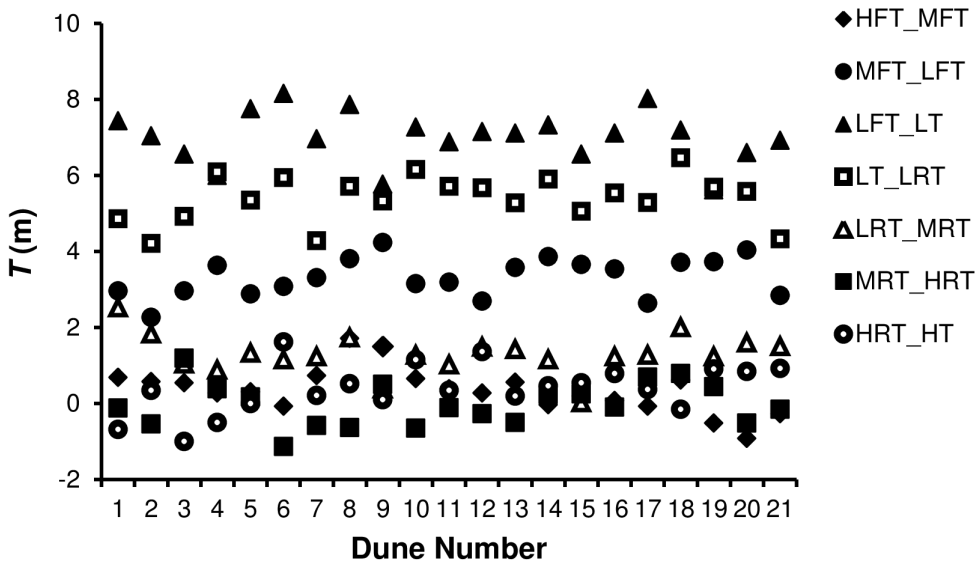

Figure A14. **Mean translation distances for each primary dune for each survey interval. Dune 1 is the upstream-most primary dune.**

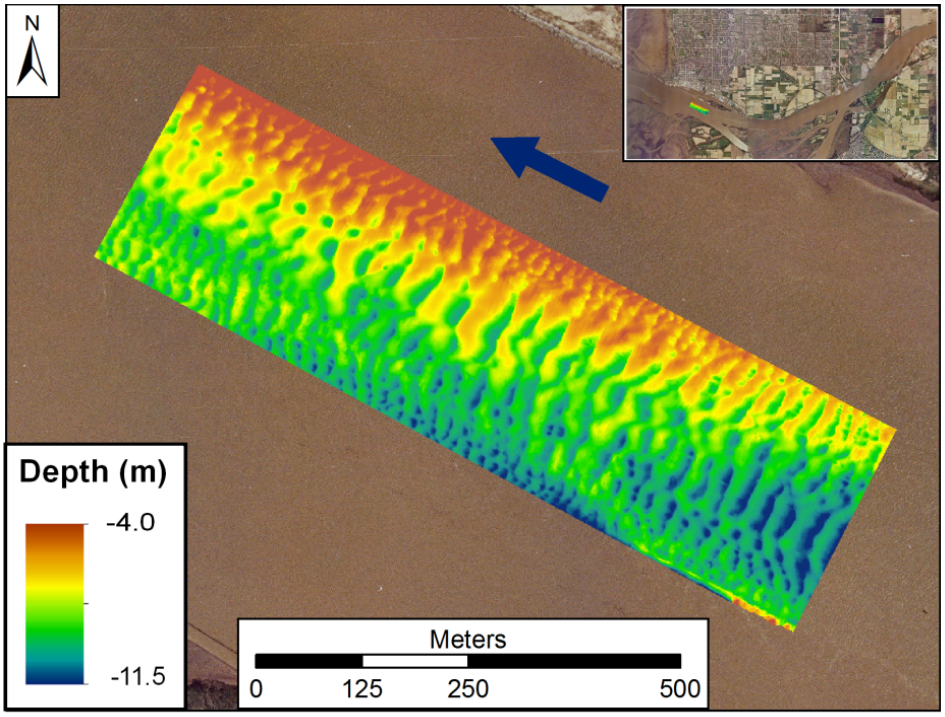

Figure A15. **Bathymetric map of survey site at High Falling Tide.**

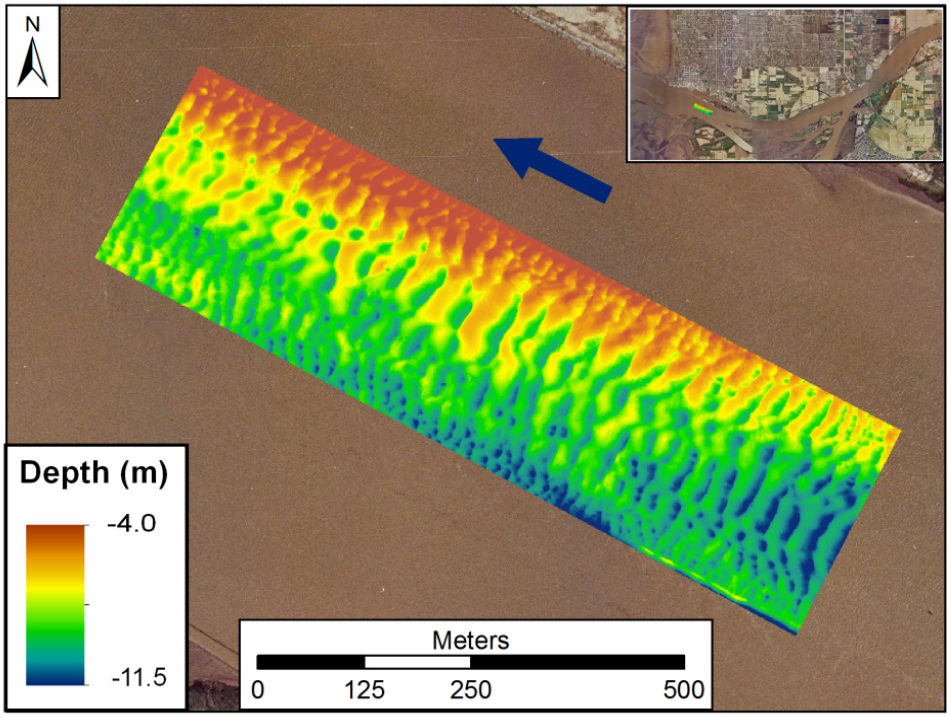

Figure A16. Bathymetric map of survey site at Mid Falling Tide.

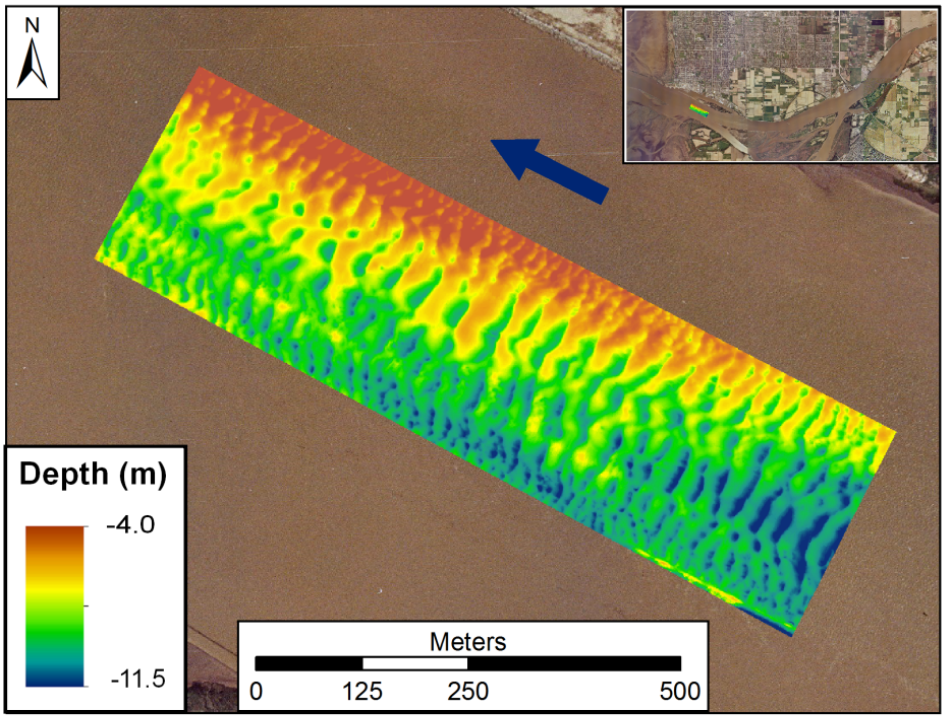

Figure A17. Bathymetric map of survey site at Low Falling Tide.

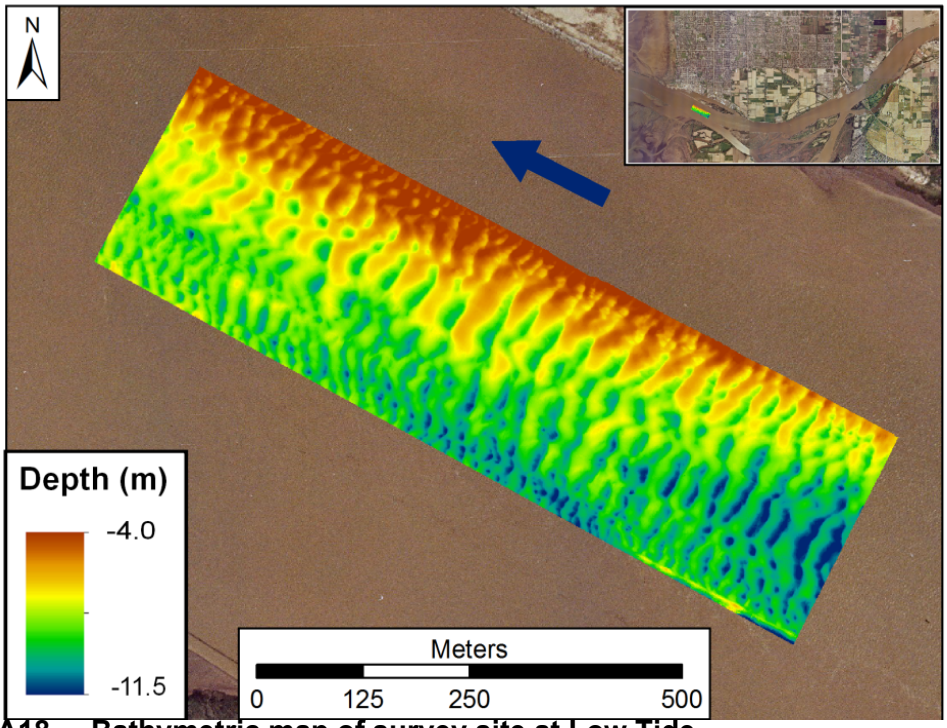

Figure A18. Bathymetric map of survey site at Low Tide.

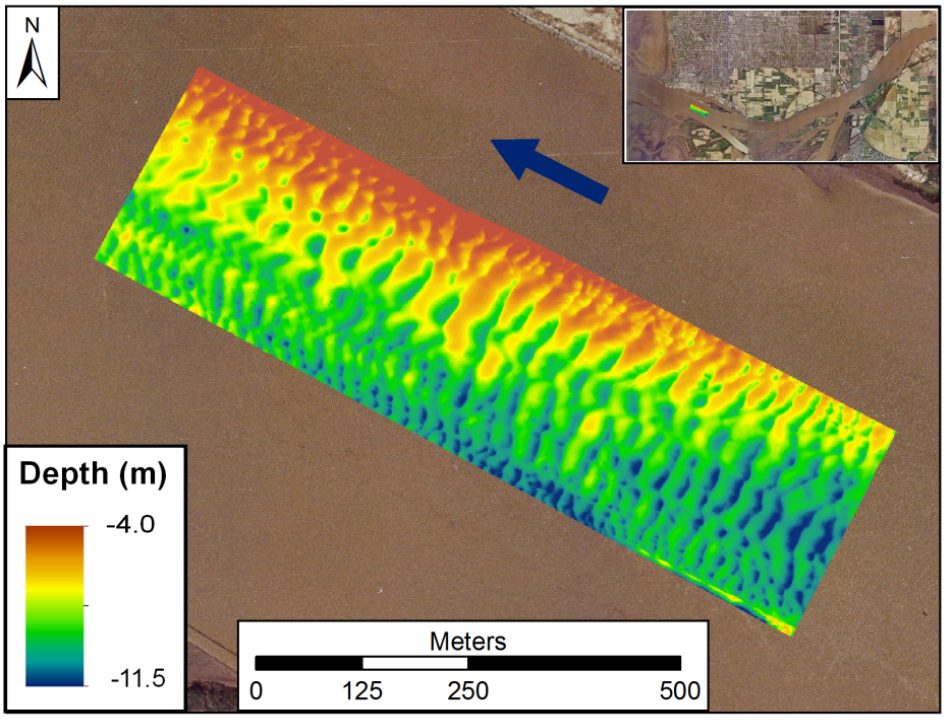

Figure A19. Bathymetric map of survey site at Low Rising Tide.

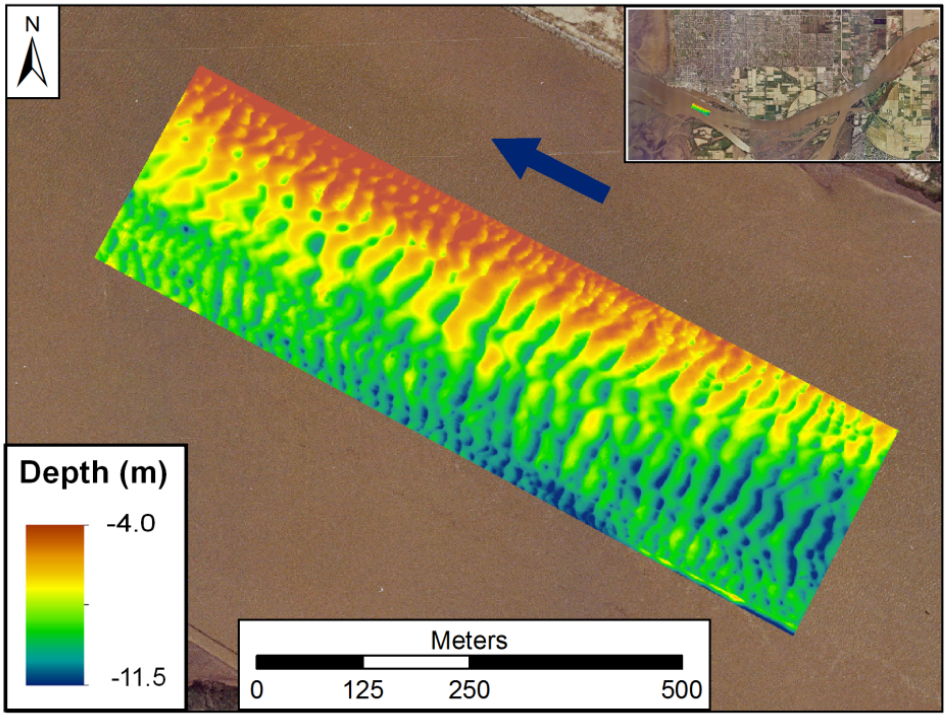

Figure A20. Bathymetric map of survey site at Mid Rising Tide.

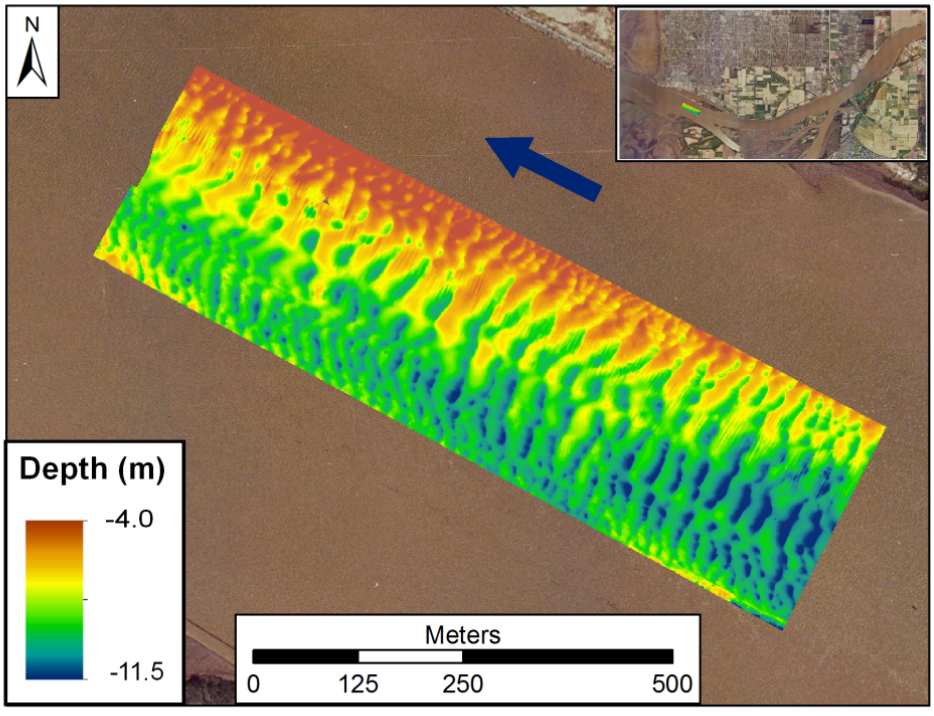

Figure A21. Bathymetric map of survey site at High Rising Tide.

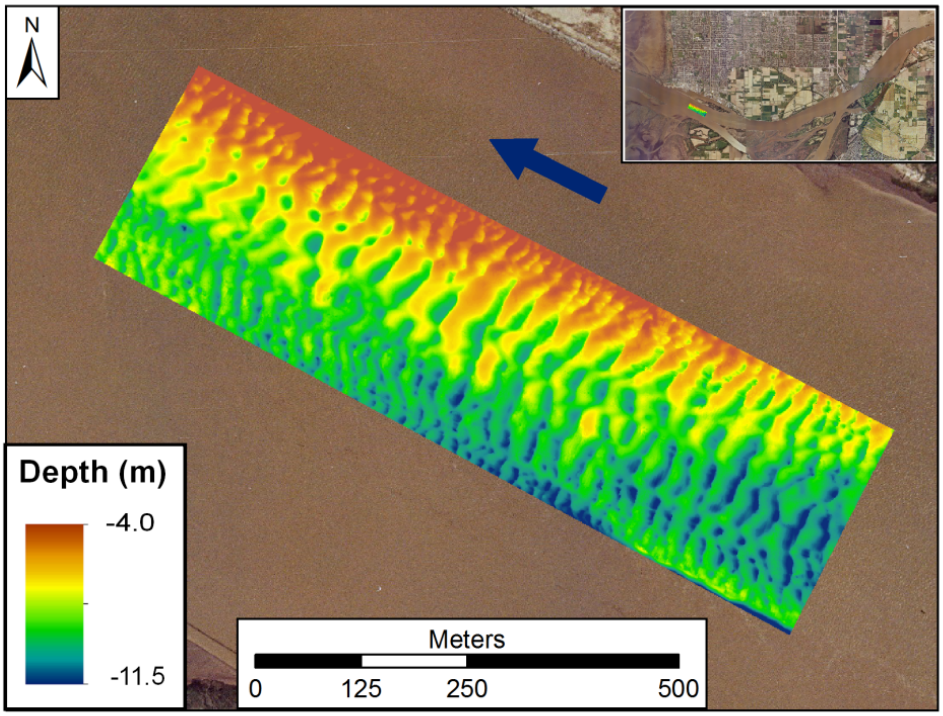

Figure A22. Bathymetric map of survey site at High Tide.

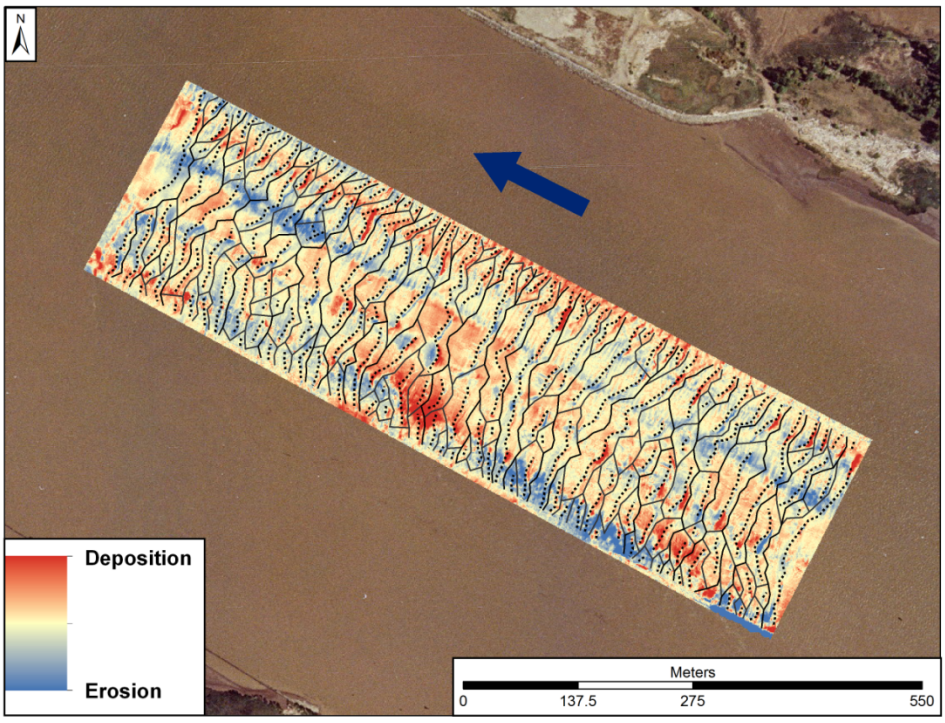

Figure A23. Map of difference in elevations between HFT and MFT.

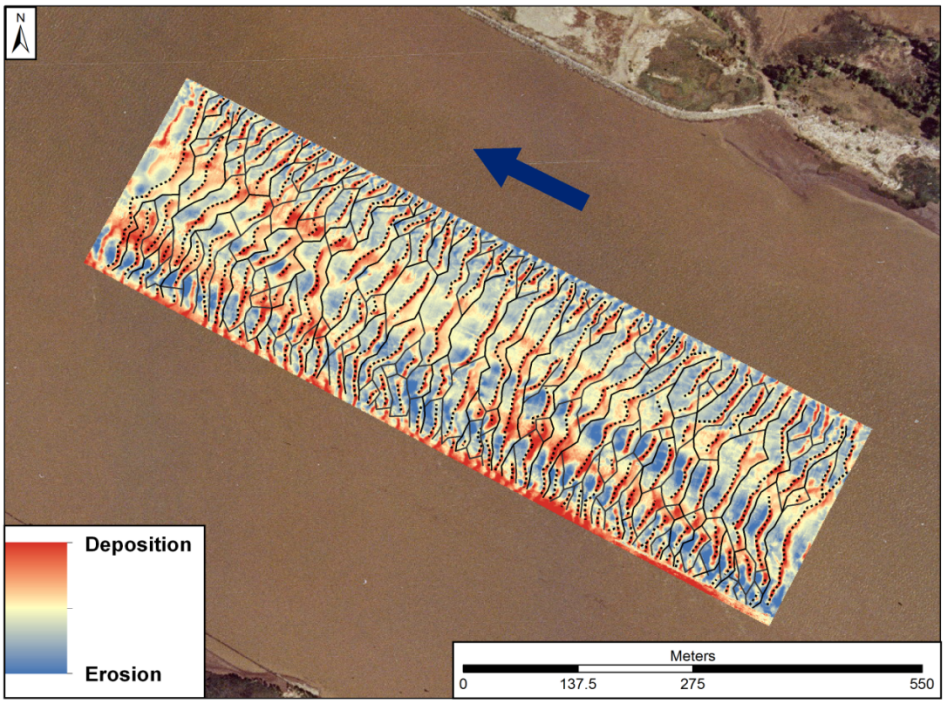

Figure A24. Map of difference in elevations between MFT and LFT.

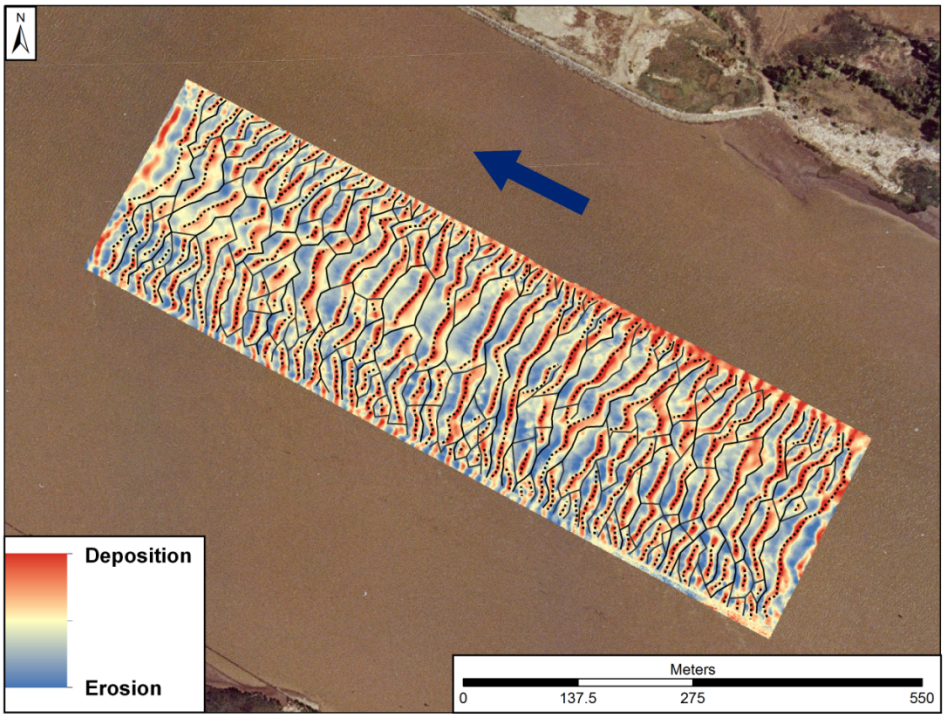

Figure A25. Map of difference in elevations between LFT and LT.

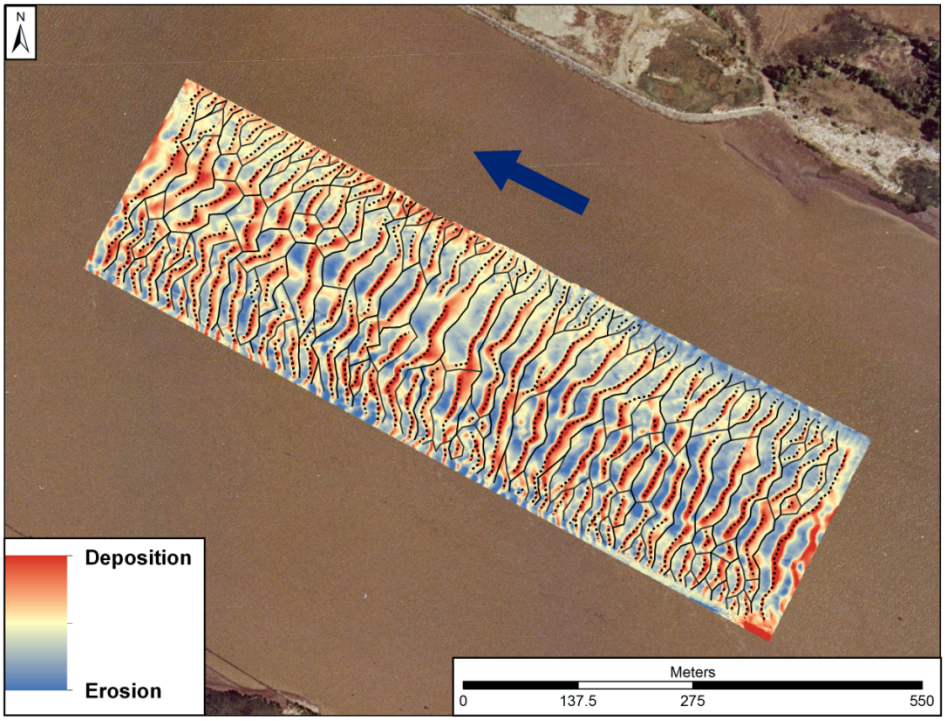

Figure A26. Map of difference in elevations between LT and LRT.

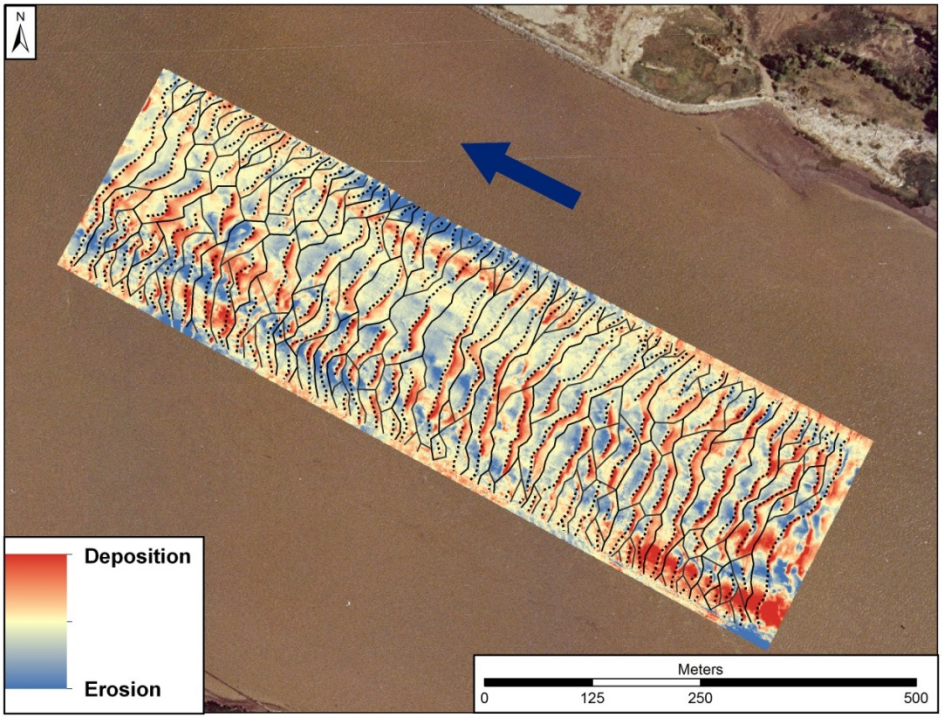

Figure A27. Map of difference in elevations between LRT and MRT.

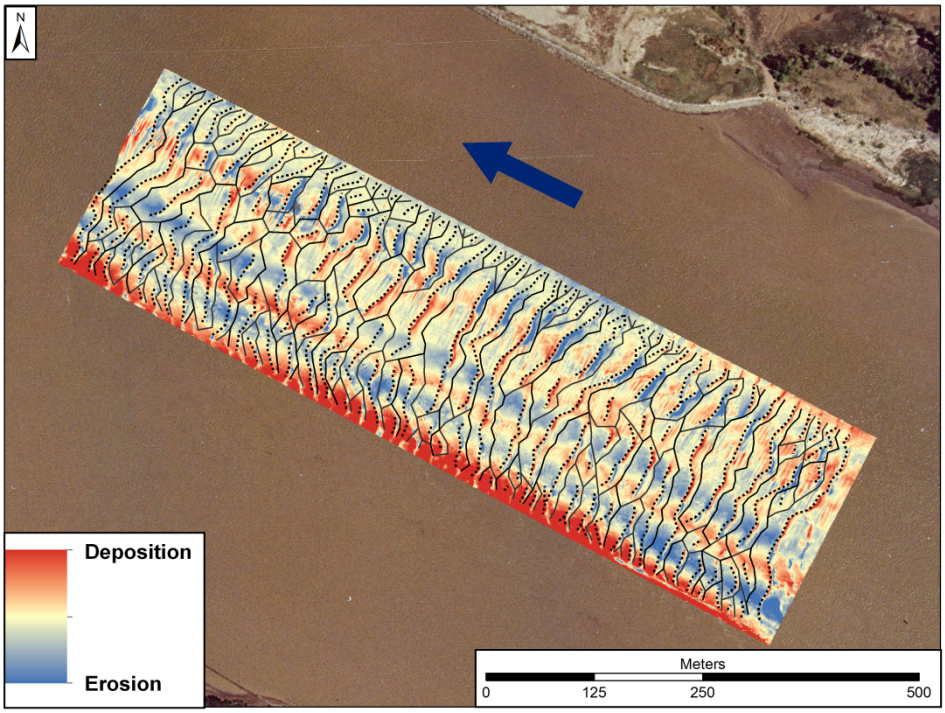

Figure A28. Map of difference in elevations between MRT and HRT.

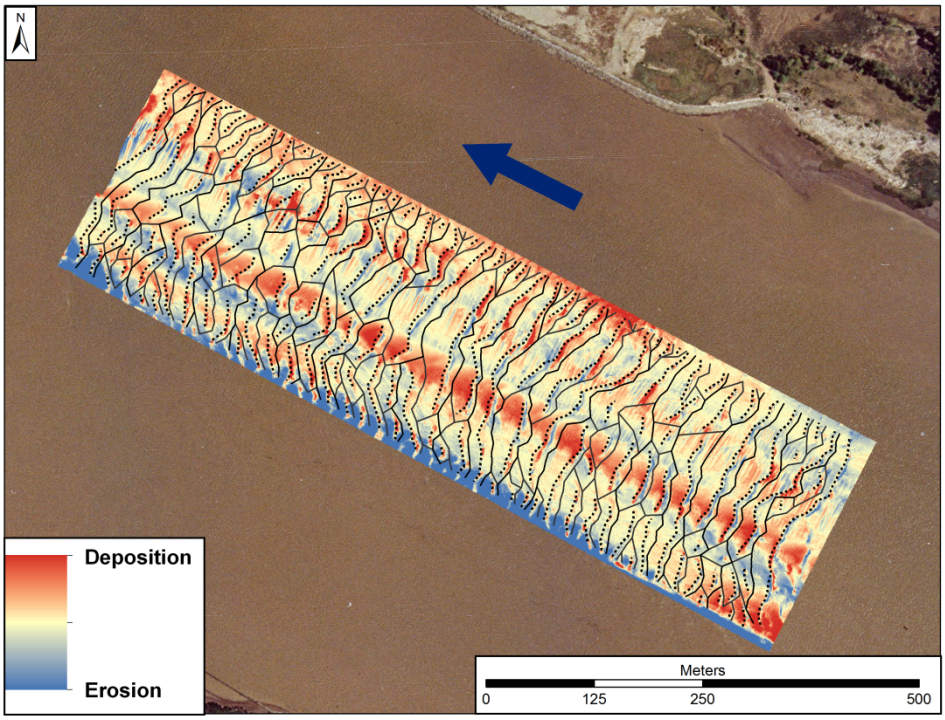

Figure A29. Map of difference in elevations between HRT and HT.

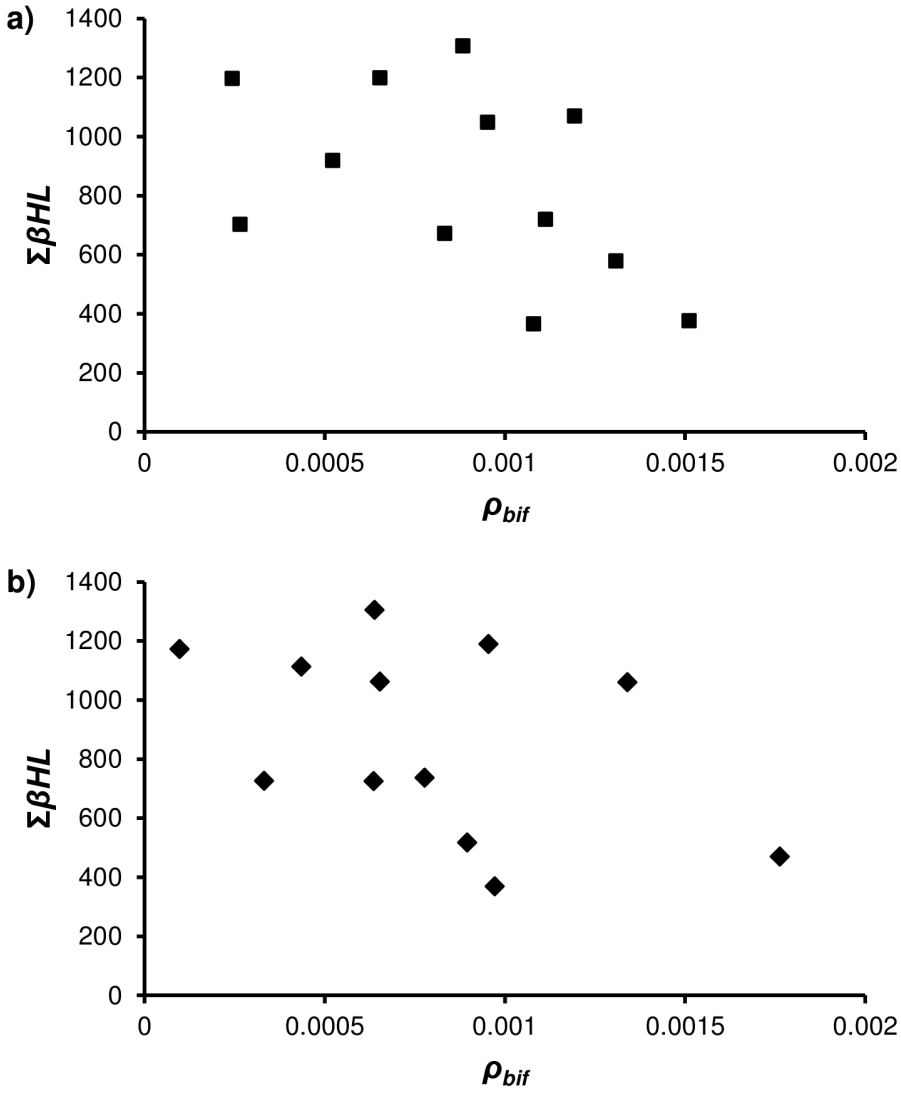

Figure A30. Graphs showing the sum mass by volume for each polygon from Irregular Grid 2 for a) LFT to LT, and b) LT to LRT.

Table A1. Skewness and kurtosis values for H, L, and H/L for each survey period over the tidal cycle.

	H (m)		*L* (m)		*H/L*		θ_{Lee} (°)	
	Skew	Kurtosis	Skew	Kurtosis	Skew	Kurtosis	Skew	Kurtosis
HFT	0.54	0.14	0.21	-0.49	0.12	0.00	0.51	0.08
MFT	0.62	0.43	0.22	-0.50	-0.16	0.23	0.25	-0.75
LFT	0.56	0.19	0.38	-0.24	0.41	1.03	0.35	-0.60
LT	0.40	-0.29	0.17	-0.58	0.02	-0.08	0.17	-0.90
LRT	0.46	-0.39	0.04	-0.71	0.58	0.94	0.25	-0.70
MRT	0.49	-0.11	0.04	-0.73	-0.06	-0.14	0.11	-0.88
HRT	0.49	-0.02	0.15	-0.70	0.06	-0.06	0.30	-0.67
HT	0.40	-0.25	0.14	-0.73	-0.07	-0.25	0.35	-0.68